RESPONSE OF AN INSTRUMENTED MASONRY SHEAR WALL BUILDING WITH FLEXIBLE DIAPHRAGMS DURING THE LOMA PRIETA EARTHQUAKE

ARTURO TENA–COLUNGA
DANIEL P. ABRAMS

University of Illinois at Urbana–Champaign, 1992

Urbana, Illinois

ABSTRACT
RESPONSE OF AN INSTRUMENTED MASONRY SHEAR WALL BUILDING WITH FLEXIBLE DIAPHRAGMS DURING THE LOMA PRIETA EARTHQUAKE

The subject structure of this study is a two−story office building located at Palo Alto, California. The structure was built in 1974. Recorded peak ground accelerations were as high as 0.21g and peak roof accelerations as high as 0.53g. Considerable amplifications of the peak accelerations between the ground and the roof were observed. The building withstood the Loma Prieta Earthquake with little damage.

Masonry construction used in Northern California is similar throughout the United States. Because moderate earthquakes are expected east of the Rocky Mountains, the response of the office building at Palo Alto can help foretell the earthquake hazard in the eastern and midwestern United States. The ground motions recorded at the office building at Palo Alto represent an upper bound for assessing possible hazards associated with similarly constructed buildings in the eastern United States. Since the building was not appreciably damaged, even with these high accelerations, there is hope that similar historic buildings across the nation may survive a future earthquake. However, such extrapolation is not warranted unless a detailed investigation is done to examine the reasons for the superior performance.

The objectives of this study are the following :

1) Investigate the reasons of the survival of the office building at Palo Alto with the use of both simplified and state−of−the−art methods.

2) Assess the effectiveness of a discrete MDOF dynamic model on the seismic evaluation of this building and similar masonry buildings with flexible diaphragms.

3) Correlate the recorded, observed and computed response at the office building at Palo Alto with estimates of dynamic response and prescribed strength by state−of−the−art masonry and seismic codes.

ACKNOWLEDGEMENTS

TABLE OF CONTENTS

LIST OF TABLES

LIST OF FIGURES

x

CHAPTER 1
INTRODUCTION

Masonry is one of the oldest forms of building construction. Nevertheless, the behavior of masonry structures is still one of the least understood. Masonry construction has usually been targeted as unreliable in seismic zones due to the damage experienced by some unreinforced masonry structures in major earthquakes. However, masonry structures can behave well when subjected to strong ground motions. For example, during the 1989 Loma Prieta Earthquake, a three–story unreinforced masonry building that was across the street from the failed Interstate 880 freeway structures in Oakland remained intact.

Another good example that masonry structures can survive strong ground shaking was the behavior of the old firehouse of Gilroy, California (Ref. 33), a two–story historic unreinforced masonry building that survived the Loma Prieta Earthquake with little damage. Gilroy is located approximately 15 km south east of Loma Prieta (Fig. 1.1). An array of instruments in Gilroy recorded accelerations higher than in other cities. Several of the 1989 acceleration records from the Gilroy array recorded peak ground accelerations from 0.30g to 0.50g (Refs. 10, 18, 32, 33).

Modern masonry construction has also had a satisfactory performance in recent earthquakes. The behavior of grouted brick walls systems is of particular interest. A two–story office building of this characteristics located at Palo Alto was instrumented by California Strong Motion Instrumentation Program (CSMIP, Ref. 32). The recorded peak ground acceleration in orthogonal directions were 0.21g and 0.20g. Peak acceleration at roof level were as high as 0.53g at the center of the flexible diaphragm and 0.34g at the exterior walls. The structure had a satisfactory behavior despite the intensity of shaking. The study of the survival of the two–story office building at Palo Alto can enhance the understanding of how similar masonry structures might act in other parts of the nation when subjected to moderate and strong ground motions.

1

1.1 Objectives and Scope

The subject structure of this study is a two–story office building located at Palo Alto, California. The structure was built in 1974. The lateral force resisting system consists of two two–way grouted brick walls tied with flexible diaphragms. The building is founded in spread footings. Prior to the Loma Prieta Earthquake, the building was instrumented by CSMIP with seven accelerometers (Ref. 7). Recorded peak ground accelerations were as high as 0.21g and peak roof accelerations as high as 0.53g. Considerable amplifications of the peak accelerations between the ground and the roof were observed. The subject building withstood the Loma Prieta Earthquake with no appreciable structural damage.

Masonry construction used in Northern California is similar throughout the United States. Because moderate earthquakes are expected east of the Rocky Mountains, response of the two–story office building at Palo Alto can help foretell the earthquake hazard in the eastern and midwestern United States. Though the Loma Prieta Earthquake was considered to be moderate in intensity, an equivalent motion in the eastern United States would be considered strong. If an earthquake at the New Madrid fault were to occur some time within the next 250 years, there would be only a 8% probability that ground accelerations measured at the firehouse (maximum of 0.21g) would be exceeded (Refs. 21, 22). Thus, the ground motions recorded at the two–story office building at Palo Alto represent an upper bound for assessing possible hazards associated with similarly constructed buildings in the eastern United States.

Little attention has been paid to reproduce the dynamic response of masonry structures with flexible diaphragms. Nonetheless, a simplified discrete MDOF dynamic model has been recently proposed for the seismic evaluation of masonry structures with flexible diaphragms (Refs. 33, 34). The study of the two–story office building at Palo Alto using this approach could corroborate the applicability of the discrete model to the study of masonry structures with flexible diaphragms.

The objectives of this study are the following :

1) Assess the applicability of the simplified discrete MDOF dynamic model for the seismic evaluation of the two−story office building at Palo Alto and similar masonry shear wall buildings with flexible diaphragms.

2) Correlate the recorded, observed and computed response at the two−story office building at Palo Alto with estimates of dynamic response and prescribed allowable stress limits by state−of−the−art masonry and seismic codes.

1.2 The Loma Prieta Earthquake

The Loma Prieta Earthquake of October 17, 1989, was the largest in intensity to hit the San Francisco Bay Area since 1906. The earthquake struck at 5:04 p.m (PDT), disrupting most of the communities of the Bay Area and shocking the nation that was getting ready to enjoy the nationally broadcast opening game of the 1989 baseball World Series scheduled at San Francisco's Candlestick Park at that time.

The earthquake had a surface−wave magnitude of 7.1 and its epicenter was located about 10 miles northeast of Santa Cruz and 60 miles southeast of San Francisco (Fig. 1.1). The hypocenter was about 11 miles beneath the earth's surface. The earthquake ruptured a 25−mile segment of the San Andreas fault and was felt from Los Angeles in the south, to the Oregon border to the north, and Nevada to the east. The strong shaking lasted less than 15 seconds, but caused more than $7 billion damage (Ref. 10).

The single greatest catastrophe occurred when the Cypress Street Viaduct, a one−mile elevated segment of the Interstate Highway 880 collapsed and claimed 42 lives (Refs. 8, 9, 10, 11, 25, 30). The earthquake killed 62 people, injured 3,757, destroyed 367 businesses, and left more than 12,000 people homeless (Ref. 10).

1.2.1 Performance of URM Structures

Several aspects of the Loma Prieta Earthquake have been extensively reported in the literature (Refs. 7, 8, 9, 10, 11, 17, 18, 25, 30, 32). Of particular interest is the performance of unreinforced masonry structures. Unreinforced masonry structures are usually demonized by their somewhat spectacular damage during earthquakes, however, many of them performed well during the Loma Prieta Earthquake.

In the city of San Francisco (Fig. 1.1), out of 1947 URM buildings surveyed (Ref. 10), only 36 were identified to have suffered heavy or severe damage (1.8%). Damage in Chinatown, where 15% of San Francisco URM buildings are located, varied from minor to moderate. There was ample evidence that most of this damage was caused by pounding due to the lack of building separation (Ref. 30). On the other hand, damage in the south of Market district, where 25 to 30 percent of San Francisco's URM are located, was extensive and varied from minor cracking to partial collapse.

The distribution of damage to URM buildings in San Francisco illustrates the effects of soil type on building response (Ref. 30). URM buildings on the stiff rock−like soils (uphill Chinatown) were less damaged than similar buildings founded on softer soils (bay mud and landfill of south of Market district). Peak ground accelerations recorded at San Francisco varied from 0.06g at the Pacific Heights district to 0.33g at the San Francisco International Airport (Ref. 10).

In Oakland (Fig. 1.1), the downtown area suffered significant damage mostly in steel−framed buildings with masonry cladding and URM buildings (Ref. 25). Damage observed in low−rise URM buildings consisted primarily of collapsed parapets, separation of masonry walls at the roof level(Ref. 18), and some partial out−of−plane brickwork collapses of the masonry walls caused by the pushing of the flexible diaphragms (Ref. 25). Peak ground accelerations nearby the downtown Oakland area measured between 0.26g and 0.29g (Refs. 10, 32).

4

The damage observed at Hollister (Fig. 1.1) was nearly equal to that observed at Oakland (Ref. 18). Peak ground accelerations of 0.18g and 0.38g were recorded in orthogonal directions and 0.20g in the vertical direction (Refs. 10, 32).

Palo Alto (Fig. 1.1) experienced similar peak ground accelerations (0.21g to 0.38g, Ref. 10). However, damage to URM structures was reduced. Most of the damage was observed at the campus of Stanford University, where unreinforced sandstone masonry buildings suffered different levels and extent of damage. The more common type of damage was flexural cracking at the bottom and top of slender piers between openings, mild shear cracking in piers and at corner intersections of walls, and tensile cracking in arches.

There was an array of instruments in Gilroy which recorded higher peak ground accelerations than in other cities (Refs. 10, 18, 32). Several of the 1989 acceleration records from the Gilroy array recorded peak ground accelerations from 0.30g to 0.50g (Ref. 10). Many buildings in the main street and downtown area of Gilroy were essentially undamaged, although the town hall was severely damage by the shaking. One of the structures that withstood the earthquake handily was the historic old firehouse building, only two blocks north from the town hall (Ref. 33). The survival of the firehouse attracted the attention of some post−earthquake investigation teams (Refs. 10, 30).

Santa Cruz (Fig. 1.1) was the city that suffered the more dramatic URM damage during the earthquake. Many of the old URM buildings in the Pacific Garden Mall in downtown Santa Cruz were damaged or destroyed (Refs. 10, 30). Structural damage observed in the URM buildings in the Pacific Garden Mall can be described as out−of−plane brickwork failure, in−plane brickwork failure, diaphragm flexibility/failure and pounding. Santa Cruz is located 10 miles from the epicenter. Free−field accelerograms recorded in Capitola, within 6 miles from Santa Cruz and 9 miles from the epicenter, recorded peak ground accelerations of 0.47g and 0.54g in orthogonal directions and 0.60g in the vertical direction (Refs. 10, 30, 32).

Recorded peak ground accelerations at the University of California at Santa Cruz were 0.44g and 0.47g in orthogonal directions and 0.66g in the vertical direction (Ref. 10).

Watsonville and Los Gatos (Fig. 1.1) were other cities where some URM structures suffered severe structural damage, yet the level of damage was not uniform (Ref. 18). Some unbraced parapets survived. Existing wall anchorage was adequate in many instances. URM walls that exceeded code recommended heights were stable. Diagonal shear cracking in URM walls was not universal and could be commonly related to the quality of the existing masonry and the building configuration. Peak ground accelerations recorded in Watsonville were 0.28g and 0.39 g in orthogonal directions and 0.66g in the vertical direction (Refs. 10, 32). Peak ground accelerations within or above 0.40g are inferred for Los Gatos from instrumental records at Saratoga and Santa Cruz (Ref. 18).

The most severe damage of URM structures during the Loma Prieta Earthquake occurred in places were peak ground accelerations higher than 0.38g were recorded (Santa Cruz, Watsonville and Los Gatos). A substantial number of URM buildings in the cities of Hollister, Palo Alto, Oakland and San Francisco survived without damage that would have threatened the life of occupants or those on the adjacent public way (Ref. 18). Peak ground accelerations recorded in these cities were typically between 0.20g to 0.30g.

The earthquake investigation team of the International Masonry Institute (Ref. 17) made the following observations regarding the behavior of unreinforced masonry structures during the Loma Prieta Earthquake :

    ❏ Unreinforced masonry buildings that had been retrofitted for seismic safety appeared to have performed well.

    ❏ Buildings with flexible structural frames, designed to deform under seismic loads, appeared to experience damage to exterior claddings when insufficient provisions were made to accommodate the frame deformations.

    ❏ Some older unreinforced masonry structures, constructed before the advent

of engineering practices and building codes, experienced varying degrees of damage.

☐ Improper or nonexistent connections between walls and roof or floor diaphragms appear to have caused several failures of older URM buildings.

☐ Unbraced and unreinforced masonry parapet walls appear to have caused several failures.

Therefore, poor connections and poor detailing of URM structures seem to be responsible for most of the failures of these structures rather than the assumed brittle nature of the masonry, which is instead often blamed.

1.4 Organization

The study is divided into seven chapters. In Chapter 2, the description of the building is presented. The observed damage and the recorded motions at the firehouse during the Loma Prieta Earthquake are discussed in Chapter 3. In Chapter 4, preliminary estimates of strength and their correlation with different code provisions are addressed. In Chapter 5, the effectiveness of the use of the discrete MDOF dynamic models on the prediction of the recorded dynamic response at the building is studied. In Chapter 6, estimates of dynamic response outlined by state−of−the−art seismic codes are compared to those measured at the office building. A summary of the investigation and the conclusions are offered in Chapter 7.
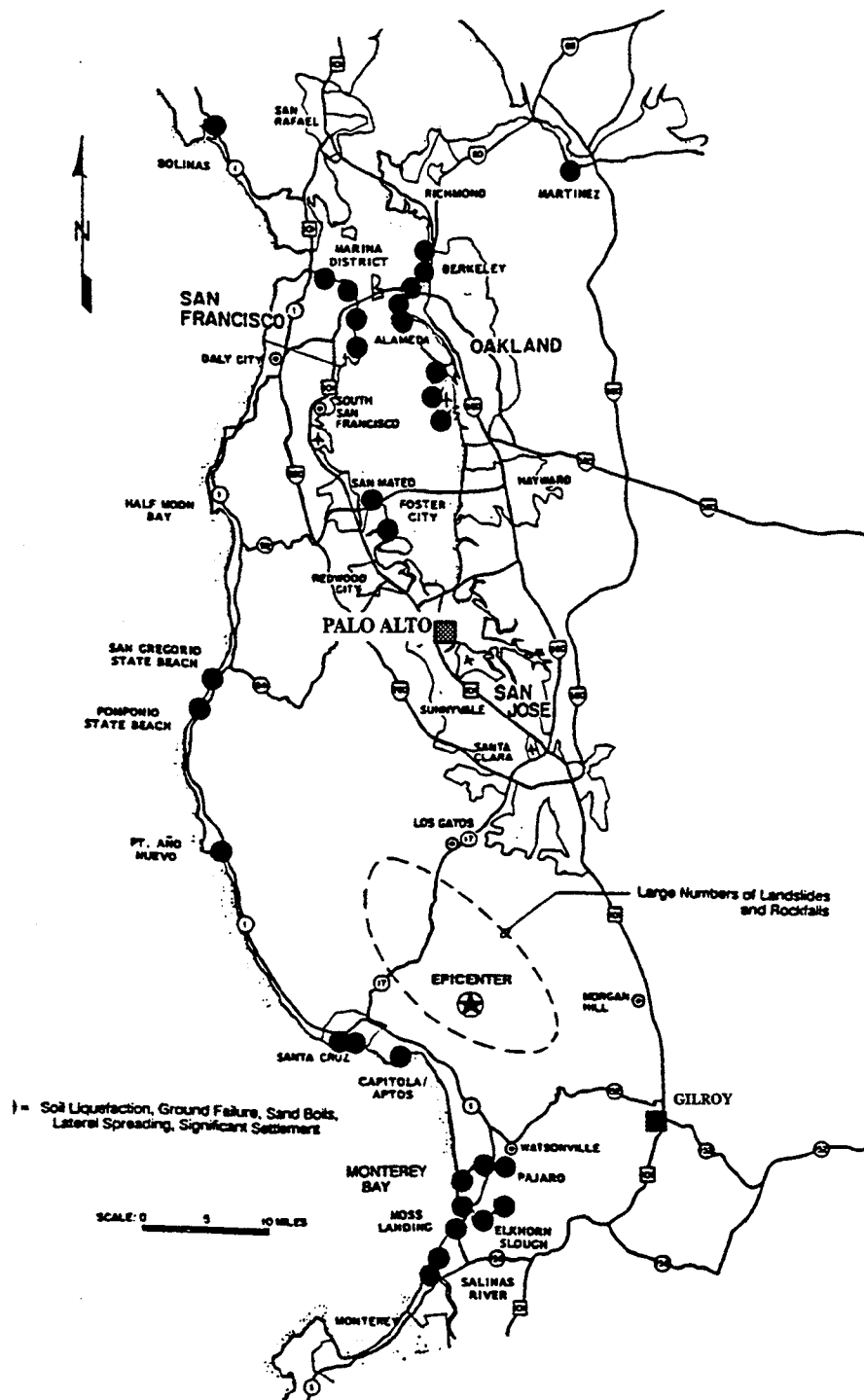
Figure 1.1 Affected area by the Loma Prieta Earthquake

8

CHAPTER 2
DESCRIPTIVE INFORMATION

2.1 Description of the Building

A two−story office building, located at Palo Alto, California, is the subject of this investigation. The structure was constructed in 1974. The building is presented in Figure 2.5. Plan views are presented in Fig. 2.1. The building is of rectangular shape, where the lateral force resisting system is composed of two−way grouted masonry brick walls at north and south ends together with flexible diaphragm floor systems. In addition, the vertical load carrying system is also composed of interior tubular steel columns (ϕ= 3 1/2", t = 3/8") and exterior glulam columns (Fig. 2.1). Many of those interior and exterior columns are only located at the fist floor level (Fig. 2.1). The building is found on spread footings.

2.1.1 <u>Diaphragms</u>

The two−story office building at Palo Alto has a peculiar mixture of floor systems. The second floor consist of 1.5" thick light weight concrete over 3/4" thick plywood mounted on 36" open truss joists running in the E−W direction every 2 ft. Two interior 5 1/8" x 15" glulam beams running in the N−S direction and four exterior 5 1/8" x 16 1/2" glulam beams running in both directions complete the floor system (Fig. 2.1). The specified compressive strength of the light weight concrete, f'_c, was 2500 psi. The plywood sheathing and the glulam beams used are type Douglas Fir. On the other hand, the roof diaphragm consist only of a 1/2" thick Douglas Fir plywood together with deep interior and exterior glulam Douglas Fir beams running in both directions (Fig. 2.1). The roof diaphragm is considerably more flexible than the first floor diaphragm. The aspect ratio of the diaphragm (length/ width) is 1.87.

2.1.2 <u>Grouted Walls</u>

The lateral force resisting system is composed of four L−shaped two−way grouted brick walls. A detail of the dimensions and location of the grouted walls at the base level is

presented in Fig. 2.2. The typical cross section of the two-way grouted brick walls is presented in Fig. 2.3. Walls are 12" thick. The joining grout is 7" thick. Bricks are grade MW (moderate weathering) conforming to ASTM C-62 (Ref. 20). The bricks were joined with a mortar mix with volumetric proportions of Portland cement : hydrated lime : sand of 1 : 0.5 : 4.5, corresponding to a type S mortar according to ASTM C-270 specifications (Ref. 20). Bricks were prewetted to have initial rate of absorption not in excess of 0.25 oz/in^2/min, according to ASTM C-67 provisions (Ref. 20). The grout was mixed according to ASTM C-476-63 table 3.1, course grout, with an specified compressive strength f'$_c$ of 2000 psi and a slump of 10 inches.

The grouted walls were reinforced both horizontally and vertically with bars # 4 @ 12" (Fig. 2.2) . Additional # 8 bars were provided in the vertical direction at the corners (Fig. 2.2). All reinforcement steel is grade 40. All reinforcement steel is continuos; laps are 50 diameters at splices in the grouted brick walls. Splices are staggered in adjacent bars. Walls were specially inspected during the construction of the building.

2.1.3 Connection between diaphragms and walls

Ledgers of the diaphragms are tied to the grouted walls by 3/4" φ steel rods anchored in the the interior reinforcement of the grouted walls by a hook. These ledgers are nominally placed every 24" in both directions. Plywood is connected to the ledgers through nails.

2.1.4 Foundation system

The first floor slab is a 4" thick reinforced concrete slab. The foundation consist of spread footings for the grouted brick walls, the exterior columns, and the interior steel columns. Between the slab and there is an engineered fill which consists of 1" thick sand, a 6 mm thick polyethylene film lapped every 6 inches, and a 4" pea gravel (Fig. 2.4). The footings are built over a sandy clay fill with a capacity of 2000 psf , according to a soil-mechanics study (Ref. 7). The wall are founded on spread footings 3 ft wide (Fig. 2.4). The depth of the footings at the walls are 1'6" in the N-S running walls, and 2'6" in the E-W running walls. Connection

details of the grouted brick walls and the footings are presented in Fig. 2.4. The width of the spread footings for the exterior and interior columns is 8" and their depth is 1'6".

2.2 Mass Considerations

The total mass of the building was estimated based on the information given on blueprints. The uniformly distributed dead load of the diaphragms at the second story level was estimated as 25.5 psf, and the live load as 50psf. At the roof level, the uniformly distributed dead load was estimated as 15 psf, and the live load as 20 psf. Self weight of the brick masonry walls was assumed to be 10 psf per inch of thickness. Volumetric weight of glulam was taken as 30 pcf. Self weight of glass was taken as 8 psf. The computed masses for the building for the dynamic analyses are 1,383.6 $lb-sec^2/in$ (weight = 534 kips) at the roof level and 3,046.5 $lb-sec^2/in$ (weight = 1,177 kips) for the second floor level. The total mass of the structure at the base without including the first floor slab and the foundation is 4,737.7 $lb-sec^2/in$ (weight = 1,830 kips). The total mass of the building including the first floor slab and the foundation is 10,439.6 $lb-sec^2/in$ (weight = 4,032 kips).

154'10"

5'5"

12' (typ.)

5 1/8" x 16 1/2" edge beams (typical)

12" Grouted brick walls

5 1/8" x 15" beams

9'4"

82'10"   5'4"

9'4"

36" truss joists @ 24" o.c.o running E−W ('typ)

5'5"   12' (typ.)

First Story Plan (Second floor diaphragm)

← N$_{ref}$

154'10"

5'5"

24' (typ.)

8 3/4" x 16 1/2"   4" x 8"   8 3/4" x 21"   4" x 8"   8 3/4" x 21"   4" x 8"   8 3/4" x 16 1/2"   4" x 8"   8 3/4" x 21"   4" x 8"   8 3/4" x 21"   4" x 8"   8 3/4" x 16 1/2"

4" x 14"   4" x 14"   2" x 14"   2" x 14"   4" x 14"   4" x 14"

82'10"   6" x16"   4" x 14"   4" x 14"   4" x 14"   4" x 14"   4" x 14"   4" x 14"   6" x16"

4" x 14"   4" x 14"   2" x 14"   2" x 14"   4" x 14"   4" x 14"

8 3/4" x 16 1/2"   4" x 8"   8 3/4" 21"   4" x 8"   8 3/4" 21"   4" x 8"   8 3/4" x 16 1/2"   4" x 8"   8 3/4" 21"   4" x 8"   8 3/4" 21"   4" x 8"   8 3/4" x 16 1/2"

5'5"   24' (typ.)

Second Story Plan (Roof diaphragm)

NOTES :

■ 24" x 12" glue–laminated column (full height)

▦ 24" x 12" glue–laminated column (first story only)

⊛ Tubular steel colums φ = 31/2", t=3/8" (full height)

○ Tubular steel colums φ = 31/2", t=3/8" (first story only)

Figure 2.1 Palo Alto – 2–story office building plan views (CSMIP station No. 58264)

12

Figure 2.2 Dimensions and location of the grouted brick walls at the base (typical)
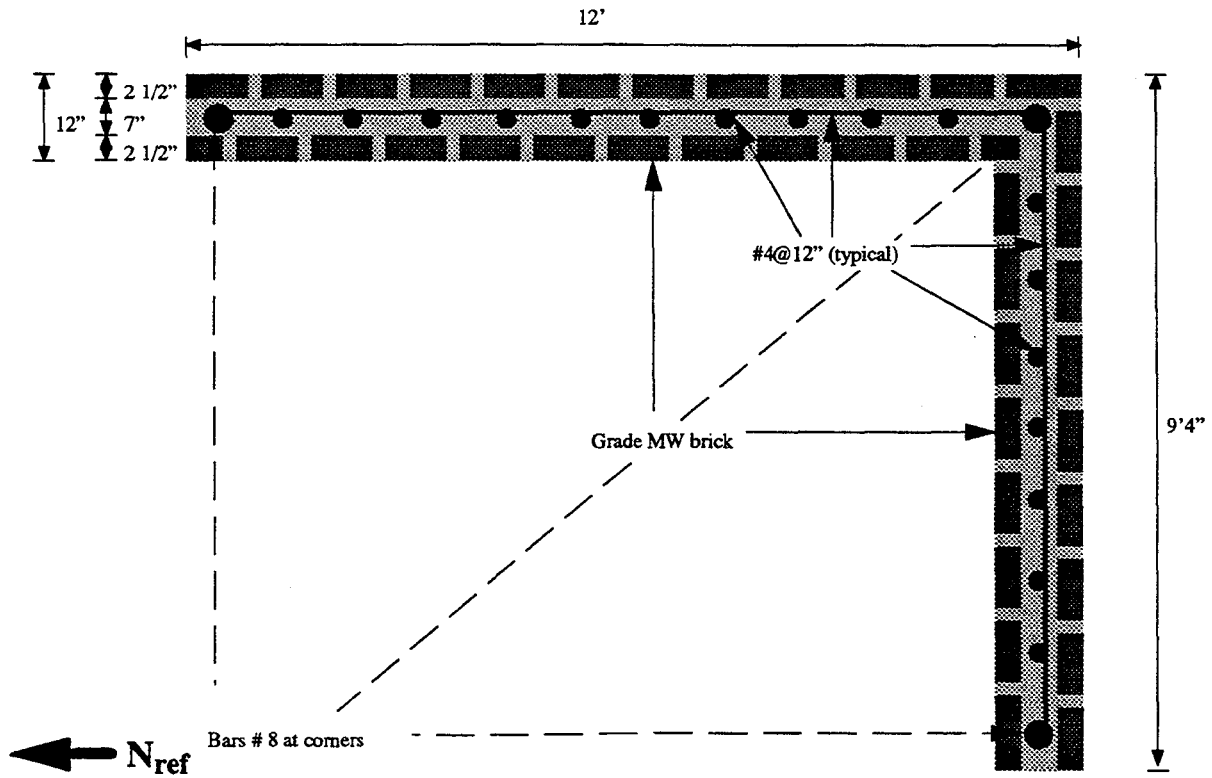
Figure 2.3 Cross section and reinforcement of the grouted brick walls (typical)

13

#4@12" (typical)

Fist Floor slab

9"

1'6"

2#8 at center
#3 @ 16"
4#6 at corners

3'

a) N–S running footing at walls (typical)

#4@12" (typical)

Fist Floor slab

9"

2'6"

4 # 11

#3 @ 16"

3 # 6

3'

b) E–W running footing at walls (typical)
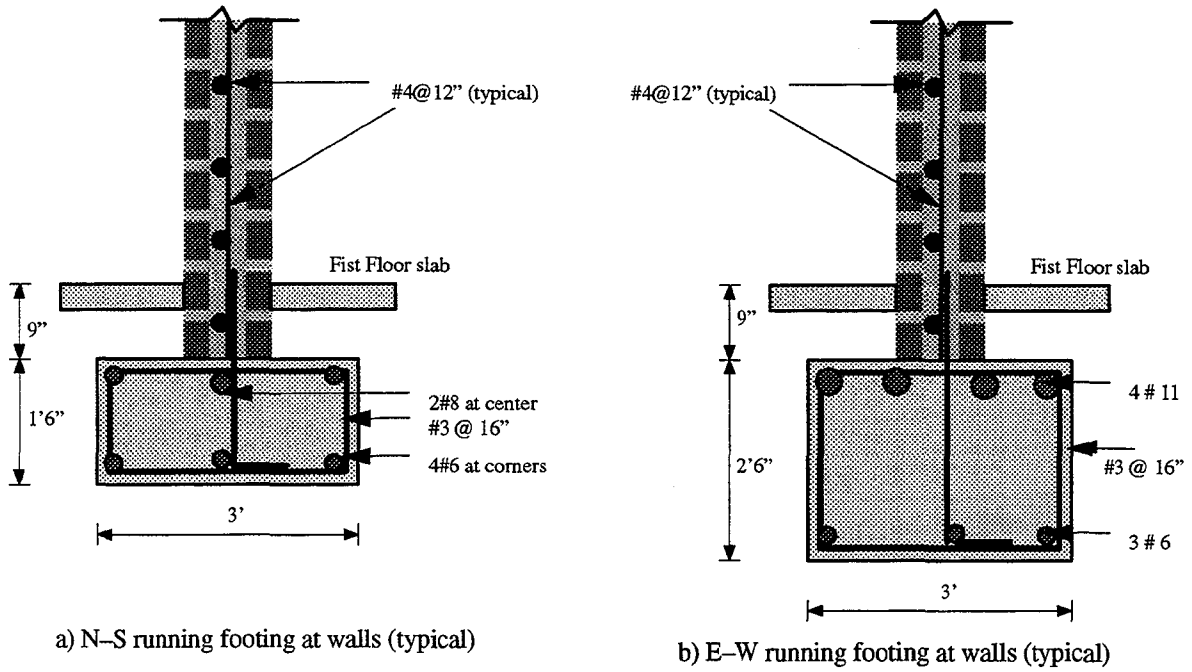
Figure 2.4 Connection details of the grouted brick walls with the foundation (typical)
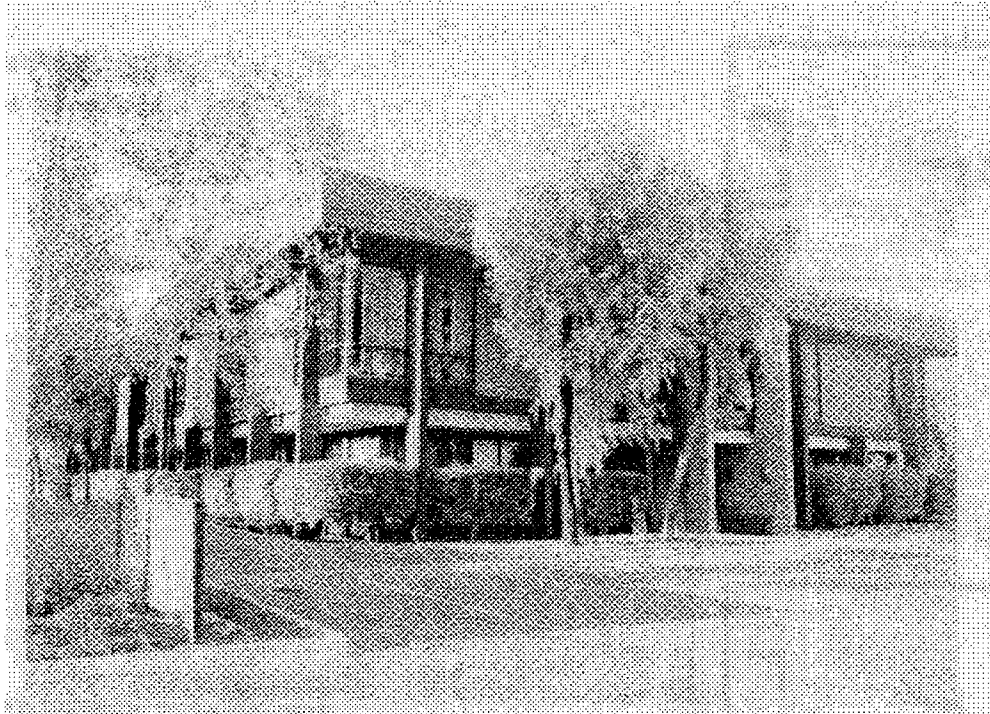
Figure 2.5 View of the office building at Palo Alto (from Shakal et al, Ref. 32)

14

CHAPTER 3
OBSERVED RESPONSE DURING THE LOMA PRIETA EARTHQUAKE

3.1 Observed Damage

There is not specific information available regarding the extent of damage at the building after the Loma Prieta Earthquake. However, it is assumed that the building did not suffer structural damage during the event.

3.2 Recorded Motions During the Loma Prieta Earthquake

The structure was instrumented by the California Strong Motion Instrumentation Program (CSMIP) with seven sensors (Refs. 7, 32). The distribution of the sensors is shown schematically in Fig. 3.1. Three sensors recorded ground motions (sensors 1 to 3, Figs. 3.1 and 3.2), and four recorded motions at the roof level (sensors 4 to 7, Figs. 3.1 and 3.2).. The sensors recorded 60 seconds, however, only 10 seconds can be considered of significant ground motions. The location of the sensors at the ground suggest that some interaction between the ground and the structure may have affected the recorded records. (Fig. 3.1). The first 25 seconds of corrected and synchronized recorded motions are presented in Fig. 3.2. Peak accelerations are summarized on Table 3.1.

3.2.1 Observed Response in the East—West Direction

Considerable amplification of peak acceleration between the ground and the roof records was observed in the east—west direction. The north wall experienced a peak acceleration of 0.41g at the roof level (sensor 4, Fig. 3.2), while at the center of the diaphragm a peak acceleration of 0.53g was experienced at the same level (sensor 5, Fig. 3.2). The peak ground acceleration in that direction was 0.21g (sensor 3, Fig. 3.2). Therefore, there were amplifications of 1.60

times between the peak ground and top wall accelerations, and 1.56 times between the walls and the diaphragm.

Table 3.1 Peak accelerations recorded at the firehouse of Gilroy	
Sensor I.D.	Peak acceleration (g)
1	0.20
2	0.08
3	0.21
4	0.34
5	0.53
6	0.32
7	0.36

The maximum relative displacements between the ground and the roof records were determined by subtracting the displacement time history of the ground from the displacement time histories of the roof records, therefore identifying the peak dynamic drifts. The computed maximum dynamic drifts between the ground level and the center of the diaphragm at the roof computed this way was 0.80" (using the recorded motions of sensors 3 and 5), whereas between the central wall at the roof level and the ground was 0.41"(using the records of sensors 3 and 4). Therefore, a maximum dynamic in−plane distortion of 0.14% times the height was experienced at the north and south walls, and a maximum dynamic out−of−plane distortion of 0.28% times the height was experienced at the diaphragm in this direction.

Absolute acceleration response spectra for different damping ratios (Fig. 3.3) suggests that the response of a system with natural period in the neighborhood of 0.35−0.45 seconds would

be highly amplified for systems with damping ratios of 5% or more. Normalized Fourier amplitude spectra computed for the east−west ground motion (Fig. 3.4) identifies that relatively large amounts of energy were input within period ranges from 1.00 to 1.25 seconds. Ground accelerations in this direction included pulses with fairly long periods of approximately 1.25 seconds (sensor 3, Fig. 3.2). This fact suggest that the natural period of the engineered fill soil is 1.25 seconds.

The normalized Fourier amplitude spectra for the north wall (Fig. 3.5) suggests that the walls were rigid and mostly reproduced and amplified the ground motions. It can also be observed in Fig. 3.5 that the amplitudes of long period ranges are decreased whereas in the small period range are increased in the normalized Fourier amplitude spectra for the time frame of 8 to 14 seconds, where the strongest motions were recorded. This observation suggest that the natural period of the structure may be in this short period range, especially in the peak located at the 0.40 seconds mark. The same observations can be made from the normalized Fourier amplitude spectra for the south wall (Fig. 3.6). As a matter of fact, the amplitude and frequency content are almost identical in both walls, as it can be observed in Figs. 3.2 and 3.7. The comparison of the normalized Fourier amplitude spectra for sensors 3 and 4 presented in Fig. 3.8 confirms the fact that the walls were rigid and they primarily reproduced the ground motions. It can also be observed that the amplitude of the response in the short period range is higher at the wall than at the ground, particularly at the 0.40 seconds mark.

The normalized Fourier amplitude spectra for the diaphragm (Figs. 3.9) suggests that the structure had a natural period of 0.40 seconds in the E − W direction, where most of the energy was released, however, there is a high component at the 1.00−1.25 period range that can be related to the ground motions. As a matter of fact, this component is considerably decreased when the strongest phase is considered (8−14 seconds, Fig. 3.9). The comparison of the normalized Fourier amplitude spectra of the diaphragm and the ground records confirms these observations (Fig. 3.10).

The identified peak response of the building in the E−W direction is compared against the absolute acceleration response spectra for different damping ratios in Fig. 3.11. It is assumed in this figure that structural response in the E−W direction may be represented by a single−degree−of−freedom oscillator. It can be observed that under this assumption, the equivalent damping ratio experienced by the structure could have been as high as 12%. There is no data available in the literature regarding the observed damping ratios in reinforced grouted brick walls. However, Paulson and Abrams have reported damping ratios of 6% in reinforced concrete block masonry structures when subjected to high amplitude motions in the elastic range, and 13% to 16% when a considerable inelastic action took place (Ref. 27).

3.2.2 Observed Response in the North−South Direction

Amplifications between the roof motions and the ground were also observed in the north−south direction. The peak acceleration of the center of the diaphragm was 0.36g (sensor 7, Fig. 3.2). The peak ground acceleration in that direction was 0.20g (sensor 1, Fig. 3.2). Therefore, there was an amplification of 1.79 times between the peak ground and the roof diaphragm accelerations in the north−south direction. From the records, a maximum relative displacement of 0.29" between the roof diaphragm and the ground was computed, corresponding to an out−of−plane distortion of 0.10% times the height.

Absolute acceleration response spectra for different damping ratios (Fig. 3.12) identified peak responses in the 0.35 to 0.45 seconds period range. Normalized Fourier amplitude spectra computed for the north−south direction(Fig. 3.13) suggested that an important amount of energy was input at a dominant period of about 0.37 and 1.13 seconds, with important energy inputs in the other period ranges. The normalized Fourier amplitude spectra for the diaphragm record at the roof (Fig. 3.14) indicates that the structure had a natural period of 0.37 seconds in the north−south direction, while significant components in other period ranges were also observed. The amplitude of the high period range components

18

is considerably decreased when the strong motion phase is considered (8−14 seconds, Fig. 3.14).

The identified peak response of the building in the N−S direction is compared against the absolute acceleration response spectra for different damping ratios in Fig. 3.15. It is assumed in this figure that structural response in the N−S direction may be represented by a single−degree−of−freedom oscillator. It can be observed that under this assumption, the equivalent damping ratio experienced by the structure in this direction could have been as high as 14%. This result is similar to what was observed in the E−W direction.

3.2.3 Vertical Ground Motions

Vertical accelerations are a concern in masonry structures since they can adversely affect the stresses due to gravity loads, especially if these accelerations are high. The recorded vertical ground accelerations are presented in Fig 3.2 (sensor 2). The recorded accelerations present a wide range of frequencies, even in the low frequency range. It shown in Table 3.1 that the peak recorded vertical ground acceleration was 0.10g, which is too low to have any significant impact in the magnitude of the gravitational load stresses.

3.2.4 Directivity Effects of the Incoming Seismic Waves

From the observation of the ground motion records presented in Fig. 3.2 and the proximity in the absolute value of the peak ground accelerations recorded in both directions (0.21g for the east−west direction, 0.20g in the north−south direction), it is believed that the seismic waves hit the structure in an incoming oblique angle. The recorded and computed data from the sensors suggested that the firehouse was more severely shaken in the east−west direction than in the north−south direction. This was also directly related to the intrinsic characteristics of the resisting structural system in each direction, since the rectangular shape of the diaphragm makes the structure more vulnerable in the E−W direction.

19

E/W Elevation

Ground Floor Plan

Roof Plan
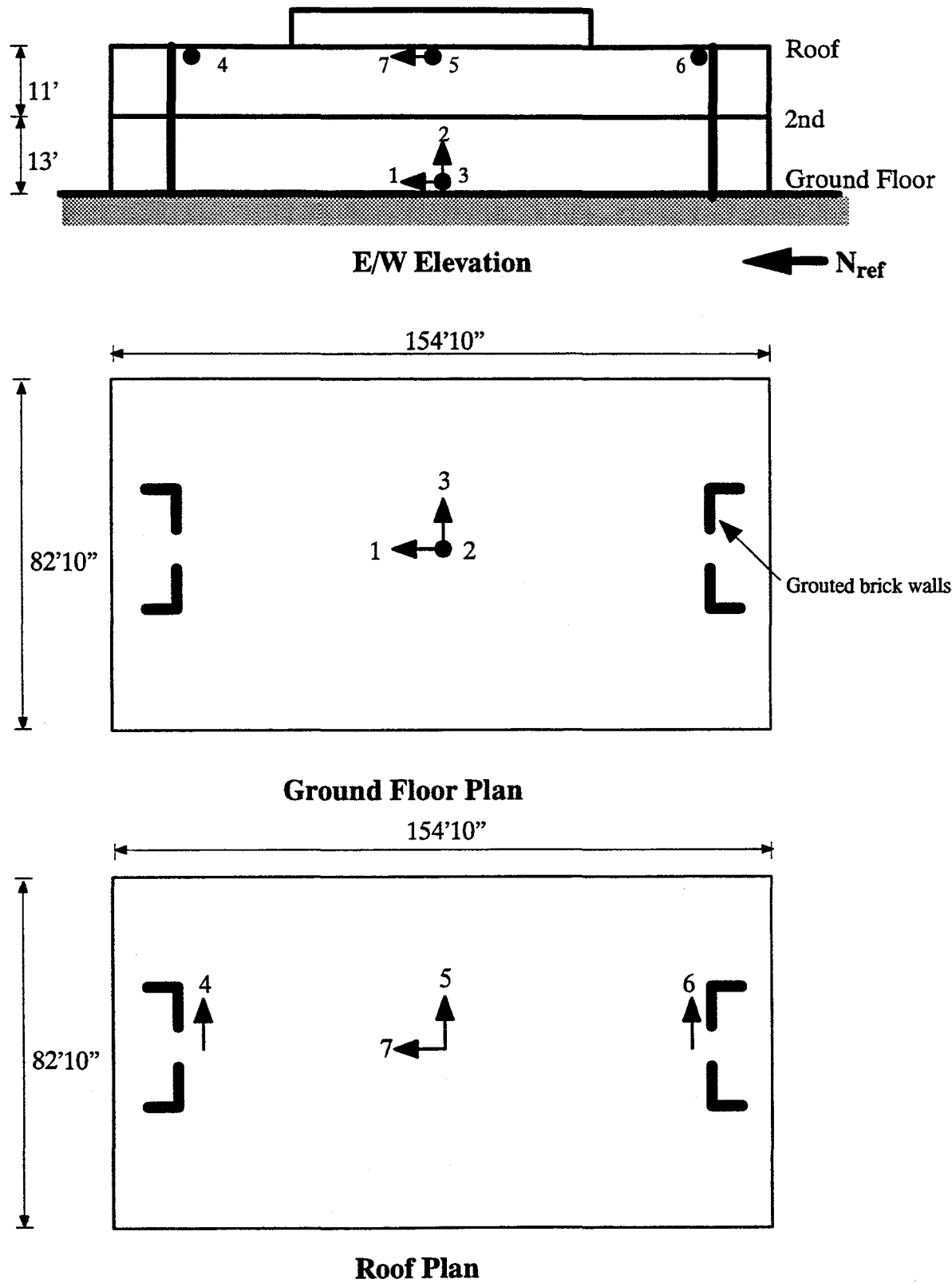
Figure 3.1 Location of sensor at Palo Alto –2–story office building (CSMIP station No. 58264)
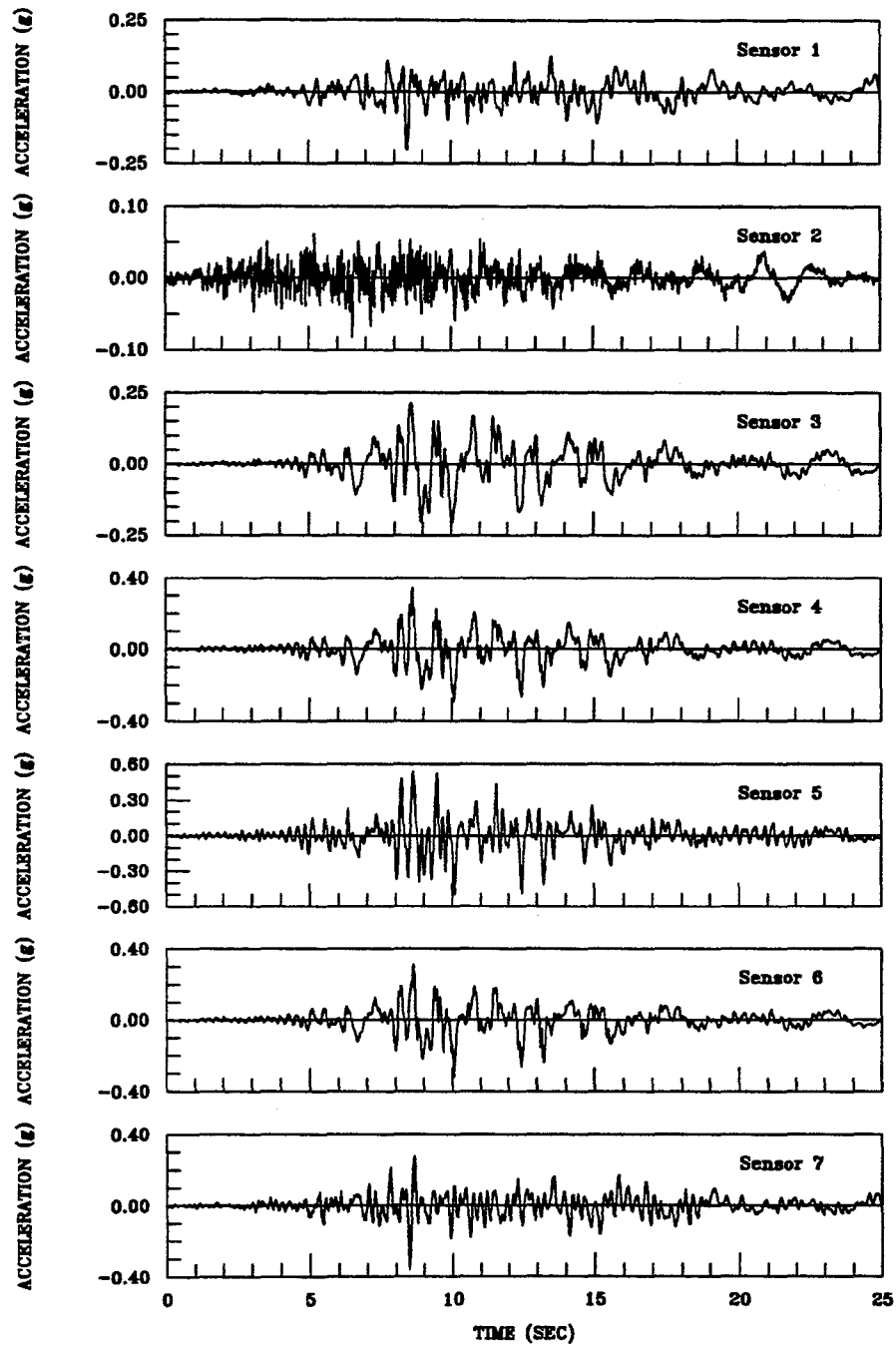
Figure 3.2 Recorded motions at the building during the Loma Prieta Earthquake

21
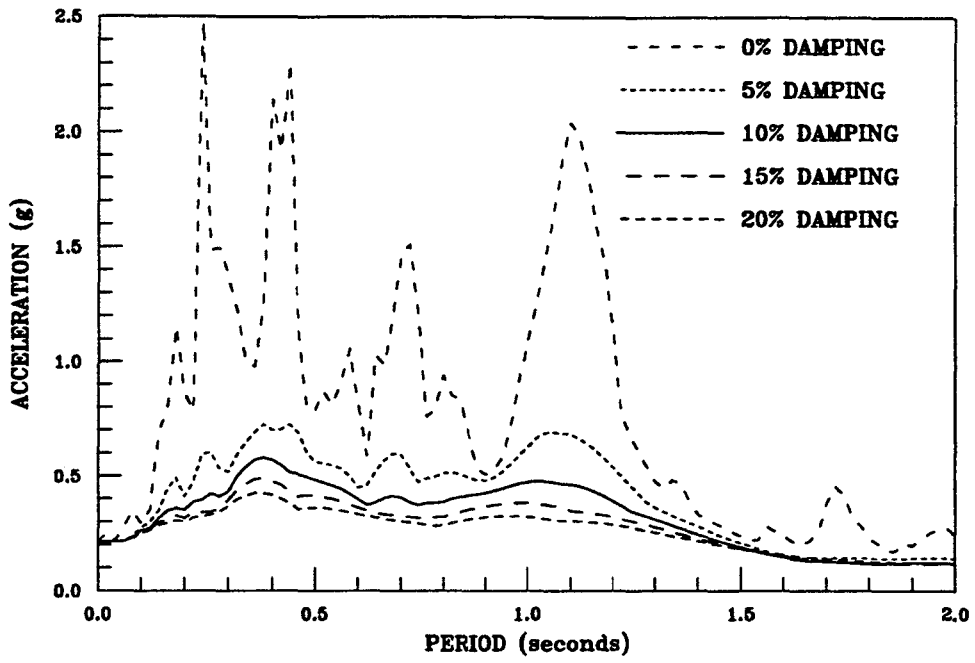
Figure 3.3 Absolute acceleration response spectra for sensor 3
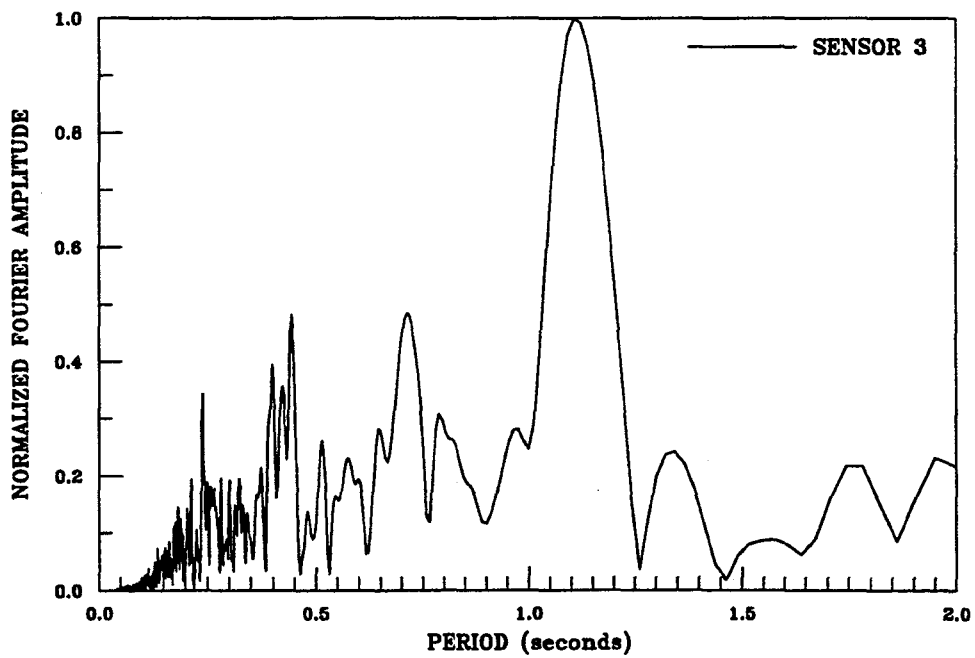
Figure 3.4 Normalized Fourier amplitude spectra for sensor 3

22
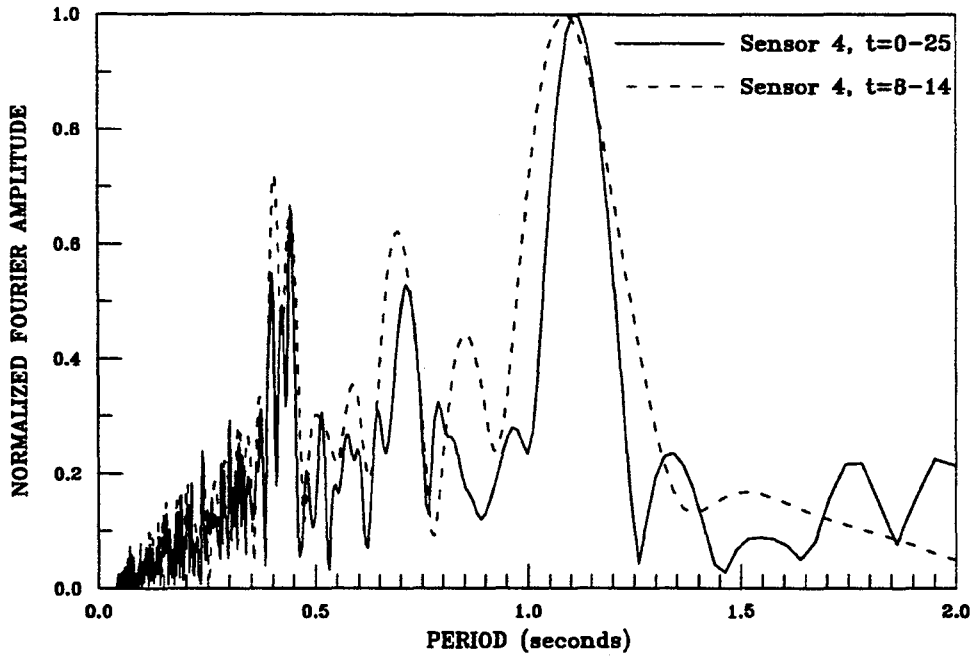
Figure 3.5 Normalized Fourier amplitude spectra for sensor 4
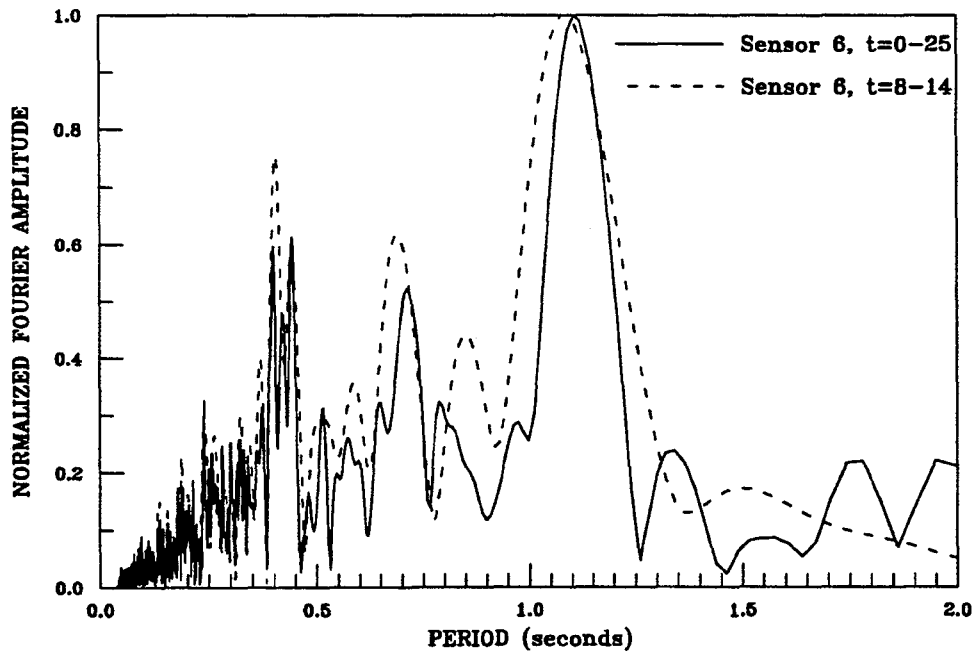
Figure 3.6 Normalized Fourier amplitude spectra for sensor 6

23
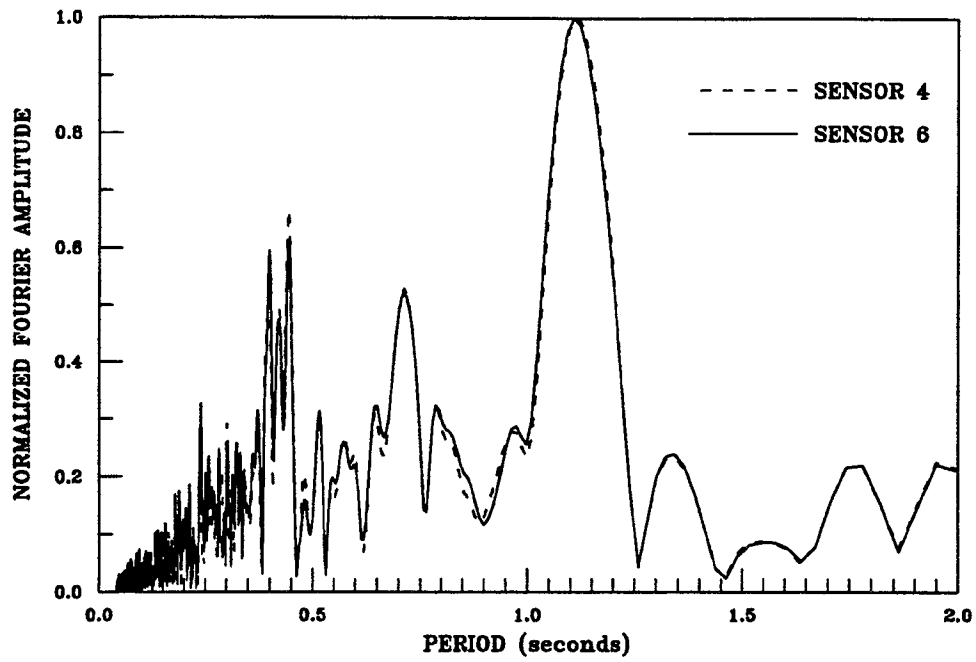
Figure 3.7 Comparison of normalized Fourier amplitude spectra for sensors 4 and 6
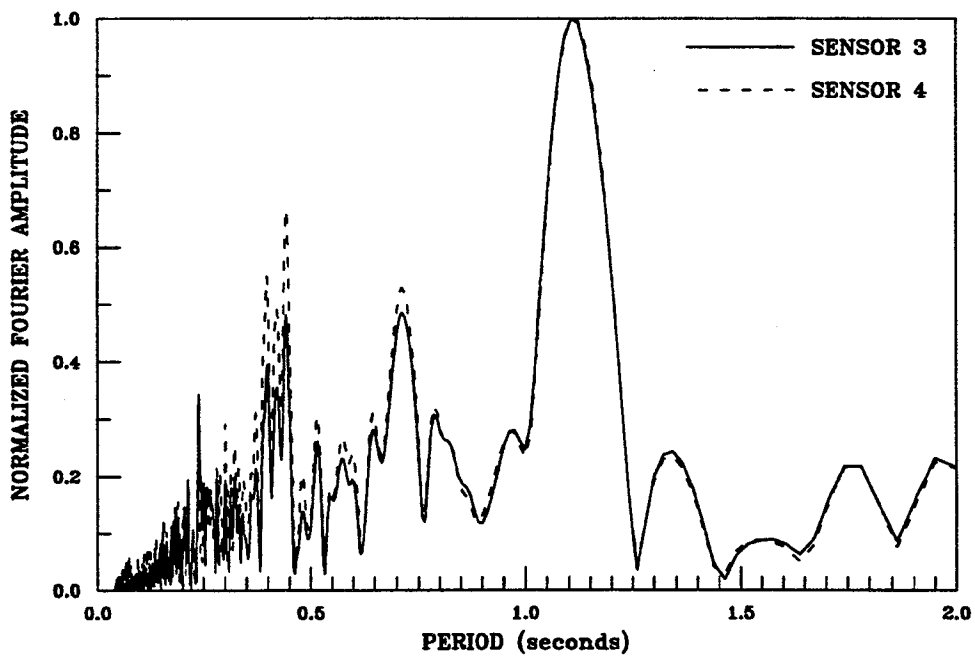
Figure 3.8 Comparison of normalized Fourier amplitude spectra for sensors 3 and 4

24
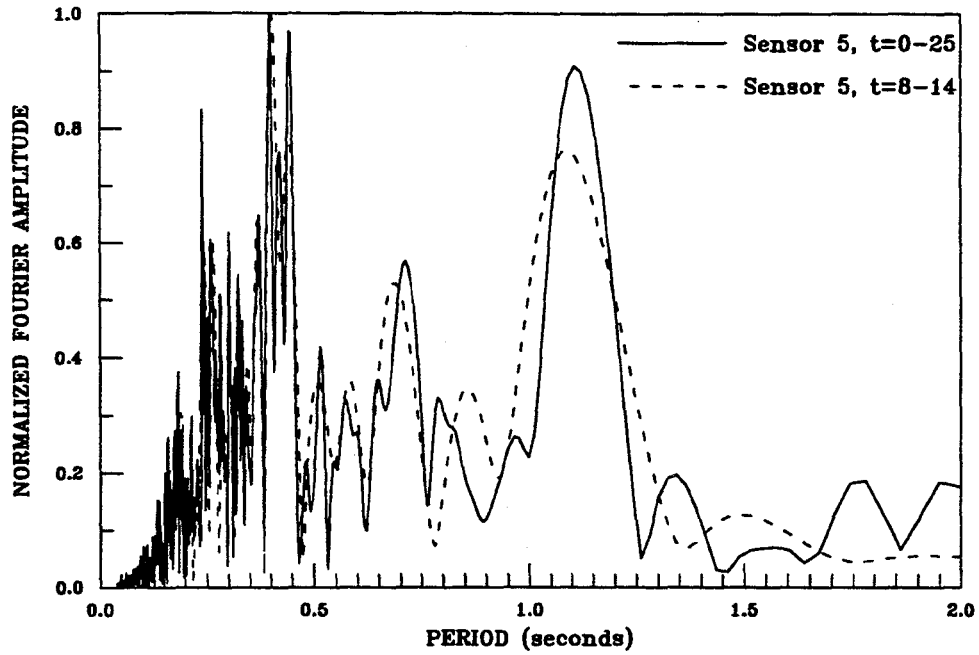
Figure 3.9 Normalized Fourier amplitude spectra for sensor 5
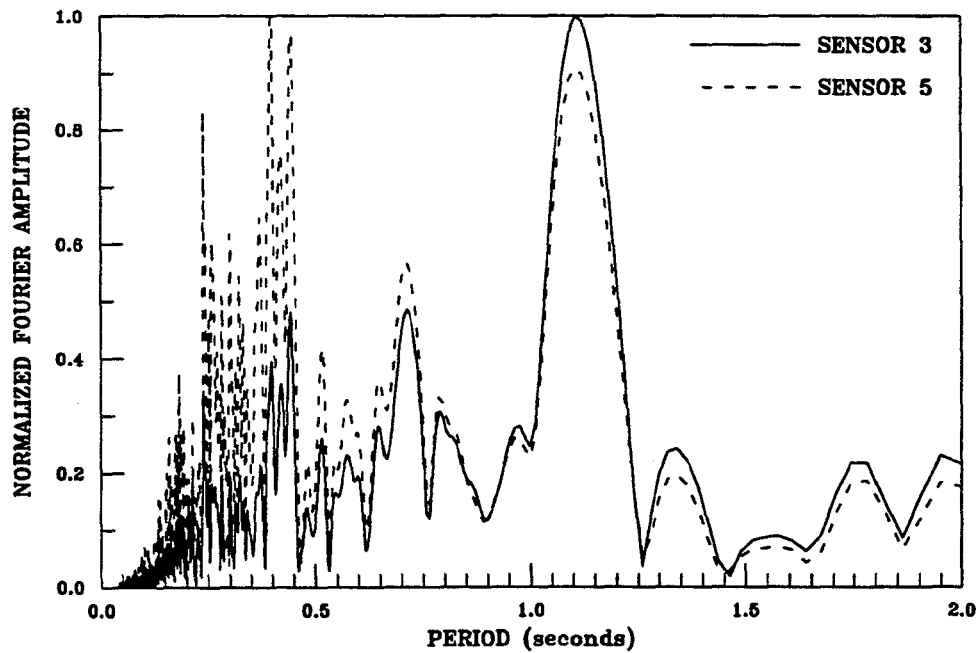
Figure 3.10 Comparison of normalized Fourier amplitude spectra for sensors 3 and 5

25
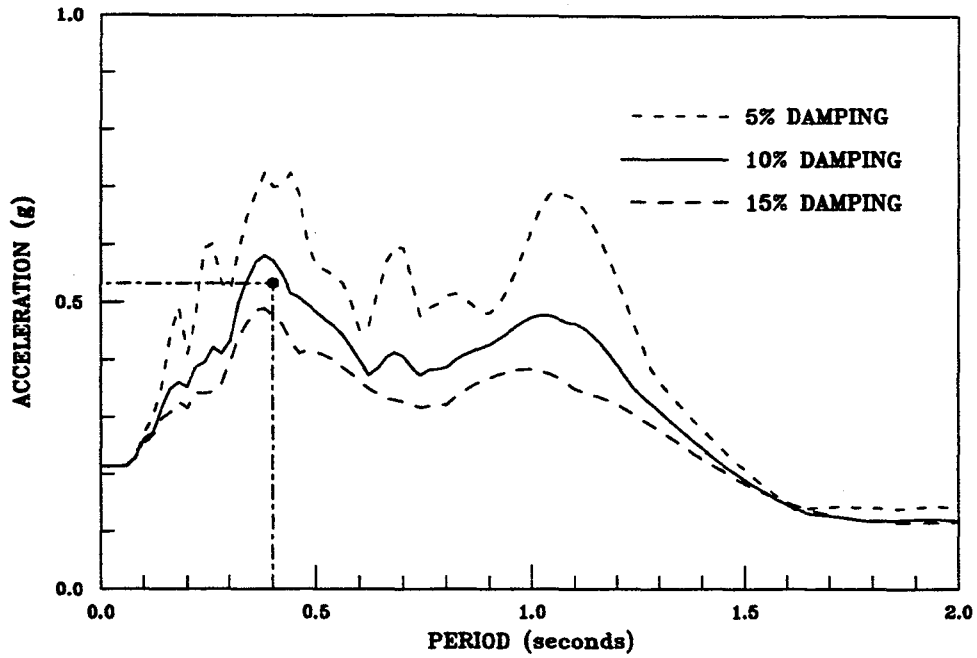
Figure 3.11 Absolute acceleration response spectra vs identified peak response (E–W direction)
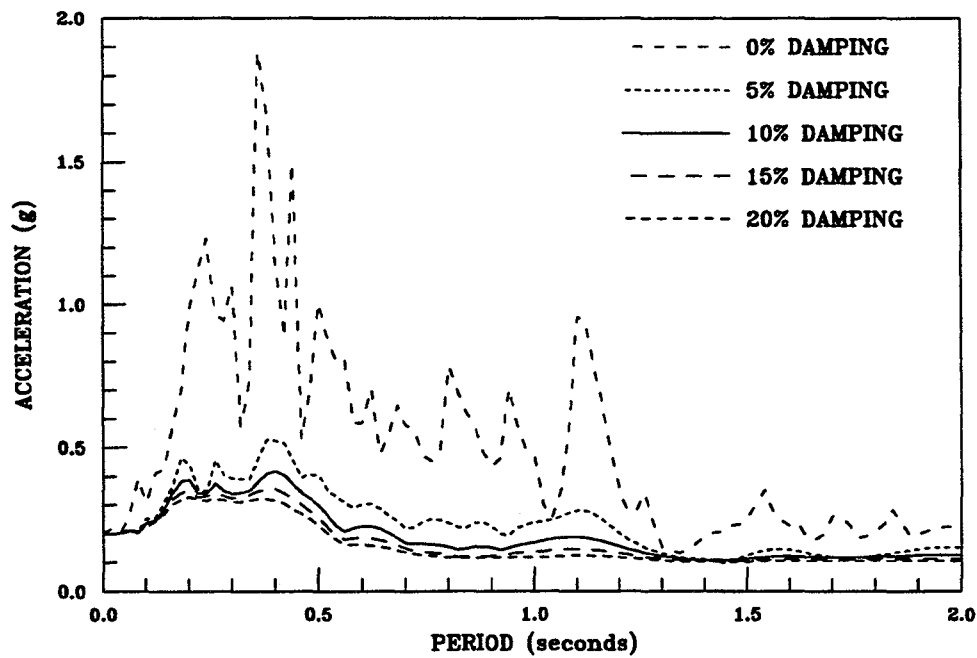
Figure 3.12 Absolute acceleration response spectra for sensor 1
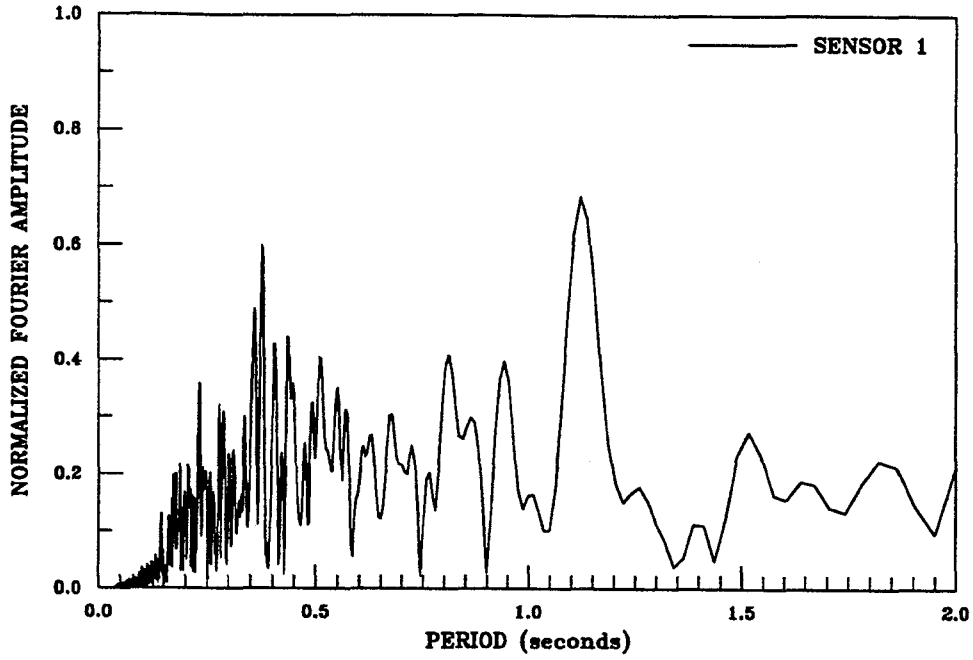
Figure 3.13 Normalized Fourier amplitude spectra for sensor 1
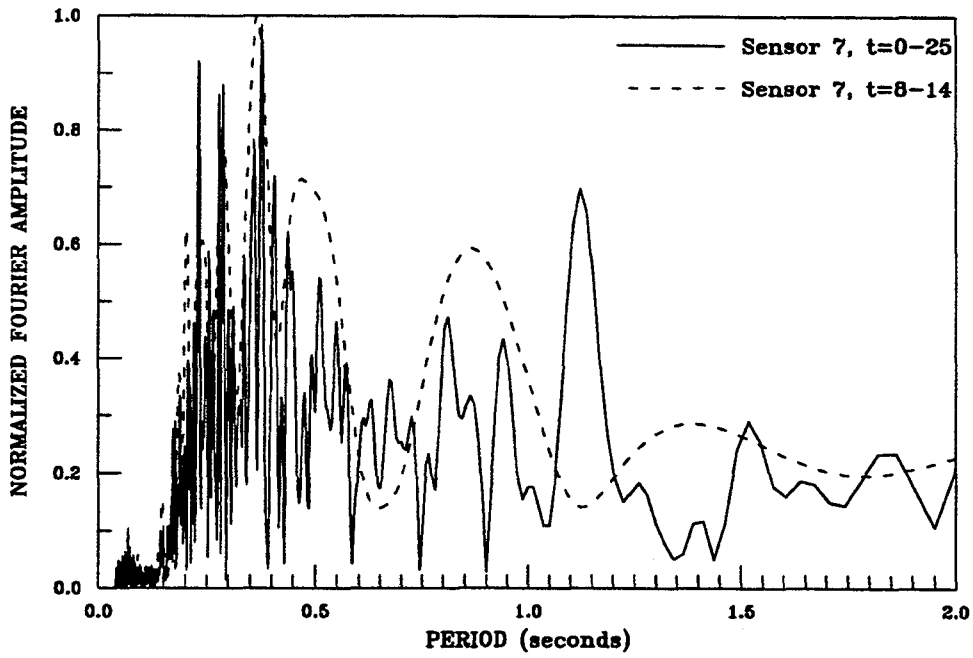
Figure 3.14 Normalized Fourier amplitude spectra for sensor 7

27
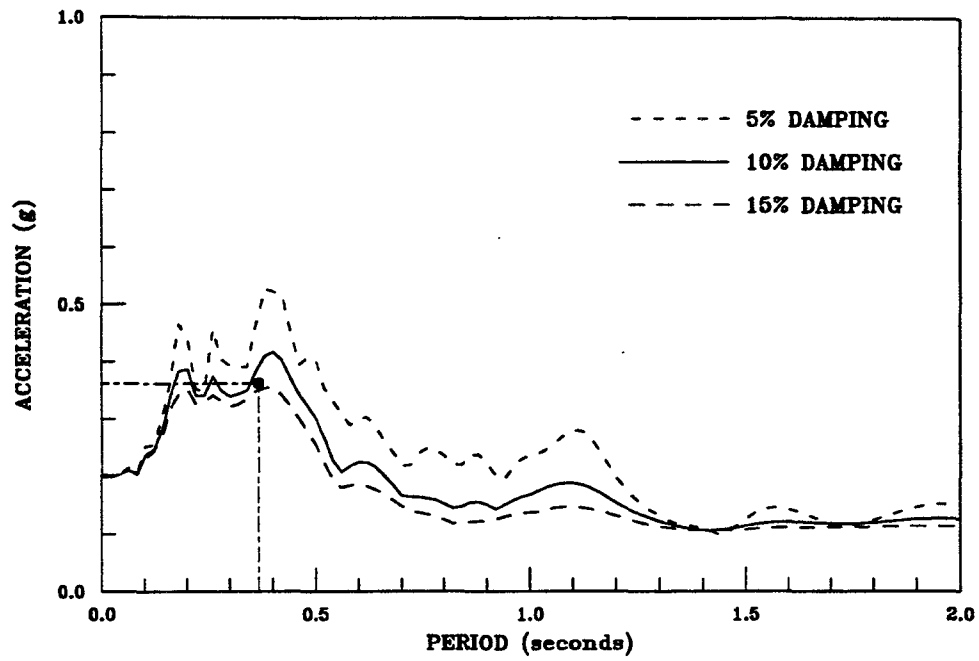
Figure 3.15 Absolute acceleration response spectra vs identified peak response (N–S direction)

CHAPTER 4
PRELIMINARY ESTIMATES OF NOMINAL STRENGTH

It is expedient to use simplified methods of analysis to make crude estimates of seismic response. Such analyses should suggest reasons why a structure may survive or not when subjected to earthquake motions. Nominal shear and overturning moment capacities of the walls can be easily computed by traditional methods. They can be compared against the suspected acting peak base shear and overturning moments obtained from the recorded motions at the structure.

4.1 Maximum Overturning Moments and Base Shears Based Upon the Recorded Motions

Reasonable estimates of the maximum base shears and overturning moments to be resisted by each shear wall in the E−W direction can be obtained from the recorded motions. This is possible because there were recorded motions in both walls (Figs 3.1 and 3.2). The distribution of the accelerations within the wall were assumed to vary linearly, based upon the peak responses recorded at sensors 4 and 3 (Figs. 3.1 and 3.2), for the north wall as illustrated in Fig. 4.1. This can be done because the peak accelerations at the ground and the walls were recorded roughly at the same time (Fig. 3.2). A similar distribution is obtained for the south wall using the peak recorded responses at sensors 6 and 3.

For the N−S direction, an extrapolation must be made because of the lack of recorded motions at the walls in this direction. Taking into account that the ground motions were similar in both directions, and the fact that the diaphragm is less flexible in the N−S direction and experienced lower accelerations (Figs 3.1 and 3.2, Table 3.1), it can be conservatively assumed that the peak acceleration recorded at the south wall in the E−W direction would be similar to those experienced by the walls in the N−S direction.. This assumed distribution is presented in Figure 4.2.

The distribution of the total mass of the building among individual walls can be reasonably assumed to be proportional to the tributary areas of those walls in the direction under consideration for flexible diaphragms. The computed masses for each wall at each level are presented in Table 4.1.

Estimates of the maximum base shears and overturning moments to be resisted by each shear wall in both the E−W and N−S directions obtained according to the assumptions presented above are summarized in Table 4.1. In Table 4.1 and following tables, it should be understood that the north wall and the south wall are composed by the two L−shaped walls. Therefore, the reported forces and capacities are those of these 2−L shaped walls (Figs. 4.1 and 4.2). Overturning moments reported are equal to 2M according to the nomenclature of Figs. 4.1 and 4.2. The magnitude of the maximum average shear stress of 63 psi seems to be within reconcilable ranges.

Table 4.1 Estimates of maximum base shears and overturning moments to be resisted by the shear walls in both the E−W and N−S directions							
Wall	Mass ($lb-sec^2/in$)		Acceleration (g)		Base Shear	Shear Stress	Overturning Moment
	1st floor	roof	1st floor	roof	(kips)	(psi)	(k−ft)
South (E−W)	1014.5	457.3	0.27	0.32	162.	60.4	2736.
North (E−W)	1014.5	457.3	0.28	0.34	170.	63.2	2867.
South (N−S)	1014.5	457.3	0.27	0.32	162.	60.4	2736.
North (N−S)	1014.5	457.3	0.27	0.32	162.	60.4	2736.

4.2 Nominal Shear Strength vs Maximum Base Shear

Estimates of the nominal shear strength of the north and south were made according to the information provided from blueprints which is presented in Chapter 2. The typical reinforcement of a single L–shaped wall is presented in Fig. 2.3. According to Fig. 2.3, the shear reinforcement ratio, ρ_h, is 0.0014. The yield stress of the reinforcement steel, f_y, was taken as 40 ksi (Grade 40 steel). The compressive strength of the grouted masonry, f'_m, was assumed as 1500 psi, corresponding to a lower bound of the strength for a MW brick masonry ($f'_b \geq 2500$ psi, Ref. 29) with type S mortar.

The nominal shear strength of the reinforced grouted brick wall was computed according to the provisions of Chapter 24 of the 1988 UBC code (Refs. 16 and 36). According to Section 2412(d) 6 of the 1988 UBC code, the nominal shear strength of a masonry wall can be computed with Equations 12–13 to 12–15 of Chapter 24 of the code :

$$V_n = V_m + V_s \qquad \qquad \text{... 4.1)}$$

$$V_m = C_d A_{mv} \sqrt{f'_m)} \qquad \qquad \text{... 4.2)}$$

$$V_s = A_{mv}\rho_n f_y \qquad \qquad \text{... 4.3)}$$

where :

V_n = nominal shear strength

V_m = nominal shear strength provided by the masonry

V_s = nominal shear strength provided by the shear reinforcement

C_d = masonry shear strength coefficient as obtained from Table No. 24–L. of the code

A_{mv} = net area of masonry section bounded by wall thickness and length of section in the direction of the shear force considered, square inches

f'_m = specified compressive strength of masonry at the age of 28 days, psi.

f'_y = specified yield strength of the reinforcement, psi

31

ϱ_n = ratio of distributed shear reinforcement on a plane perpendicular to plane of A_{mv}

The nominal shear strength of the walls in both the E−W and the N−S directions computed according to Equations 4.1 to 4.3 are presented in Table 4.2, where they are compared with the maximum base shears obtained in Section 4.1. Both the south and the north wall have enough nominal shear strength to resist the maximum acting base shear in both the E−W and the N−S direction. The walls have more shear capacity in the N−S direction because the flange of the L section is larger in the N−S direction (Fig. 2.3). The contribution of the rectangular walls was neglected in both directions.

Table 4.2 Nominal shear strength vs maximum acting base shear (ksi)				
Wall	Nominal shear strength		Maximum base shear	
	E−W	N−S	E−W	N−S
South	274.	353.	162.	162.
North	274.	353.	170.	162.

4.3 Nominal Moment Capacity vs Maximum Overturning Moment

Estimates of the nominal moment capacity of the north and south were made according to the information provided from blueprints which is presented in Chapter 2. The typical reinforcement of a single L−shaped wall is presented in Fig. 2.3. The vertical reinforcement ratio, ϱ_v, is 0.0020 (Fig. 2.3). The yield stress of the reinforcement steel, f_y, was taken as 40 ksi (Grade 40 steel). Young's modulus of the steel reinforcement was taken as 29,000 ksi. The compressive strength of the grouted masonry, f'_m, was assumed as 1500 psi. Young's modulus of the masonry was taken as $750 f'_m$, according to 1988 UBC code (Refs. 16 and 36).

The nominal moment capacity of the reinforced grouted brick walls was computed according to the provisions of Chapter 24 of the 1988 UBC code (Refs. 16 and 36). Whitney's rectangular stress distribution was assumed. Ultimate strain of the masonry under compression, ε_m, was 0.003. Yield strain of the reinforcement steel, ε_y, was 0.0014. Nominal moment capacities and its associated curvature were obtained for the L flanged walls considering the lever arm of each reinforcement bar in tension according to the assumptions outlined above and geometry presented in Fig. 2.3. The moment capacities were computed considering 2 cases : a) absence of axial load; and, b) a nominal axial load corresponding to the dead load carried by each flanged wall (P=102.3 kips).

The nominal moment capacity of both the south and the north wall is the sum of the moment capacity of the two L−shaped walls in the E−W direction. For the E−W direction, the moment capacity is the sum of the capacities of the L−shaped walls considering that the flange of one L−shaped wall is under compression whereas in the other wall, the flange in is tension, as it can be observed in Fig. 4.1. The computed moment capacities and associated curvatures in the E−W direction are presented in Table 4.3, where they are compared with the maximum acting overturning moments obtained in Section 4.1.

Table 4.3 Nominal moment capacities vs maximum overturning moments (E−W)					
Wall	Nominal Moment (k−ft)		Nominal Curvature (rad/in)		Overturning Moment (k−ft)
	P =0	P=P_{dl}	P =0	P = P_{dl}	
South	1995.	2403.	0.00020	0.00013	2737.
North	1995.	2403.	0.00020	0.00013	2867.

The nominal moment capacity considering the axial dead load is 84% the estimated maximum overturning moment. This suggest that the walls may have yielded in this direction when subjected to the peak accelerations. A larger moment capacity could have been developed if the grade 40 reinforcement steel would have had a larger yielding capacity than the assumed

40 ksi. This could be possible due to the manufacturing process, because many Grade 40 bars in the market are Grade 60 bars where quality control was not optimum. Assuming an effective yielding stress of the bars of 50 ksi, the nominal moment capacity including the axial dead load would be equal to the maximum overturning moment.

For the N−S direction, the moment capacity of the L−shaped wall depends on the direction of loading. The moment capacities were computed when the flange of both L−shaped walls were under compression (Flange "C") and when they were in tension (Flange "T"). The contribution of the facade walls running in the N−S direction (Figs. 2.2 and 4.2) were also considered. The computed moment capacities and associated curvatures are presented in Table 4.4. Curvatures correspond to those of the L−shaped walls. The contribution of the facade walls to the moment capacities were only 9% when the flange of the L−shaped walls were under compression and 4.6% when the flange of the L−shaped walls were under tensile stresses.

Table 4.4 Nominal moment capacities vs maximum overturning moments (N−S)								
Wall	Nominal Moment (k−f)				Overturning Moment (k−ft)	Nominal Curvature (rad/in)			
	Flange "C"		Flange "T"			Flange "C"		Flange "T"	
	$P=0$	$P=P_{dl}$	$P=0$	$P=P_{dl}$		$P=0$	$P=P_{dl}$	$P=0$	$P=P_{dl}$
South	1938.	2337.	3642.	4598.	2737.	0.0015	0.00109	0.0002	0.00014
North	1938.	2337.	3642.	4598.	2737.	0.0015	0.00109	0.0002	0.00014

The nominal moment capacity considering the axial dead load is 85% the estimated maximum overturning moment when the flange of the L−shaped walls are under compression (Flange "C"). This suggest that the walls may have yielded in this direction when subjected to the peak accelerations if the flange was certainly under compression. However, the nominal capacity

of the walls when the flange of the L–shaped walls are under tension (Flange "T") is 168% the estimated maximum overturning moment, then, if the flange was under tension, the walls may have not yield. Therefore, the directivity of loading should have played a key role in the survival of the walls in the N–S direction.

4.4 Provided Reinforcement vs Minimum Reinforcement Provisions

For reinforced masonry shear walls The 1988 UBC code (Refs. 16 and 36) specifies a minimum wall reinforcement that should be provided (Section 2407 h 4B). All walls shall be reinforced with both vertical and horizontal reinforcement. The sum of the areas of horizontal and vertical reinforcement shall be at least 0.002 times the gross cross–sectional area of the wall. The minimum area of reinforcement in either direction shall not be less than 0.0007 the gross cross–sectional area of the wall. That is :

$$\varrho_v + \varrho_h \geq 0.002 \qquad \text{... 4.4)}$$

$$\varrho_v \geq 0.0007 \qquad \text{... 4.5)}$$

$$\varrho_h = 0.0007 \qquad \text{... 4.6)}$$

The provided reinforcement ratios for all walls were ϱ_v = 0.002 (flexural reinforcement), and ϱ_h = 0.0014 (shear reinforcement). Therefore, the provided steel ratios were more than the minimum requirement of the 1988 UBC code. The walls also fulfill the requirements contained in Section 2412(d) 4 of the code. The nominal moments were much more than 3 times the cracking moment (flexural failure mode, Section 2412 d 4B). In the E–W direction, they were 23.5 times higher, in the N–S direction they were 21 times higher. The shear reinforcement ratio was more than half the flexural reinforcement ratio (Section 2412 d 4D). The maximum spacing of the flexural and shear reinforcement of 12 inches did not exceed three times the nominal thickness of the wall (3t = 36 in.) nor 24 inches (Section 2412 d 4E).

The NEHRP provisions (Ref. 21) are similar to those of the 1988 UBC code. However, the minimum reinforcement ratios in either direction shall not be less than 0.0015 the gross

cross—sectional area of the wall, unless the shear walls are constructed using running bond (Section 12.6.2 A). In the latter case, the NEHRP provisions are identical to the 1988 UBC code provisions. Since the walls were constructed using running bond, they fulfill the NEHRP minimum requirements as well. The maximum spacing of the reinforcement allowed by the NEHRP provisions (Section 12.6.2 A) differ from those of the 1988 UBC code, however, they were fulfilled as well. The maximum spacing of the flexural and shear reinforcement of 12 inches did not exceed one—third the height and the length of the wall (h/3 = 44 in., L/3 = 37.3 in.), nor 48 inches. The minimum grout space for structural reinforced grouted masonry of 3.5 inches for high—lift construction (Section 12.7.1) was also fulfilled, as the current grout thickness of the walls is 7 inches (Fig. 2.2).

4.5 Summary

Despite the crude nature of the procedures used to estimate the seismic response of the structure, important issues have come up. The design of the walls satisfy current seismic codes. Provided reinforcement ratios are more than the minimum requirements of current seismic codes. The nominal shear strength of the walls were sufficient to withstand the maximum base shears to which they were subjected. The failure mode of the walls was on flexure. The nominal moment capacity of the walls was tight in the E—W direction and they may have yielded when subjected to the estimated maximum overturning moment. The moment capacity of the walls in the N—S direction was sufficient if the flange of the L—shaped walls were under tension, however, the moment capacity was tight if the flange of the L—shaped walls were under compression.
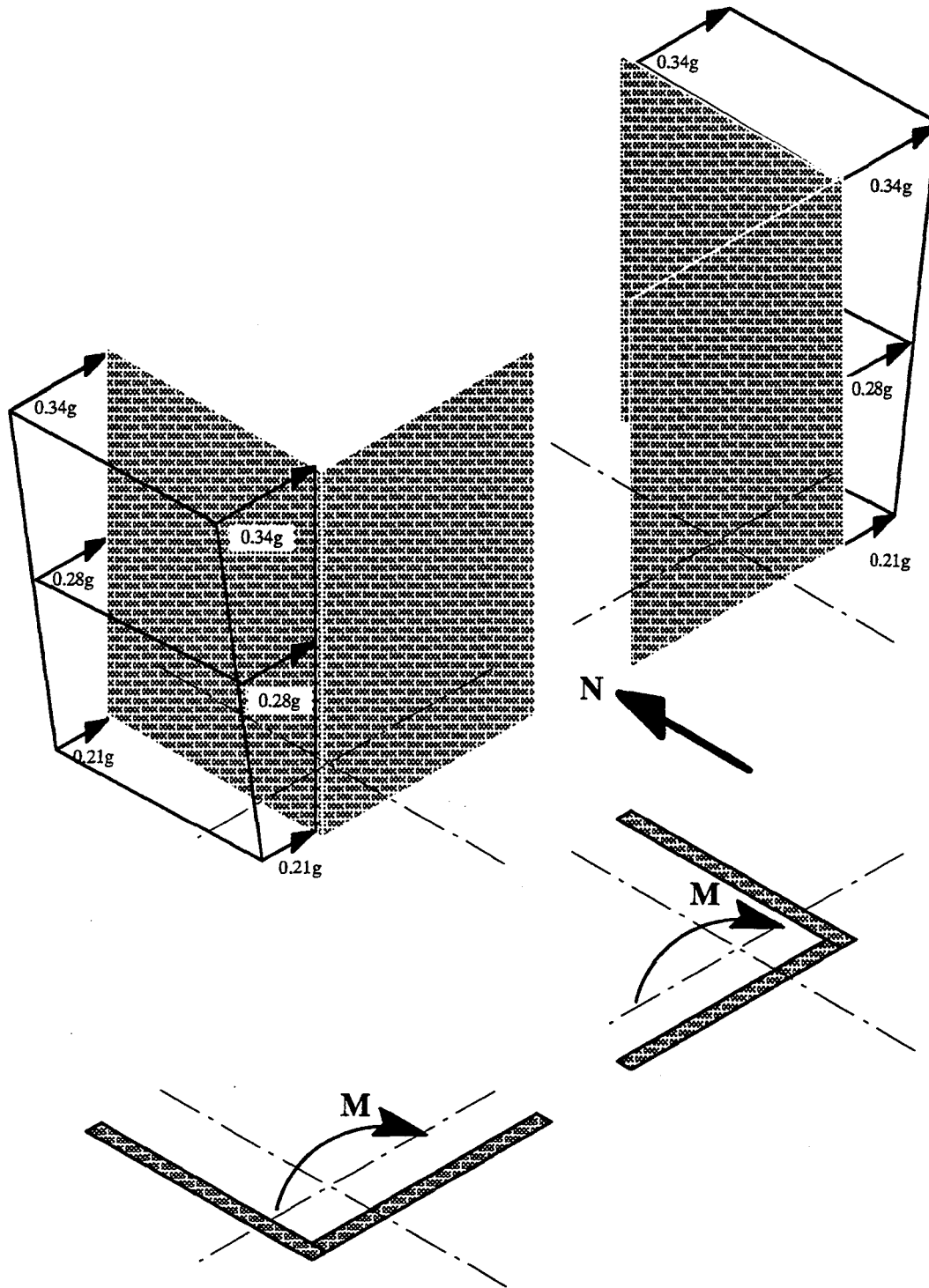
Figure 4.1 Lateral acceleration distribution assumed at the walls in the E−W
direction based upon the recorded peak accelerations at the walls
and the ground. Acting E−W overturning moments.
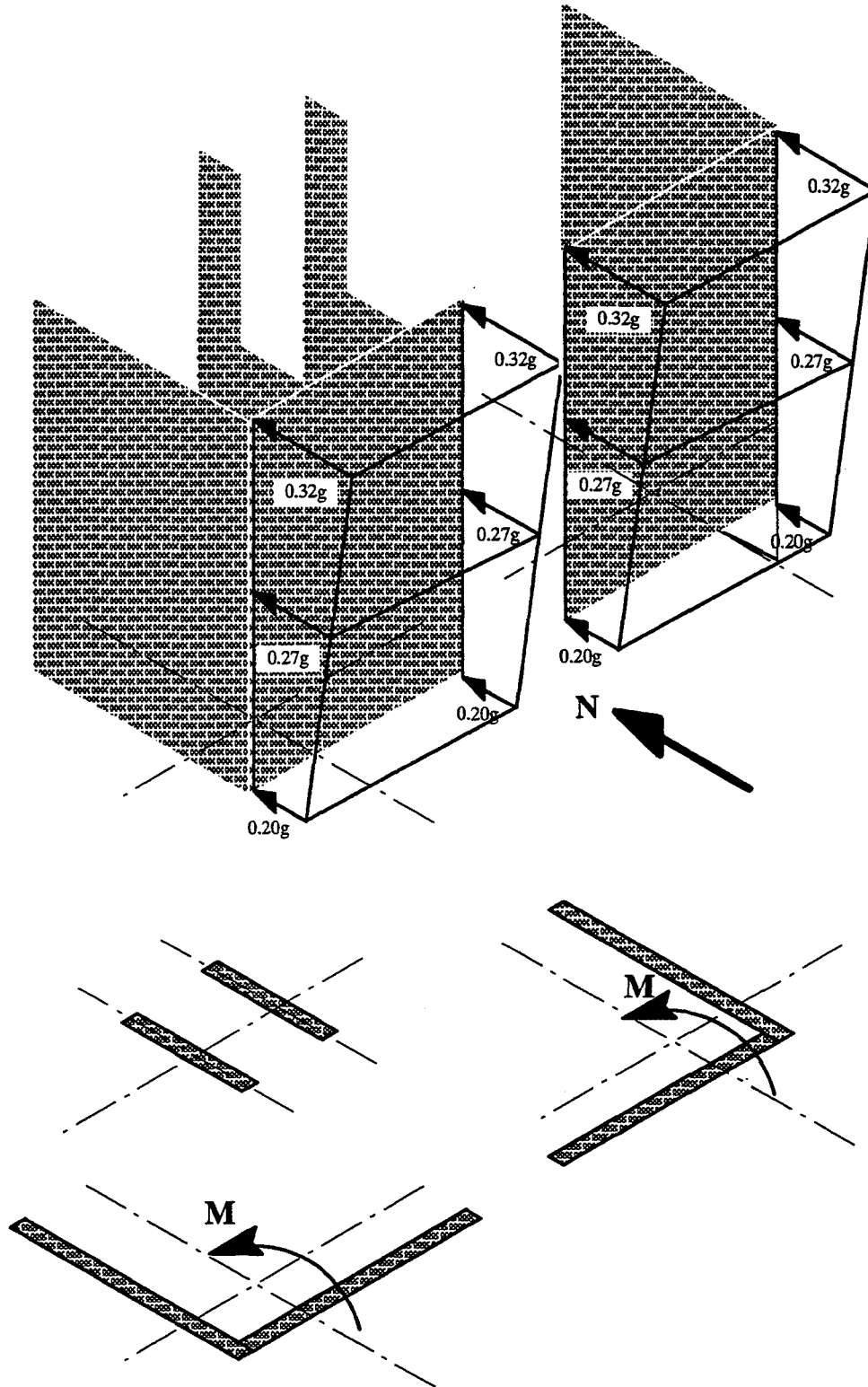
Figure 4.2 Lateral acceleration distribution assumed at the walls in the N–S
direction based upon the recorded peak accelerations at the walls (E–W)
and the ground (N–S). Acting N–S overturning moments.

CHAPTER 5
COMPUTED RESPONSE WITH DISCRETE MDOF DYNAMIC MODELS

Discrete linear−elastic, MDOF dynamic models of the building were made to study the behavior of the structure in both the east−west and the north−south directions. The discrete linear−elastic, MDOF dynamic model is described extensively elsewhere (Refs. 33 and 34).

Several analyses were performed to study the sensitivity of the proposed model to different sets of mechanical properties structure. Each set of values was the result of changes in the mechanical properties of the materials and components of the structure. The analyses allowed to identify the structure as well.

5.1 Discrete Linear−Elastic, MDOF Dynamic Model

The discrete linear−elastic multi−degree−of−freedom (MDOF) dynamic model was developed to study the response of low−rise URM buildings where elastic response may be expected during an earthquake. The method considers both the effects of flexibility of the diaphragms and the rotations of the walls in the overall response of the system.

The discrete MDOF dynamic model can be visualized as an equivalent system of condensed beams (representing the perforated cantilever URM walls) linked by elastic springs (representing the flexible floor systems). Response is measured by the translational degrees of freedom of these elements. Masses are lumped at the dynamic degrees of freedom, as illustrated in Figs. 5.1, 5.2, 5.16 and 5.17.

Flexible diaphragms in the direction of interest are represented by elastic springs. In most cases, support conditions allow the diaphragm to shear, therefore, elastic shear springs are used to represent the diaphragm action (Figs. 5.1 and 5.2). On a few cases, the diaphragms are reduced to a strut due to the support conditions (see the diaphragm support conditions in the N−S direction, Fig 2.1). Elastic axial springs are used to represent the diaphragm action in such cases (Figs. 5.16 and 5.17).

39

Walls resisting lateral forces in the direction under study are represented by equivalent condensed beams with translational degrees of freedom in that direction, as shown in Figs. 5.1, 5.2, 5.16 and 5.17. The equivalent condensed beam elements for solid walls can be easily obtained by direct static condensation of the stiffness matrix of the walls idealized as equivalent wide columns.

Soil−structure interaction effects can be easily incorporated in the analysis by computing the average lateral diminished stiffness matrix, $\hat{K}$, from the average lateral stiffness matrix $\overline{K}$, and the foundation flexibility represented by two generalized springs, as presented by Hjelmstad and Foutch (Ref. 15). A generalized spring with stiffness k_θ is introduced to represent the resistance of the soil−foundation system to rocking, while the other generalized spring with stiffness k_δ represents the resistance of the soil−foundation system to direct lateral displacement, as shown in Figs. 5.1, 5.2, 5.16 and 5.17

The equation of motion for the system represented in those figures is :

$$M\ddot{x} + C\dot{x} + \hat{K}x = -M\underline{1}\ddot{x}_g \qquad \text{... 5..1)}$$

where the average lateral diminished stiffness matrix, $\hat{K}$, is given by (Ref. 15) :

$$\hat{K} = I - \left[\frac{k_\theta(1 + \beta_\theta)\overline{K}\underline{1}\underline{1}^T - (\underline{1}^T\overline{K}\underline{H})[\overline{K}\underline{1}\underline{H}^T + \overline{K}\underline{H}\underline{1}^T] + k_\delta(1 + \beta_\delta)\overline{K}\underline{H}\underline{H}^T}{k_\theta k_\delta[1 + \beta_\theta + \beta_\delta + (1 - \gamma)\beta_\theta\beta_\delta]} \right] \overline{K} \qquad \text{... 5.2)}$$

where :

$\overline{K}$ = average lateral stiffness matrix of the fixed end structure.

$\hat{K}$ = average lateral diminished stiffness matrix of the soil−structure system.

$\underline{1} = \{1,1,...,1\}$ is a vector of ones.

$\underline{H} = \{h_1,...,h_n\}$ is a vector containing the heights of the masses above the

base.

k_θ = generalized spring stiffness against rotation.

k_δ = generalized spring stiffness against direct lateral displacement.

40

β_θ and β_δ and γ are non−dimensional parameters defined as :

$$\beta_\theta = \frac{\underline{H}^T \overline{K} \underline{H}}{k_\theta} \qquad \qquad ...5.3)$$

$$\beta_\delta = \frac{\underline{1}^T \overline{K} \underline{1}}{k_\delta} \qquad \qquad ...5.4)$$

$$\gamma = \frac{(\underline{1}^T \overline{K} \underline{H})^2}{(\underline{1}^T \overline{K} \underline{1})(\underline{H}^T \overline{K} \underline{H})} \qquad \qquad ...5.5)$$

The values of the generalized spring constants k_θ and k_δ depend on the type of soil where the foundation is built on, as well as the type, depth and geometry of the foundation itself. The parameters needed to determine the generalized spring constants can be obtained from the data of in−situ soil tests or by using the recommendations given by a code, such as the ATC 3−06 code (Ref. 3).

5.2 East−West Direction Modeling

A 6 DOF discrete, linear−elastic dynamic model considering soil−structure interaction effects was used to study the response of the two−story office building at Palo Alto in the E−W direction, as shown in Figs. 5.1 and 5.2. The masses off the building were lumped and distributed according to a tributary area criteria , and their values are presented in Table 5.1.

Table 5.1 Lumped masses for the E−W discrete 6 DOF dynamic model (Figs. 5.1 and 5.2)	
DOF	Mass (lb−sec^2/in)
1	1014.50
2	457.33
3	1017.52
4	468.90
5	1014.50
6	457.33

The average lateral stiffness of each wall was obtained through static condensation of the global stiffness matrix, as outlined in Section 5.1. An average Young's modulus of 1125 ksi $(750 f'_m)$ was considered according to 1988 UBC code provisions. The stiffness constant of the springs representing the flexible diaphragms were estimated assuming typical values for the shear modulus of plywood (90 ksi) and its Young's modulus (1,700 ksi). (Refs. 5, 14, 35, 37).

The equivalent effective thicknesses for plywood diaphragms suggested by the American Plywood Association (APA, Refs. 14, 35) were also considered. For the roof diaphragm, the secondary beams running in the E−W direction were considered to contribute to the shear stiffness of the diaphragm. The secondary beams contributed to 66% of the total stiffness of the diaphragms. Truss joists and sheathing were neglected in the calculations at the roof level. For the second floor diaphragm, the shear stiffness was computed as the sum of the stiffness of the 1.5" thick light−weight concrete and the 3/4" plywood. Secondary beams, truss joists and sheathing were neglected in the calculations at the second floor. The stiffness of the second floor diaphragm is clearly controlled by the light−weigh concrete. The 3/4" thick plywood contributed only to the 5.4% of the total stiffness of the diaphragm of the second floor. The second floor is considerably stiffer than the roof (8.7 times stiffer). The preliminary estimates of the stiffnesses of the springs which are identified in Figs 5.1 and 5.2 are presented in Table 5.2.

Table 5.2 Preliminary spring constants for the 6 DOF discrete model of Figs. 5.1 and 5.2		
SPRING ID	Diaphragm's Thickness (in)	Stiffness (k/in)
K_{D1}	1.5 (c) + 0.75 (plwd)	433.8
K_{D2}	0.50 (plwd)	50.0

Soil−structure interaction effects were incorporated according to Section 5.1. The values of the generalized spring constants k_θ and k_δ were calculated based upon the procedure outlined

by the Applied Technical Council for footing foundations (ATC 3−06, Ref. 3). According to the ATC procedure, k_θ and k_δ can be computed with its equations C6−18 to C6−22 for footing foundations. These equations have been rewritten here in terms of our notation :

$$k_\delta = \Sigma k_{\delta i} \qquad \qquad \text{... 5.6)}$$

$$k_\theta = \Sigma k_{xi} y_i^2 + \Sigma k_{\theta i} \qquad \qquad \text{... 5.7)}$$

$$k_{\delta i} = \frac{8 G_i \, r_{ai}}{2 - v}\left[1 + \frac{2}{3}\frac{d_i}{r_{ai}}\right] \qquad \qquad \text{... 5.8)}$$

$$k_{xi} = \frac{4 G_i \, r_{ai}}{1 - v}\left[1 + 0.4\frac{d_i}{r_{ai}}\right] \qquad \qquad \text{... 5.9)}$$

$$k_{\theta i} = \frac{8 G_i \, r_{ai}^3}{2(1 - v)}\left[1 + 2\frac{d_i}{r_{mi}}\right] \qquad \qquad \text{... 5.10)}$$

$$r_{ai} = \sqrt{\frac{A_{oi}}{\pi}} \qquad \qquad \text{... 5.11)}$$

$$r_{ai} = \sqrt[4]{\frac{4 I_{oi}}{\pi}} \qquad \qquad \text{... 5.12)}$$

where :

k_δ = generalized horizontal stiffness of the foundation.

k_θ = generalized rocking stiffness of the foundation.

$k_{\delta i}$ = horizontal stiffness of the ith footing.

$k_{\theta i}$ = rocking stiffness of the ith footing.

k_{xi} = vertical stiffness of the ith footing.

y_i = normal distance from the centroid of the ith footing to the rocking axis of the foundation.

G_i = shear modulus of the soil beneath the ith footing at large strain levels.

d_i = depth of the effective embedment for the ith footing.

r_{ai} = radius of a circular footing that has the area of the ith footing, A_{oi}.

43

r_{mi} = radius of a circular footing, the moment of inertia of which about a horizontal centroidal axis is equal to that of the ith footing, I_{oi}, in the direction in which the response is being evaluated.

In the computation of the generalized spring stiffnesses k_δ and k_θ, d_i was taken as 39 inches (Fig. 2.4 b). The average shear modulus of the soil beneath the footings at large strain levels, G_i, was computed based upon the ATC 3−06 recommendations given by :

$$G_i = k_G \frac{\gamma}{g}\left(\frac{v_s}{k_v}\right)^2 \qquad\qquad \text{... 5.13)}$$

where :

G_i = the average shear modulus for the soils beneath the foundation at large strain levels.

v_s = the average shear wave velocity for the soils beneath the foundation at large strain levels.

k_G = value of G/G_0 according to Table 6−A of the ATC 3−06 provisions.

k_v = value of v_s/v_{s0} according to Table 6−A of the ATC 3−06 provisions.

G_0 = the average shear modulus for the soils beneath the foundation at small strain levels.

v_{s0} = the average shear wave velocity for the soils beneath the foundation at small strain levels.

γ = the average unit weight of the soils.

g = gravity constant

The soil was identified as a sandy clay fill in blueprints . Therefore, the values of γ, v and v_s were obtained from the information provided for engineered fill soils (bearing dead load plus live load capacity of 2000 psf) by Lew, Chieruzzi and Campbell (Ref. 19). The average unit weight for this type of soils, γ, varies from 110 to 125 lb/ft^3, the average Poisson ratio is v=0.35, and the values of v_s range from 560 ft/sec to 940 ft/sec. The values of k_G and k_v were

determined from Table 6−A of ATC 3−06 code (Ref. 3), interpolating linearly for the peak ground acceleration of 0.21g recorded in the E−W direction. The average shear modulus for the soil beneath the foundation at large strain levels (G_i, computed from Equation 5.13) was determined as 13.05 ksi using mean values (γ= 125 lb/ft^3, v = 0.35, and v_s = 710 ft/sec). Therefore, the initial estimation of the generalized spring constants k_θ and k_δ computed from Equations 5.5 to 5.12 based upon these assumptions are k_δ = 10,655 k/in, and k_θ = 6.827x10^9 k−in/rad.

The amount of the effective damping factor for the structure−foundation system, $\tilde{\xi}$, was determined according to ATC 3−06 Equation C6−29, which in our notation is written as:

$$\tilde{\xi} = \xi_0 + \frac{\xi_i}{(\tilde{T}/T)} \qquad \text{... 5.14)}$$

where :

$\tilde{\xi}$ = effective damping factor for the structure−foundation system.

ξ_i = structural damping factor.

ξ_0 = foundation damping factor as specified in Fig. 6−1 of ATC 3−06.

$\tilde{T}$ = effective period of the structure−foundation system.

T = period of the structure fixed at the base.

The foundation damping factor ξ_0, incorporates the effects of energy dissipation in the soil due to the radiation of waves away from the foundation and the hysteretic or inelastic action in the soil. The structural damping factor ξ_i was assumed as 0.06, according to reported values obtained experimentally by Paulson and Abrams for grouted reinforced masonry blocks subjected to moderate shaking (Ref. 27).

Time−step integration analyses of the 6 DOF discrete model were carried out by means of a special purpose program which integrates the equation of motion using the implicit direct methods algorithm (Refs. 12 and 13). Newmark−β method with γ = 0.5, β = 0.25, and a

time−step integration of 0.001 seconds was used throughout the analyses. Frequency analyses were simultaneously done by solving the eigenvalue problem with a special purpose program that uses Lanczos algorithm.

5.2.1 Considerations for Sensitivity Analyses in the E−W Direction

Several analyses were carried out to identify the response of the structure and to study the sensitivity of the modeling to variations in the stiffness of walls, diaphragms, and soil. The stiffnesses of the wood was varied up to a 30% increment (k_d, $1.15k_d$, $1.25k_d$, and $1.30k_d$), that is, no increment was considered on the light−weight concrete of the second floor. Young's modulus of the masonry walls was varied within a 50% (0.75E, E, and 1.25E).

The nominal stiffness of the generalized foundation springs was varied to identify the frequency ranges of responses of the firehouse. Thus, the average shear modulus for the soil beneath the foundation ($G_i = 13.05$ ksi) was varied within the range obtained from the the studies of Lew and Campbell ($0.57G_i$ to $1.82G_i$) considering the depth of the effective embedment of the footings. This is the case illustrated in Figs. 5.5 to 5.7. Damping ratios varied according to the amount of soil−structure interaction in each given analyses as deducted from Equation 6.14. Modal damping was used throughout the study.

The fixed−based condition was studied to assess the influence of the soil−structure interaction effects. The rigid diaphragm condition was also studied to compare it against the flexible diaphragm condition. The results of the sensitivity analyses in the E−W direction are presented and discussed in the following sections.

5.2.2 Sensitivity with Respect to Soil−Structure Interaction Considerations

Soil−structure interaction effects had a considerable impact in the response of the structure, especially in the amplitude of the response. This can be illustrated by comparing the response of the fixed−base system with respect to the response of systems where the flexibility of the soil−foundation system is considered. The mode shapes for the fixed−base consideration

computed from the discrete model based upon the original data given in Section 5.2 are shown in Fig. 5.3.

The mode shapes of Fig. 5.3 describe in−plane motions and are presented schematically in the equivalent system composed by condensed beams and elastic springs (Fig. 5.3). The natural period of this model was 0.43 seconds, approximately 8.5% larger than the identified natural period of the building in the E−W direction of 0.40 seconds. The first three mode shapes suggest that the diaphragm action controls the response of the structure. The first two are identical because of the symmetry in mass and stiffness of the model. The amplitude of the movement of the walls under the lower modes for the fixed−base condition is very small compared to the amplitudes observed at the diaphragms (Fig. 5.3).

The amplitude of the peak responses was determined by performing a time−step analysis of this fixed−base system considering 6% viscous damping for the first mode. The damping was increased for higher modes through a modal damping assumption. The computed peak accelerations were 0.06g at the walls at the roof level, and 0.44g at the center of the diaphragm at the same level. The recorded peak accelerations were 0.34g and 0.53g for the north wall and the diaphragm at the roof level respectively (Fig. 3.1, Table 3.1).

The maximum computed relative displacements between the roof and the base were 0.05" for the walls and 0.89" for the center of the south diaphragm. The maximum relative displacements computed from the recorded motions were 0.41" and 0.80" for the walls and the center of the diaphragm at the roof level with respect to the base respectively. The fixed−base model seems to represent the response of the diaphragm well, however, the response of the walls is considerably underestimated.

Soil−structure interaction effects were introduced to improve the model. The computed mode shapes for the model which includes soil−structure interaction are presented in Fig. 5.4. Mode shapes of Fig. 5.4 describe the in−plane motions, and they are presented schematically in the equivalent system composed by condensed beams and elastic springs

47

(Figs. 5.2 and 5.4). The average shear modulus for the soil beneath the foundation was considered.

The first three mode shapes of Fig. 5.4 are plenty of diaphragm action, however, it is clear that the flexible support induces higher responses in the walls. This is corroborated with the time−step analysis, where an associated 6.1% effective viscous damping for the first mode of the soil−structure system was determined from Equation 5.14. The computed peak accelerations at the roof level for the walls and the center of the diaphragm were 0.16g and 0.52g respectively. The maximum computed relative displacements between the roof and the base were 0.14" for the walls and 1.04" for the diaphragm.

The computed response with the discrete model considering soil−structure interaction effects is, in general, much improved with respect to the computed response with the fixed−base discrete model. This is especially true for the response of the walls, as it can be deducted from the values of Table 5.3. These values show that peak responses of these two conditions are improved when compared to the peak recorded responses. Therefore, it is clear from Table 5.3 that the inclusion of soil−structure interaction becomes very important in the discrete modeling of the building (identified as "Flexible Base Model"). Soil−structure interaction has been important to improve the overall amplitude of the recorded response.

Table 5.3 Recorded vs computed peak responses at the roof level of the original discrete MDOF dynamic modeling of the office building at Palo Alto (E−W).						
Parameter	North and South Walls			Center of the Diaphragm		
	Re-corded	Fixed−Base Model	Flexible Base Model	Re-corded	Fixed−Base Model	Flexible Base Model
Accel.	0.34g	0.06g	0.16g	0.53g	0.44g	0.52g
Drift	0.41"	0.08"	0.14"	0.80"	0.89"	1.04"

On the other hand, these original set of analyses suggest that the initial estimations of structural response were within the range of observed dynamic response in the firehouse. Several studies have been carried out to identify the recorded response of the structure and the sensitivity of this discrete modeling to variations of the parameters involved in the modeling (Section 5.2.1). These parameters interact among themselves, therefore, it is difficult to isolate the effect of a single parameter.

The variation of the natural period of the model structure with respect to variations of the stiffness of the foundation is presented in Figs. 5.5 and 5.6. In these figures, the period is expressed as a function of the assumed average shear modulus of the soil beneath the foundation (G_i).

In the curves shown in Fig. 5.5, Young's modulus of the grouted brick walls is kept constant and it is equal to the estimated average value ("E", E = 1125 ksi). Each curve shows the influence of the variations of the average shear modulus of the soil for a given assumed stiffness of the plywood of the diaphragms. Each curve is identified with a label which is expressed as a function of the nominal stiffnesses of the plywood. For example, label "$1.15k_d$" marks the curve of a discrete model where the stiffnesses of the plywood and secondary wood beams were increased by 15%. The curve connecting full circles corresponds to the "original" discrete model which is defined by the initial considerations presented in Section 5.2. The vertical dashed line represents the natural period of 0.40 seconds of the building in the east−west direction. The horizontal dashed lines define the range of variation of G_i for engineered fill soils, according to the information provided by the studies of Lew, Chieruzzi and Campbell (Ref. 19).

The computed natural period increases relatively fast for each curve of Fig. 5.5 in the narrow range considered when more soil−structure interaction is present (i.e., smaller assumed G_i), that is what should have been expected. The curves show that, as the system approaches the fixed−base condition, variations within a 30% of the stiffness of the diaphragms are

49

important in the determination of the period of the model structure. On the contrary, as the soil−structure interaction is more pronounced, the influence of the variation of the stiffness of the diaphragms in the computed natural period of the structure is attenuated as the curves tend to approach to each other.

Curves of Fig. 5.6 were similarly obtained by varying Young's modulus of the walls within a 50% of the estimated average value for the cases where the nominal stiffness of the plywood was increased by 15% and 25% ("$1.15k_d$" and "$1.25k_d$"). The curves connecting full geometric sections correspond to the cases where an average Young's modulus was considered. As the walls get more flexible, more soil−structure interaction is needed to match a given period. Therefore, soil−structure interaction affects more severely the natural period of stiffer structures than those of flexible structures.

The patterns of the curves of Fig. 5.6 also suggest that as the model approaches to the fixed−base condition, variations within 50% of the nominal stiffness of the walls are not significant in the estimation of the period of the structure. On the other hand, when soil−structure interaction is more pronounced, these variations are important in the determination of the natural period of the structure. Therefore, the observations made about Fig. 5.6 for variations in the stiffness of the walls contrast with what is observed in Fig. 5.5 for variations in the stiffness of the diaphragms.

The variation of the non−dimensional parameters β_θ and β_δ (Section 5.1) with respect to the variation of the average shear modulus of the soil is presented in Fig. 5.7 for all the sensitivity case studies in the E−W direction. Both parameters, β_θ and β_δ, identify the proportion of soil−structure interaction due to rocking and lateral translation respectively. It is clear from Fig. 5.7 that these parameters are practically unaffected by changes in the stiffness of the diaphragms. However, variations in the stiffness of the walls do affect these parameters. Comparing the curves in Fig. 5.7 for β_θ and β_δ, it can be concluded that soil−structure interaction effects are more dependent on the translational action of the foundation rather

than on rocking. This behavior is typical of short, squatty structures according to the ATC 3−06 provisions (Ref. 3). The instrumented two−story office building at Palo Alto fulfills this description.

Up to this point, it can be concluded that soil−structure interaction effects are indeed important in the discrete modeling of the building. Amplitudes of structural responses are best represented when soil−structure interaction effects are considered. Soil−structure interaction effects in the building are governed by the translational action of the foundation because the building is rather stocky. Variations within a 50% of the nominal stiffness of the walls of the discrete model are much more sensitive to soil−structure interaction effects when computing the natural period of the model, than increments within 30% of the nominal stiffness of the plywood of the diaphragms. The computed natural periods with the discrete models were more sensitive to soil−structure interaction when the walls were stiffer. Values of average shear stiffness of the soil beneath the foundation required by the model to match the identified natural period of the firehouse in the east−west direction are within the identified range for the type of soil under study.

5.2.3 Sensitivity with Respect to Variations in the Stiffness of Diaphragms

The flexibility of the diaphragms controls the dynamic response of the building in the E−W direction. This is illustrated in Figs. 5.3 and 5.4, where the mode shapes for the fixed−based discrete modeling and the discrete modeling taking into account soil−structure interaction are presented. The first mode shape is characterized by the roof diaphragm action in both cases.

Several analyses were carried out to study the sensitivity of the discrete modeling of the building due to variations in the stiffness of the diaphragms. As shown earlier in Section 5.2.2, increments up to 30% of the nominal stiffness of the plywood diaphragms affect very significantly the natural period of the fixed−base structure. However, the range of variation

of the stiffness of the plywood diaphragms becomes less important when soil—structure interaction starts to take place.

The sensitivity of peak structural responses with respect to variations within a 30% increment of the nominal stiffnesses of the plywood diaphragms are presented in Figs. 5.8 and 5.9. For these curves, Young's modulus of the grouted brick walls was kept constant and equal to the nominal average value obtained according 1988 UBC code specifications. Figure 5.8 presents the variation of the predicted peak accelerations for the walls and the center of the diaphragm at the roof level with respect to the computed natural period for increments up to 30% of the nominal stiffness of the plywood diaphragms. As stated in Section 5.2.2, the notation "1.xyk$_d$" identifies the curve of a discrete model where the stiffness of the plywood diaphragms were increased by xy percent. The vertical dashed line represents the identified natural period of the building in the E—W direction. The lower horizontal dashed lines identify the recorded peak accelerations at the north and south walls at the roof level (0.34g and 0.32g respectively). The upper horizontal dashed line identifies the recorded peak acceleration at the center of the diaphragm at the roof level (0.53g). The curves connecting full geometric sections (circles and triangles) correspond to the "original" discrete model defined by the initial considerations presented in Section 5.2.1.

It can be observed from the curves of Fig. 5.8 that the amplitude of the peak accelerations and the natural period of the structure are sensitive to variations in the stiffness of the diaphragms. The amplitude of the accelerations is higher at the diaphragms than at the walls. The discrete model is, in general, overshooting the recorded peak acceleration at the diaphragm while undershooting the recorded peak acceleration at the walls. The curves computed for an increment of 25% of the nominal stiffnesses of the diaphragms (1.25 k$_d$) seem to represent the recorded peak responses the best. The period elongation for each case can be deducted from Figs. 5.8 and 5.9, since the leftmost points of each curve represent the peak responses for the fixed—base condition.

The patterns of the sensitivity curves with respect to variations in the stiffness of the diaphragms are rather complex because of the interaction with another parameters of the discrete modeling. For example, the increment of the predicted peak accelerations for the walls when the stiffnesses of the plywood diaphragms increases is also associated to the fact that more soil−structure interaction is needed in these cases to have structures with similar period. This can be illustrated with the mode shapes presented in Figs. 5.3 and 5.4, where it is clear that soil−structure interaction significantly increases the amplitude of the dynamic response of the walls relative to that of the diaphragms.

The curves obtained for the predicted maximum relative displacements between the roof and the base for the walls and the center of diaphragm are presented in Fig. 5.9. The horizontal dashed lines represent the computed maximum dynamic relative displacements between the roof and the base experienced by the structure at the walls (bottom dashed line, $\Delta = 0.41$ in), and at the center of the diaphragm (upper dashed line, $\Delta = 0.80$ in). The curves show a tendency to overshoot the identified maximum dynamic relative displacements of the diaphragm while undershooting at the walls. The curves corresponding to an increment of 25% of the stiffnesses of the plywood diaphragms improve the estimation of the dynamic relative displacement at the walls only. The patterns of these curves are very similar to the ones for the peak accelerations presented in Fig. 5.8.

As an attempt to assess the positive or negative impact of having flexible diaphragms instead of rigid diaphragms, a set of analyses were run considering that the building would have had rigid diaphragms instead. The stiffness of walls and soil correspond to those used in the analysis of the best−correlation discrete model for the recorded response in the E−W direction (E = 1215 ksi, G = 0.80 G_i, and 25% increment in the nominal stiffnesses of the plywood diaphragms). Both the fixed−based structure and the flexible−supported structure model were studied for this rigid diaphragm condition. Results of the analyses are summarized in Table 5.4, where they are compared to the recorded responses and to the predicted response for the best−correlation discrete model.

53

Table 5.4 Comparative study of the predicted peak responses at the roof level for the two−story office at Palo Alto, considering flexible or rigid diaphragms (E−W)

	Flexible Diaphragms			Rigid Diaphragms	
	Mea-sured	Fixed−Base	Flexible Base	Fixed−Base	Flexible Base
Natural Period	0.40	0.39	0.40	0.12	0.24

Peak Accelerations (g)					
Element	Flexible Diaphragms			Rigid Diaphragms	
	Mea-sured	Fixed−Base	Flexible Base	Fixed−Base	Flexible Base
South Wall	0.32	0.06	0.21	0.17	0.21
North Wall	0.34	0.06	0.21	0.17	0.21
Diaphragm	0.53	0.44	0.55	0.17	0.21

Maximum dynamic drifts (inches)					
Element	Flexible Diaphragms			Rigid Diaphragms	
	Mea-sured	Fixed−Base	Flexible Base	Fixed−Base	Flexible Base
South Wall	0.41	0.05	0.20	0.06	0.18
North Wall	0.41	0.05	0.20	0.06	0.18
Diaphragm	0.80	0.81	1.05	0.06	0.18

The natural period of the structure changes dramatically if the diaphragms are rigid. It is well known that rigid diaphragms lead to uniform distributions of accelerations and deformations in all connecting elements. In contrast, flexible diaphragms lead to uneven deformations of the connecting elements according to their relative stiffness.

A comparative study of the results summarized in Table 5.4 suggest that for a fixed−based structure, flexible diaphragms could induce lower accelerations at the in−plane walls than the accelerations driven by rigid diaphragms. When soil−structure interaction effects are considered ("flexible base" case), the results obtained herein suggests that a structure with rigid diaphragms shall experience similar (but lower) deformations and accelerations at the walls. A concern with the flexible diaphragms is that regardless of the supporting conditions, the diaphragms induce themselves to higher accelerations and deformations which they should be able to withstand. Moreover, these uneven high deformations are imposed to the out−of−plane walls, which should be able to resist these deformations without splitting.

In summary, the sensitivity studies regarding the flexibility of the diaphragms confirm the fact that the diaphragm action dictates the dynamic response of the structure. Increments in the nominal stiffnesses of flexible diaphragms affect the natural period of fixed−base discrete models more severely than when soil−structure interaction is accounted in the discrete modeling. Flexible diaphragms induce amplified dynamic response themselves which they should be able to withstand. Besides, these amplified motions are imposed to resisting elements in the perpendicular direction. Thus, flexible diaphragms may have a negative impact in the dynamic behavior of a structure, especially if the diaphragms remain elastic as it has been assumed throughout this study.

5.2.4 Sensitivity with Respect to Variations in the Stiffness of the Walls

The sensitivity of the discrete models with respect to variations in the stiffness of the grouted brick walls was studied as well. Young's modulus was assumed to vary within 50% of the nominal average value of 1215 ksi. For this set of analyses, the stiffness of the diaphragms considered were $1.15K_d$ and $1.25K_d$, and they were the fixed parameter.

As illustrated earlier in Section 5.2.2, the curves of Fig. 5.6 suggest that variations within 50% of the nominal stiffness of the walls do not have a considerable impact in the computed period of the structure as the discrete models approach a fixed−base condition, whereas as the

soil−structure interaction effects are more pronounced, these variations become important in the determination of the natural period of the structure.

The sensitivity of peak structural responses to variations within 50% of the nominal stiffness of the walls are presented in Figs. 5.10 and 5.11. The variation of predicted peak accelerations for all structural elements running in the E−W direction at the roof level in relation to the computed natural period for variations within 50% of the nominal stiffness of the walls is presented in Fig. 5.10. The vertical dashed line represents the identified natural period of 0.40 seconds of the building in the E−W direction. The lower horizontal dashed lines identify the recorded peak acceleration at the walls at the roof level. The upper horizontal dashed line identifies the recorded peak acceleration at the center of the south diaphragm at the roof level. The curves connecting full geometric sections (circles, squares, triangles and rhomboids), correspond to the reference discrete models defined by the increment of 15% and 25% the nominal stiffness of the plywood diaphragms.

It can be concluded from the observation of Fig. 5.10 that the predicted peak accelerations are insensitive to variations within 50% of the nominal stiffness of the walls for all period ranges. A similar conclusion can be drawn from the maximum dynamic drifts between the roof and the base. These maximum dynamic drifts are presented in Fig. 5.10 for all walls and diaphragms resisting in−plane loading in the E−W direction.. Thus, both the peak accelerations and the maximum dynamic drifts predicted with the discrete modeling are rather insensitive to variations of up to ±25% of the nominal stiffness of the walls for all period ranges.

5.2.5 Identified Structure in the East−West Direction

Based upon the extensive sensitivity analyses presented in Sections 5.2.2 to 5.2.4, it was determined that the dynamic response of the two−story office building at Palo Alto in the E−W direction was best represented with the discrete model of Figs. 5.1 and 5.2 when : 1) initially estimated stiffnesses of the plywood diaphragms are increased by a 25%; 2) the

stiffnesses of the walls are based on the nominaL average Young's modulus of 1215 ksi obtained according to the 1988 UBC code provisions; and, 3) the shear modulus of the soil beneath the foundation is 80% of the mean value initially estimated from the data taken from the studies of Lew, Chieruzzi and Campbell (G_i = 13.05 ksi), if a nominal depth is considered. The associated effective damping ratio for the first mode was 6.5% (Fig. 5.12).

The computed acceleration time histories for the walls and the center of the diaphragm at the roof level are compared against the recorded motions in Fig. 5.13. Peak accelerations and maximum dynamic drifts computed with the discrete model compare very favorably with those obtained from the recorded motions for the roof diaphragm. The peak acceleration at the center of the diaphragm at the roof level predicted by the discrete model (212. in/sec^2 = 0.55g) is only 3.2% higher than the one recorded by sensor 5 (206. in/sec^2 = 0.53g). On the other hand, the peak accelerations predicted at the walls correlate very poorly with those recorded during the earthquake. The peak acceleration for the walls at the roof level computed with the discrete model (79. in/sec^2 = 0.21g) are 56.6% lower than the one recorded by sensor 6 at the south wall (124. in/sec^2 = 0.32g) and 66.4% lower than the one recorded by sensor 4 at the north wall (132. in/sec^2 = 0.34g).

The maximum dynamic displacement between the base and the roof computed with the discrete model for the center of the diaphragm (1.05 inches) is 31.2% higher than the one computed from the recorded motions (0.80 inches). The maximum dynamic drift for the walls estimated with the discrete model (0.20 inches) is 50.6% lower than the one obtained from the recorded motions (0.41 inches).

In addition, the frequency content of the acceleration time histories computed with the discrete modeling matches remarkably well the frequency content of the recorded motions for the diaphragm. This is illustrated in Fig. 5.14 for the frequency range which is of interest in the study of the building. In contrast, the frequency content of the acceleration time histories predicted for the walls suggest that the stiffness of the walls may have been

overestimated as gross cross section properties were considered instead of those for the cracked section. The dominant response of the walls predicted by the discrete model is associated to a period of 0.25 seconds. Therefore, cracked sections properties (about 1/10 of the gross sections) would have caused the discrete model to excite the walls under the dominant period of the structure, allowing higher drifts and deformations. Therefore, although the discrete model was able to identify and reproduce the dynamic response of the diaphragm well, it is felt that a better overall correlation would have been obtained considering the properties of the cracked sections at the walls, especially because the walls may have yielded during the earthquake (Section 4.3).

5.3 North – South Direction Modeling

A six DOF discrete, linear – elastic dynamic model with soil – structure interaction effects was used to study the response of the building in the north – south direction. The model is shown in Figs. 5.16 and 5.17. The masses were lumped and distributed according to a tributary area criterion, and their values are presented in Table 5.5.

Table 5.5 Lumped masses for the N – S discrete 6 DOF dynamic model (Figs. 5.16 and 5.17)	
DOF	Mass (lb – sec^2/in)
1	1014.50
2	457.33
3	1017.52
4	468.90
5	1014.50
6	457.33

Average lateral stiffness for each wall was computed through static condensation, considering the uncracked section properties of the walls. and the nominal average Young's modulus of 1215 ksi. All walls running in the N – S direction were considered (facade walls and L – shaped

walls). Axial springs are used to represent the diaphragm because the support conditions make the diaphragm to behave as a narrow band rod in this direction by not allowing the diaphragm to shear (See Fig. 2.1). The stiffness constant of the axial springs representing the flexible diaphragms were estimated assuming a Young's modulus of plywood of 1700 ksi. Equivalent effective thicknesses for plywood diaphragms recommended by the American Plywood Association were also considered (APA, Refs. 14, 35). A width of 24 ft was considered effective to transmit the seismic forces axially in the N−S direction. This width correspond to the distance edge to edge between the L−shaped walls (Figs. 2.1 and 2.2).

For the roof diaphragm, the secondary beams running in the N−S direction were neglected to contribute to the axial stiffness of the diaphragm. Truss joists and sheathing were also neglected in the calculations at the roof level. For the second floor diaphragm, the axial stiffness was computed as the sum of the stiffness of the 1.5" thick light−weight concrete and the 3/4" plywood. Secondary beams, truss joists and sheathing were neglected in the calculations at the second floor. The axial stiffness of the second floor diaphragm is controlled by the light−weigh concrete. The 3/4" thick plywood contributed to the 30.8% of the total stiffness of the diaphragm of the second floor. The second floor is considerably stiffer than the roof (4.5 times stiffer). The preliminary estimates of the stiffnesses of the springs which are identified in Figs 5.16 and 5.17 are presented in Table 5.6.

Table 5.6 Preliminary spring constants for the 6 DOF discrete model of Fig. 5.16		
SPRING ID	Diaphragm's Thickness (in)	Stiffness (k/in)
K_{A1}	1.5 (c) + 0.75 (plwd)	412.6
K_{A2}	0.5 (plwd)	92.3

Soil−structure interaction effects were incorporated according to Section 5.1. The values of the generalized spring constants k_θ and k_δ were calculated based upon the procedure outlined by the Applied Technical Council (ATC 3−06, Ref. 3) for footing foundations. They were

already presented in Section 5.2.1. In the computation of the generalized spring stiffnesses k_δ and k_θ, d_i was taken as 27 inches (Fig. 2.4 a) for each wall running in the N−S direction. All walls running in the N−S direction were considered. The average shear modulus of the soil beneath the footings at large strain levels, G_i, was computed based upon the ATC 3−06 recommendations (Equation 5.13).

The values of γ, v and v_s needed to estimate G_i were taken from Lew, Chieruzzi and Campbell for engineered fill soils (Ref. 19). The values of k_G and k_v were determined from Table 6−A of ATC 3−06 provisions for the recorded peak ground acceleration of 0.20g in the north−south direction. The mean shear modulus for the soil beneath the foundation at large strain levels, G_i, was determined as 13.05 ksi in the N−S direction. The initial estimation of the generalized spring constants, k_θ and k_δ, are $k_\theta = 9.224 \times 10^8$ k−in/rad, and $k_\delta = 29,541$ k/in. These values were computed from Equations 5.6 to 5.12 based upon these assumptions, considering all walls (facade and L−shaped walls), and considering the depth of the effective embedment of the spread footings.

The amount of effective damping factor for the structure−foundation system, $\tilde{\xi}$, was determined according to ATC 3−06 provisions (Equation 5.14). The structural damping factor ξ_j in the north−south direction was also assumed as 0.06.

Time−step integration and frequency analyses of the 6 DOF discrete model were carried out using the same tools and methods which were employed for the analyses in the E−W direction (Section 5.2).

5.3.1 Considerations for Sensitivity Analyses

Several analyses were also carried out in the N−S direction to identify the response of the structure. The sensitivity of the modeling to variations in the stiffness of diaphragms, and soil, as well as whether or not to consider the facade walls in the modeling was also studied. The stiffnesses of the diaphragms were varied within 20% (k_d, 0.85k_d, and 0.80k_d) of the nominal

values presented in Table 5.6. Young's modulus of the masonry walls was kept constant as the nominal average value defined according to the 1988 UBC code (E =1125 ksi).

To identify the frequency ranges of response of the firehouse in this direction, the nominal stiffnesses of the generalized foundation springs were also varied. Therefore, the average shear modulus for the soil beneath the foundation (G_i = 13.05 ksi) was varied from $0.90G_i$ to $1.82G_i$, that is within the credible range of variation of the engineered fill soil under consideration. Damping ratios varied according to the amount of soil−structure interaction in each given analyses (Equation 5.14). Modal damping was used throughout the computations.

The fixed−based condition was studied in order to assess the influence of the soil−structure interaction effects. The rigid diaphragm condition was also studied to compare it against the flexible diaphragm condition. The effect of considering or neglecting the facade walls was also studied. The results of the sensitivity analyses in the N−S direction are discussed in Sections 5.3.2 to 5.3.5.

5.3.2 Sensitivity with Respect to Soil−Structure Interaction Considerations

Soil−structure interaction effects had a considerable impact in the amplitude of the response of the structure in the N−S direction. This is in correspondence with the behavior observed in the E−W direction. This can be illustrated by comparing the response of the fixed−base system with respect to the system where the flexibility of the soil−foundation system was considered. For the fixed−base consideration, the computed mode shapes from the original−data discrete model are shown in Fig. 5.18.

The mode shapes of Fig. 5.18 describe the in−plane motions. These shapes are presented schematically in the equivalent system composed by condensed beams and elastic springs (Figs. 5.17 and 5.18). The natural period of this model was 0.33 seconds, approximately 12% shorter than the identified natural period of the building in the N−S direction of 0.37 seconds. The first two mode shapes are identical due to symmetry of the structure in mass and stiffness.

61

The first three modes suggest that the diaphragm action controls the response of the structure. The amplitude of the movement of the walls in the lower modes for the fixed−base condition is small when compared to that of the diaphragms.

The amplitudes of peak responses were determined by performing a time−step analysis of this fixed−base system considering 6% viscous damping for the first mode and increasing the damping for the higher modes through a modal damping assumption. The computed peak accelerations at roof level were 0.07g at the south and north walls, and 0.32g at the center of the diaphragm. The recorded peak acceleration at the diaphragm at the roof level in the N−S direction was 0.36g (Fig. 3.1, Table 3.1).

The maximum computed relative displacements between the roof and the base were 0.06" for the south and north walls and 0.39" for the center of the diaphragm. The maximum relative displacement computed at the center of the diaphragm from the recorded motions was 0.29" in the N−S direction. The natural period shorten by 12% and the peak acceleration at the diaphragm is undershot by 17%, however, the peak dynamic drift between the diaphragm and the base is overestimated by 34%. Therefore, the fixed−base model gives a crude estimation of the overall response of the structure.

There are not recorded data available to compare any of the walls that resisted the seismic action in the N−S direction. However, based upon the observations made in the E−W direction (Section 5.2.2), it is believed that the fixed−base modeling may underestimate the amplitude of the response of the south and north walls in this direction as well.

Based upon the experience gained during the E−W direction modeling, soil−structure interaction effects were introduced to improve the modeling, particularly the amplitude of the response of the walls. The computed mode shapes presented in Fig. 5.19 correspond to a system based entirely on the initial considerations of Section 5.3, and the inclusion of soil−structure interaction effects.

Mode shapes of Fig. 5.19 describe in−plane motions, and they are presented schematically in the equivalent system composed by condensed beams and elastic axial springs (Figs. 5.16, 5.17 and 5.19). The average shear modulus for the soil beneath the foundation was 85% the average value given in Section 5.3.

The computed natural period estimated was 0.36 seconds for the discrete model based upon the initial data with soil−structure interaction. This value constitutes a 11.6% increment with respect to the fixed−base model, and is only 0.8% shorter than the identified natural period of the structure in the N−S direction. The first three mode shapes still identify a dominant diaphragm action. However, it is clear from the first and second modes that the flexibility of the base induces slightly higher responses in the walls.

This is corroborated with the time−step analysis for this condition, including a viscous damping of 10% for the first mode of the soil−structure system (Equation 5.14). The computed peak accelerations at the roof level for the south and north walls, and the center of the diaphragm, were 0.25g, 0.25g, and 0.58g respectively. The maximum computed relative displacements between the roof and the base were 0.31" for the south and north walls, and 0.92" for the diaphragm.

Soil−structure interaction effects improved the computed response of the walls as compared to the response of the fixed−base discrete model. On the other hand, soil−structure interaction worsen the overestimation of the amplitude of the dynamic responses at the diaphragms. This can be observed in Table 5.7, where the peak responses of the walls and the diaphragm under these two conditions are compared with respect to the recorded peak responses.

The original set of analyses suggested that the initial estimates of structural response crudely represent the observed dynamic response in the building in the N−S direction. The estimate of the dynamic response can be further improved considering the variability of the material properties and the effective axial areas of the diaphragms. Sensitivity analyses were carried

out to improve the prediction of the natural period of the structure and the amplitude of the response of the diaphragms. These analyses were performed by decreasing the initially estimated stiffness of the diaphragms (Section 5.3.3).

Table 5.7 Recorded vs computed peak responses at the roof level of the original discrete MDOF dynamic modeling of the two−story office building at Palo Alto (N−S).						
Parameter	South and North Walls			Center of Diaphragm		
	Re-corded	Fixed−Base Model	Flexible Base Model	Re-corded	Fixed−Base Model	Flexible Base Model
Accel.	−	0.07g	0.25g	0.36g	0.32g	0.58g
Drift	−	0.06"	0.31"	0.29"	0.39"	0.92"

As a matter of fact, several studies were carried out to identify the recorded response of the structure and the sensitivity of this discrete modeling to variations of the parameters involved in the modeling. As stated earlier for the sensitivity studies in the E−W direction, these parameters interact among themselves and they are difficult to isolate.

The variation of the natural period of the model structure with respect to variations of the stiffness of the foundation is presented in Figs. 5.20 and 5.21. In these figures, the period is expressed as a function of the assumed average shear modulus of the soil beneath the foundation, G_i, considering the depth of the effective embedment of the spread footings.

For the curves of Fig. 5.20, Young's modulus of the masonry walls was kept constant to the nominal average value. The lateral stiffness matrix of the equivalent condensed beam elements correspond to the sum of the lateral stiffness matrices of the L−shaped walls and the facade walls. Each curve identifies the influence of the variations of the average shear modulus of the soil for a given assumed stiffness of the diaphragms. Each curve is identified with a label which is expressed in function of the nominal stiffness presented in Table 5.6. Then, the label "$0.85k_d$" identifies the curve of a discrete model where the stiffnesses of the

diaphragms in Table 5.6 were decreased by 15%. The curve connecting full triangles corresponds to the "original" model. The vertical dashed line represents the natural period of 0.37 seconds of the building in the north−south direction. The horizontal dashed lines define the maximum range of variation of G_i engineered fill soils (Lew, Chieruzzi and Campbell, Ref. 19).

As noticed in the analyses for the E−W direction, it can be identified for each curve of Fig. 5.20 that the computed natural period increases fast when more soil−structure interaction is present. That is, when G_i decreases, as it should be expected. In the vicinity of the natural period of the structure, the amount of soil−structure interaction needed can be substantially different in the studied range of stiffnesses of the diaphragms ($0.8k_d$ to k_d). This is in clearly in agreement to what was observed in the sensitivity analyses for the E−W direction.

The general tendency of the curves of Fig. 5.20 agrees with the observed trend of the sensitivity analyses in the E−W direction. The gap between curves increases as the system approaches the fixed−base condition (increment on the assumed G_i), whereas the influence of variation of diaphragm stiffness in the natural period of the structure is considerably attenuated as the soil−structure interaction effects are more pronounced (decrement on the assumed G_i).

Curves of Fig. 5.21 were obtained in a similar fashion. In these curves, the stiffness of the diaphragm were decreased by 15% ($0.85k_d$). Young's modulus of the walls was kept constant. Two cases were studied : a) Considering all walls running in the N−S direction (L−shaped and facade walls) in the modeling, and b) Neglecting the contribution of the facade walls in the modeling. The curve connecting full circles corresponds to the discrete model where the stiffness of the diaphragms were decreased by 15% while maintaining Young's modulus of the walls equal to the nominal average value and considering the contribution to the lateral stiffness of all walls running in the N−S direction (case a).

Curves of Fig. 5.21 show that in the vicinity of the identified natural period of the building, to consider or neglect the contribution of the facade walls leads to much different levels of

soil−structure interaction compliance to match a given period. More soil−structure interaction was needed to match a given period for the case were all walls were considered (case a).

The variation of non−dimensional parameters β_θ and β_δ with respect to the variation of the average shear modulus of the soil is depicted in Fig. 5.22 for all the sensitivity case studies in the N−S direction. Parameters β_θ and β_δ identify the proportion of soil−structure interaction due to rocking and lateral translation respectively. It is identified from the study of Fig. 5.22 that β_θ and β_δ are practically unaffected by variations in the stiffness of the diaphragms. However, variations in the stiffness of walls do affect these parameters (case a vs case b). Comparing the curves in Fig. 5.22 for β_θ and β_δ, it can be concluded that soil−structure interaction effects in the N−S direction of the firehouse are also more dependent on the translational action of the foundation rather than on rocking.

5.3.3 Sensitivity with Respect to Variations in the Stiffness of Diaphragms

As noticed in Section 5.3.2, the flexibility of diaphragms controlled the dynamic response of the building in the N−S direction as well. This is illustrated in Figs. 5.18 and 5.19, where the mode shapes for the fixed−based discrete modeling and the discrete modeling which considers soil−structure interaction are presented. The first three mode shapes in both cases are characterized by the diaphragm action.

Several analyses have been carried out to study the sensitivity of the discrete model of the structure in the N−S direction to variations in the stiffness of the diaphragms. As discussed in Section 5.3.2 (Fig. 5.20), changes in the nominal stiffness of the diaphragms affect significantly the natural period of the fixed−base structure, but they become less important when some soil−structure interaction starts to take place.

The sensitivity of peak structural responses for values from 80% to 100% of the nominal stiffness of the diaphragms ($0.80k_d$, $0.85k_d$, and k_d) are presented in Figs. 5.23 and 5.24. In the curves of Figs. 5.23 and 5.24, Young's modulus of the masonry walls was kept constant and

equal to the computed nominal average value of 1215 ksi. The variation of the predicted peak acceleration for both walls and the center of the diaphragm at the roof level in the N–S direction with respect to the computed natural period is presented in Fig. 5.23. The vertical dashed line represents the identified natural period of the firehouse in the N–S direction (0.367 seconds). The horizontal dashed line identifies the recorded peak acceleration at the center of the south diaphragm at the roof level in this direction (0.36g). The curves connecting full geometric sections (circles, and triangles) correspond to the "original" discrete model defined by the nominal stiffness of the diaphragms presented in Table 5.6.

As it was observed for the E–W direction, the study of the curves in Fig. 5.23 suggests that the amplitude of the peak accelerations are sensitive to variations of the stiffness of the diaphragms. The amplitude of the accelerations is higher at the diaphragms than at the walls. The variation of the predicted peak accelerations is pronounced both at the walls and at the center of the diaphragms (Fig. 5.23). The discrete model is overshooting by 17% to 58% the recorded peak acceleration at the diaphragm in the N–S direction. The curves computed for 85% of the nominal stiffnesses of the diaphragms (0.85 k_d) seem to be the best representation of the recorded peak responses.

The patterns of the curves of Fig. 5.23 are rather complex because of the influence of another parameters of the discrete modeling. The increment of the predicted peak acceleration for the walls when the stiffnesses of the diaphragms are increased is also propitiated by the fact that more soil–structure interaction is needed in these cases to have structures with similar period. This can be confirmed from the comparison of the modes shapes presented in Figs. 5.18 and 5.19. In these figures is clear that soil–structure interaction increases the amplitude of the dynamic response of the walls with respect to the diaphragms..

The curves obtained for the predicted maximum relative displacements between roof and base for the south and north walls, and the center of the diaphragm are presented in Fig. 5.24. The horizontal dashed line represents the maximum dynamic relative displacement

experienced by the structure at the center of the diaphragm in the N−S direction (Δ = 0.29 in). The curves considerably overshoot the identified maximum dynamic relative displacement at the diaphragm. This could be attributed to the inherent inability of the 2−D discrete model to account for the constrains imposed by the walls running in the perpendicular direction. Also, it can be observed that the roof diaphragm is very flexible even axially, as it can be confirmed by the magnitude of the amplification between the walls curves and the center of the diaphragm curves.

A set of analyses was run considering that the building would have had rigid diaphragms. This was done to investigate the positive or negative impact of having flexible diaphragms instead of rigid diaphragms. The stiffnesses of walls and soil correspond to those of the best−correlation discrete model for the N−S direction (E, G=1.03 G_i, and 0.85k_d). Both the fixed−based structure and the flexible−supported structure models were studied for the infinitely rigid diaphragm condition.

Results of the analyses are summarized in Table 5.8, where they are compared to the recorded responses at the firehouse and to the predicted responses by the discrete model with the best correlation. The natural period of the structure is changed dramatically if the diaphragms are rigid. The comparative data summarized in Table 5.8 suggest that for a fixed−based structure, flexible diaphragms could induce lower accelerations at the in−plane walls than rigid diaphragms.

A concern with the flexible diaphragms is that regardless of the supporting conditions, the diaphragms push themselves to higher accelerations and deformations which they should be able to withstand. In addition, these uneven high deformations are imposed to the out−of−plane walls, forcing the walls to resist these deformations without splitting.

In summary, the sensitivity studies regarding the flexibility of the diaphragms in the N−S direction confirm the fact that the diaphragm action governs the dynamic response of the structure. Similar conclusions can be learned from the ones arrived at the studies for the E−W

direction. Increments in the nominal stiffness of flexible diaphragms affect the natural period of the fixed−base discrete models more severely than when soil−structure interaction is accounted in the discrete modeling.

Table 5.8 Comparative study of the predicted peak responses at the roof level for the office building at Palo Alto, considering flexible or rigid diaphragms (N−S)					
	Flexible Diaphragms			Rigid Diaphragms	
	Mea-sured	Fixed−Base	Flexible Base	Fixed−Base	Flexible Base
Natural Period	0.367	0.352	0.367	0.153	0.264
Peak Accelerations (g)					
Element	Flexible Diaphragms			Rigid Diaphragms	
	Mea-sured	Fixed−Base	Flexible Base	Fixed−Base	Flexible Base
South Wall	−	0.07	0.16	0.21	0.26
North Wall	−	0.07	0.16	0.21	0.26
Diaphragm	0.36	0.37	0.45	0.21	0.26
Maximum dynamic drifts (inches)					
Element	Flexible Diaphragms			Rigid Diaphragms	
	Mea-sured	Fixed−Base	Flexible Base	Fixed−Base	Flexible Base
South Wall	−	0.07	0.20	0.10	0.21
North Wall	−	0.07	0.20	0.10	0.21
Diaphragm	0.29	0.50	0.64	0.10	0.21

Flexible diaphragms subject themselves to amplified dynamic response which they should be able to withstand. Besides, these amplified motions are imposed to the resisting elements in the perpendicular direction. Thus, flexible diaphragms may have a negative impact in the dynamic behavior of a structure, especially if the diaphragms remain elastic as it has been assumed throughout this study.

5.3.4 Sensitivity with Respect to the Lateral Stiffness modeling of the Walls

For this study, the stiffness of the diaphragms selected were the ones equivalent to 85% of their nominal values (Table 5.6). These values were kept constant throughout these sensitivity studies. This selection was done on grounds of a better prediction of the natural period and of the amplitude of the diaphragm's response. Young's modulus was assumed kept constant as the nominal value of 1215 ksi computed according to the 1988 UBC code provisions. Two cases are studied a) All walls (L–shaped, facade walls) contribute to the lateral stiffness of the discrete model in the N–S direction,; and, b) The contribution of the facade walls to the lateral stiffness of the discrete model in the N–S direction is neglected.

The sensitivity of peak structural responses with respect to the effect of including (case a) or neglecting (case b) the stiffness of the facade walls variations is presented in Figs. 5.25 and 5.26. The variation of the predicted peak accelerations for all the walls running in the N–S direction and the center of the diaphragm at the roof level with respect to the computed natural period is presented in Fig. 5.25. The vertical dashed line represents the identified natural period of the firehouse of 0.367 seconds in the N–S direction. The horizontal dashed line identifies the recorded peak acceleration at the center of the diaphragm at the roof level in this direction. The curves connecting full geometric sections (circles and triangles) identify the "reference discrete model" in this direction (case a). This model corresponds to the case study where all walls contribute to the lateral of the discrete model, the stiffness of the diaphragms are equivalent to 85% of their nominal value presented in Table 5.6.

It can be concluded from Fig. 5.25 that the predicted peak accelerations are insensitive to the action of including or neglecting the contribution of the facade walls to the lateral stiffness of the building in all period ranges. A similar conclusion can be drawn from the maximum dynamic relative displacements between the roof and the base. These displacements are presented in Fig. 5.26 for all walls and the diaphragm resisting in−plane action in the N−S direction. The reason of this insensitivity is that the lateral stiffness matrix of the facade walls is very small compared to the stiffness of the L−shaped walls. The off−diagonal terms of the L−shape walls are 86.6 times higher than the ones for the the facade walls, which stiffness is drastically reduced as a consequence of the setback on the second floor (Figs. 2.1 and 4.2).

5.3.5 Identified Structure in the North−South Direction

It was determined from the sensitivity analyses presented in Sections 5.3.2 to 5.3.4 that the dynamic response of the office building at Palo Alto in the N−S direction was best represented with the discrete model of Figs. 5.16 and 5.17 when : 1) initially estimated stiffnesses of the diaphragms are equivalent to 85% of their nominal values; 2)Young's modulus of the grouted brick walls is equal to 1215 ksi.; and, 3) the shear modulus of the soil beneath the foundation is 3% higher of the mean value initially estimated from the studies of Lew, Chieruzzi and Campbell (G_i = 13.05 ksi), if a nominal depth is considered. The associated effective damping ratio for the first mode was 6.9%. (Fig. 5.27).

The acceleration time histories computed for the center of the diaphragm at the roof level under these considerations are compared against the recorded motions in Fig. 5.28. The peak accelerations computed with the discrete model in the N−S direction compare favorably with those obtained from the recorded motions. The peak acceleration at the center of the diaphragm at the roof level predicted by the discrete model in this direction (172. in/sec^2 = 0.45g) is 23.4% higher than the one recorded by sensor 7 (140. in/sec^2 = 0.36g).

On the other hand, the maximum dynamic relative displacements are noticeable overshot by the discrete modeling. The maximum dynamic relative displacement between the base and

the roof computed with the discrete model for the center of the south diaphragm (0.64 inches) is 121% higher than the one computed from the recorded motions (0.29 inches). The overshooting of the dynamic displacements should be expected because the discrete modeling does not include the constraints imposed by the walls running in the perpendicular direction. Also, the difference might be smaller taking into account that computing the displacement from a double integration of the recorded accelerations is not accurate.

The frequency content of the acceleration time histories computed with the discrete modeling matches well the frequency content of the recorded motions (sensor 7). This is illustrated in Fig. 5.29 for the recorded motions at the diaphragm in the N−S direction for the frequency range of interest. The frequency content of the diaphragm is reasonably represented, especially in the neighborhood of the natural frequency.

It is considered that the simplified discrete dynamic modeling presented in Section 5.3 for the N−S direction has been able to identify in a reasonable way the dynamic response of the two−story office building at Palo Alto in this direction within a reasonable range of variation of the stiffnesses of the structural elements involved in the modeling.

5.4 Summary and Observations Regarding the Modeling

The discrete MDOF discrete linear−elastic dynamic model has been able to represent for both directions the recorded dynamic response of the building during the Loma Prieta Earthquake within reasonable ranges of variation for the parameters involved.

Correlations for predicted peak accelerations were good with respect to the recorded accelerations for both directions at the diaphragm. The discrete model predicted well the observed dynamic amplification between peak accelerations at the center of the diaphragm and the walls at the roof level in the E−W direction. Predicted maximum dynamic displacements in both directions were generally overshot at the diaphragms. The overshooting should be expected because the discrete modeling does not include the dynamic constraints imposed by the walls running in the perpendicular direction.

The frequency analyses of the discrete models for both the fixed—base and the flexible—supported conditions (Figs. 5.3, 5.4, 5.18 and 5.19) corroborated that diaphragm action controls the dynamic response of the building. This was previously suspected from the observation of the recorded response during the Loma Prieta Earthquake (Sections 3.2.1 and 3.2.2). Computed mode shapes in both directions also identified that the modeling of the dynamic response of the building was best represented when soil—structure interaction effects were considered.

The fixed—base discrete models of the building in both directions were unable to predict the peak structural responses of the walls well. The predicted peak acceleration for the walls with the fixed—base model were 5.6 times smaller than the one recorded, and the predicted maximum dynamic drift were 8 times smaller. However, the fixed—base models obtained reasonable estimates of the natural frequencies of the structure.

Soil—structure interaction was considered to improve the overall modeling. Soil—structure interaction was an important factor to identify the observed dynamic response of the building. The amplitudes of structural responses were best represented when soil—structure interaction effects were considered. Soil—structure interaction effects in the discrete models of the building were more dependent on the translational action of the foundation rather than on rocking because the structure was rather stocky.

Variations in the stiffness of the walls of the discrete models were much more sensitive to soil—structure interaction effects than to variations in the stiffness of the diaphragms when the natural periods of the discrete models were computed. The computed natural periods from the discrete models were more sensitive to soil—structure interaction effects when the walls were stiffer. The values of the average shear stiffness of the soil needed to match the identified natural period of the firehouse in both directions were within the identified range of variation for the type of soil under study.

The considered range of variation in the stiffness of the diaphragms was within reasonable margins in both directions. In the E−W direction, a 25% increment in the stiffness of the diaphragms was required to identify the recorded response. In the N−S direction, an decrement of 15% was required for the same purpose.

Sensitivity studies regarding the flexibility of the diaphragms in the both directions confirmed the fact that diaphragm action controlled the dynamic response of the structure. Increments of the nominal stiffness of the flexible diaphragms affect the natural period of the fixed−base discrete models more severely than when soil−structure interaction is accounted in the discrete modeling. Flexible diaphragms subject themselves to amplified dynamic responses that they are forced to withstand. In addition, flexible diaphragms impose these amplified motions to the resisting elements in the perpendicular direction. Thus, flexible diaphragms may have a negative impact in the dynamic behavior of a structure, especially if the diaphragms remain elastic as it has been assumed throughout this study.

Sensitivity analyses for both directions revealed that the peak accelerations and the maximum dynamic displacements predicted with the discrete models were rather insensitive to the range of variation of the nominal stiffnesses of the walls considered for all period ranges.

In synthesis, the extensive sensitivity studies done with the discrete models of the building in both directions revealed that the natural frequency and the amplitude of the dynamic response of the structure is sensitive to variations in the stiffness of the diaphragms and to soil−structure interaction considerations. At the same time, it is rather insensitive to the variation in the stiffness of the walls.
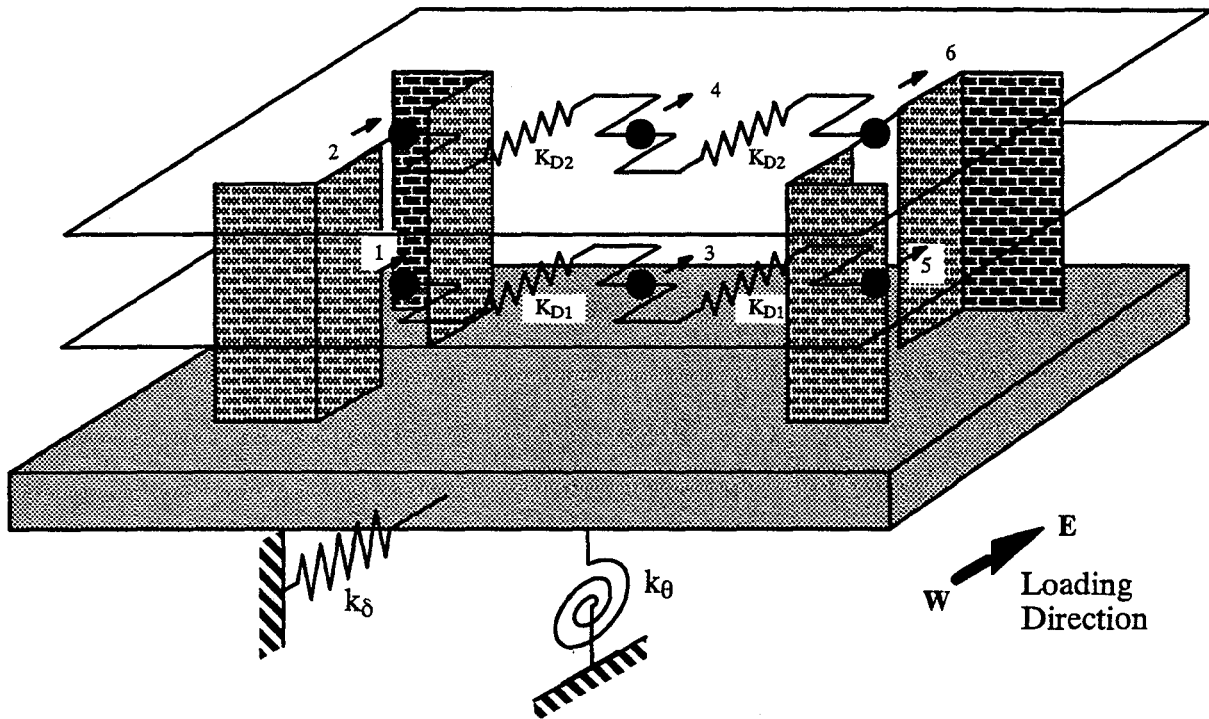
Figure 5.1 Discrete MDOF dynamic model considering soil−structure interaction
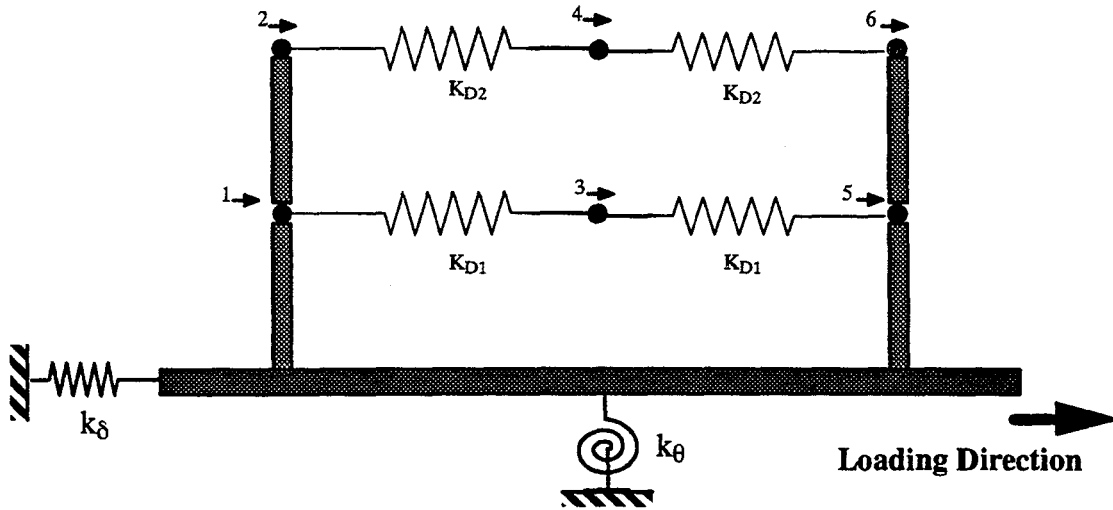for the E−W direction

Figure 5.2 Schematic representation of the discrete MDOF dynamic model of Fig. 5.1
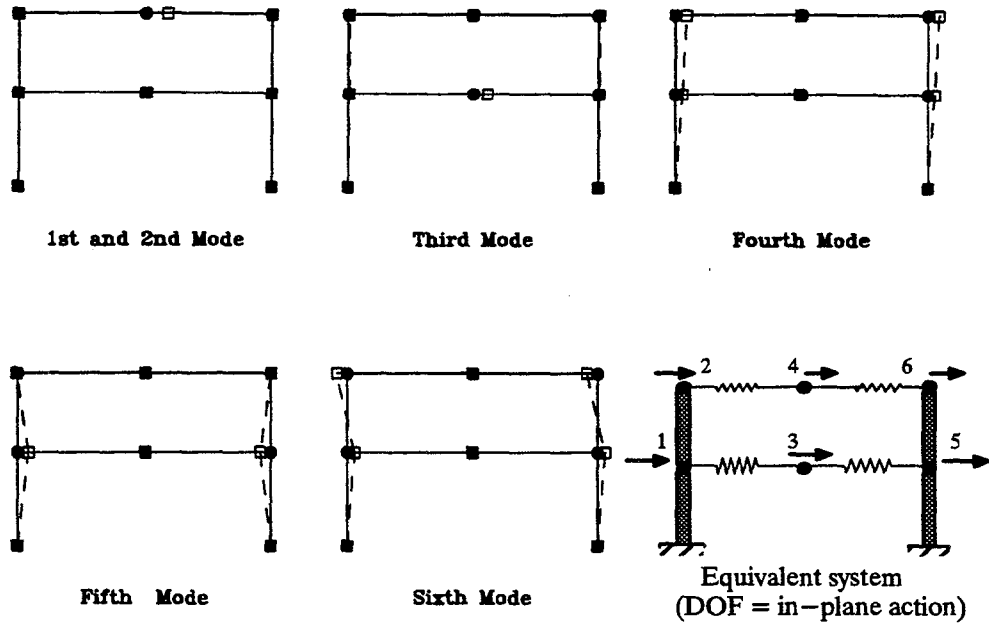as an equivalent system of condensed beam elements and elastic springs

Figure 5.3 Schematic representation of the mode shapes for the fixed–base discrete model of the building in the E–W direction
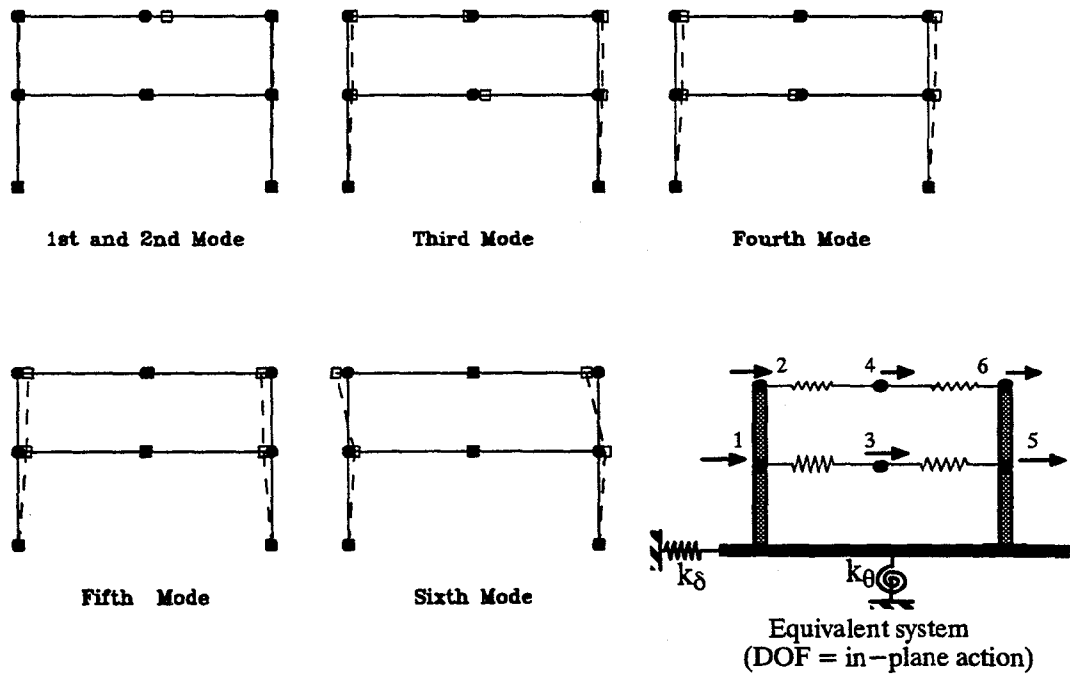

Figure 5.4 Schematic representation of the mode shapes for the flexible–base discrete model of the building in the E–W direction
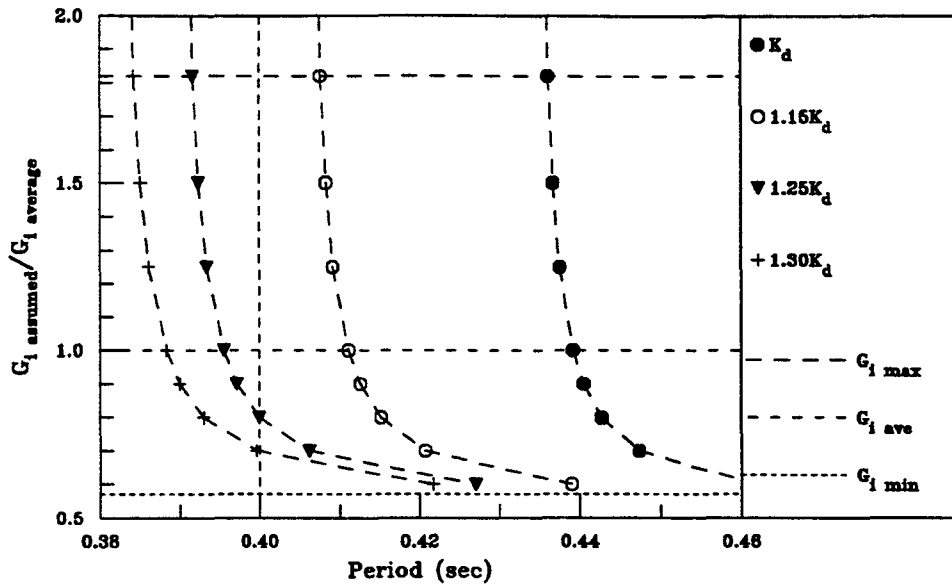
76

Figure 5.5 Sensitivity of the natural period of the discrete model with respect to the variability of the stiffnesses of the soil and the diaphragms (E–W direction)
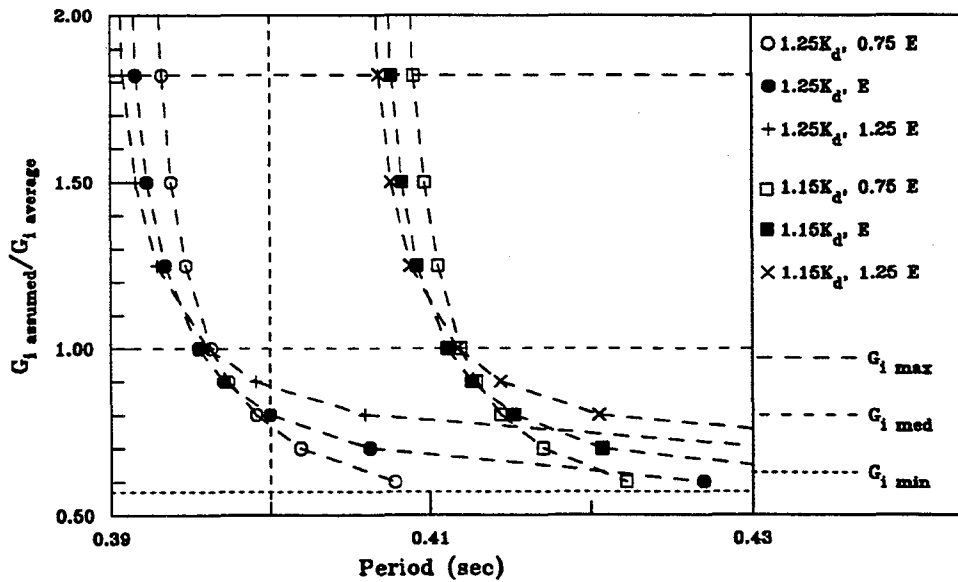

Figure 5.6 Sensitivity of the natural period of the discrete model with respect to the variability of the stiffnesses of the soil and the walls (E–W direction)
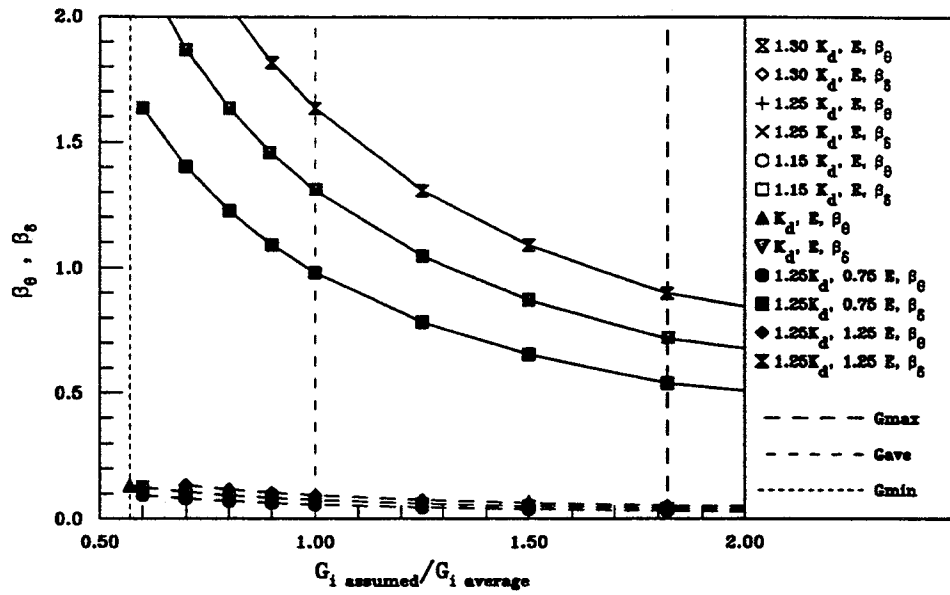
Figure 5.7 Sensitivity of the soil–structure interaction parameters β_θ and β_δ to the variability of the stiffnesses of the soil, walls and diaphragms (E–W)

Figure 5.8 Sensitivity of peak accelerations at the roof level predicted with the discrete model to the variability of the stiffnesses of the diaphragms (E–W direction)

Figure 5.9 Sensitivity of maximum dynamic drifts at the roof level predicted with the discrete model to the variability of the stiffnesses of the diaphragms (E–W)

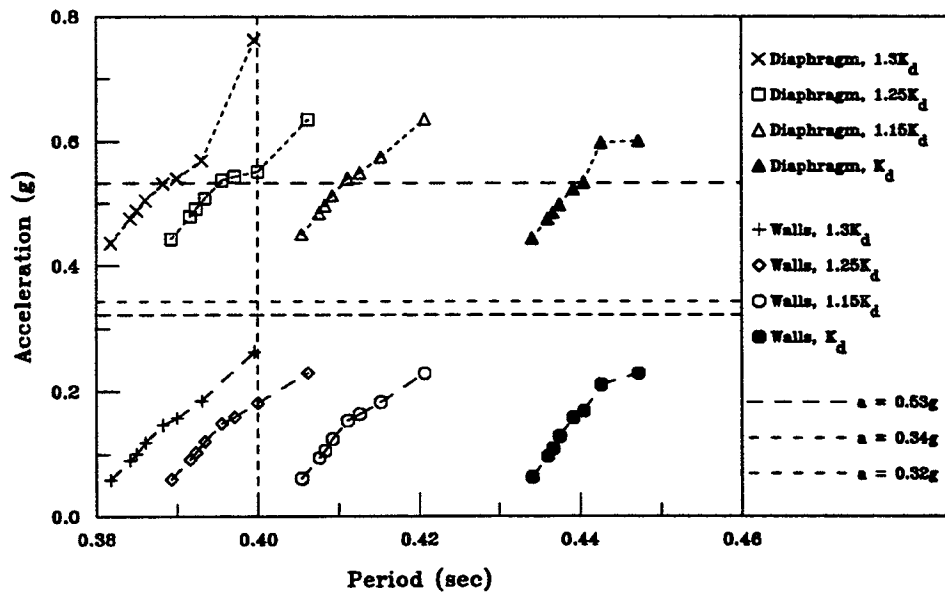Figure 5.10 Sensitivity of peak accelerations at the roof level predicted with the discrete model to the variability of the stiffnesses of the walls (E–W)
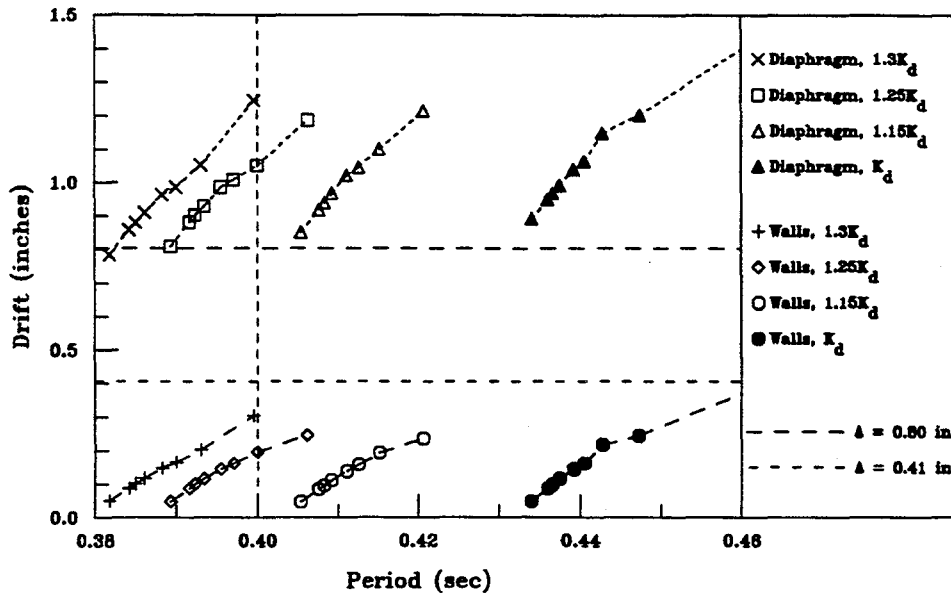
79
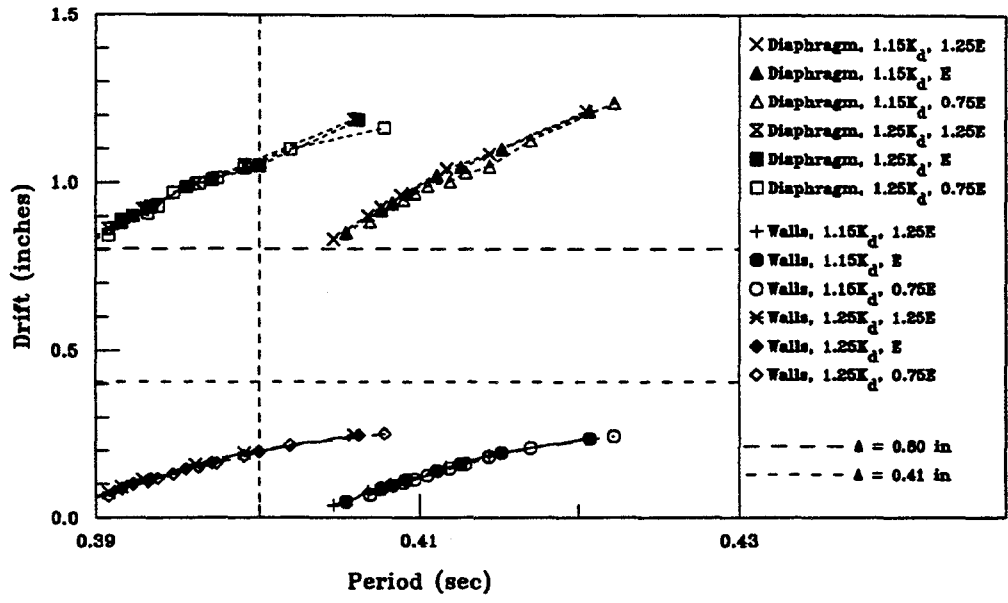
Figure 5.11 Sensitivity of maximum dynamic drifts at the roof level predicted with the discrete model to the variability of the stiffnesses of the walls (E–W)
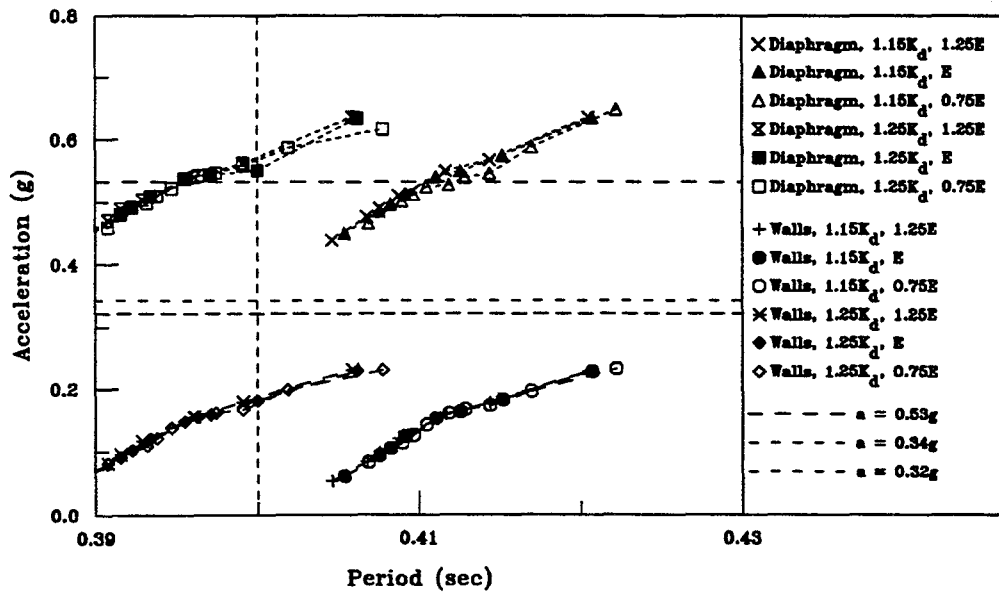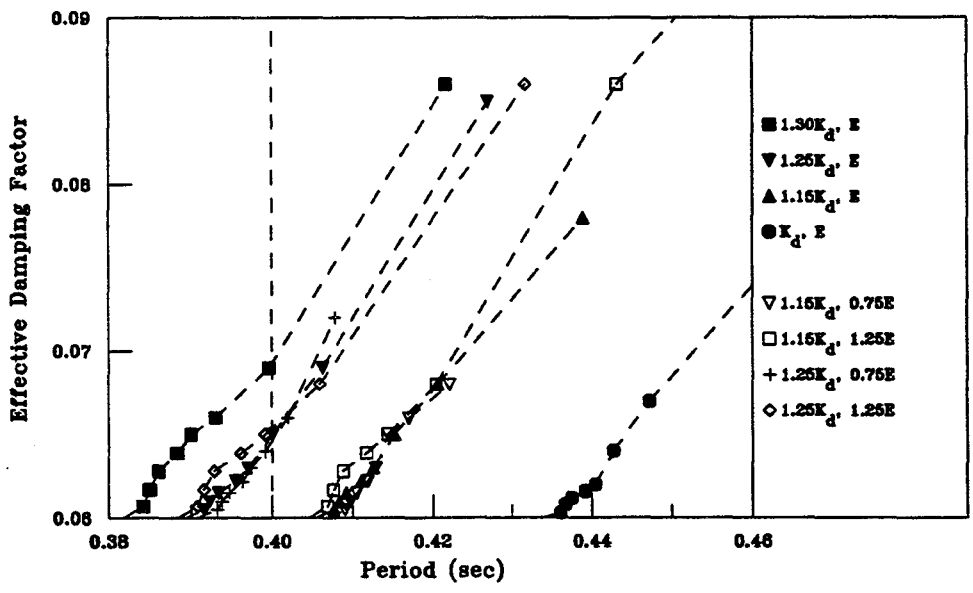
Figure 5.12 Effective damping factors used for the sensitivity studies in the E–W direction expressed as function of the natural period of the discrete models
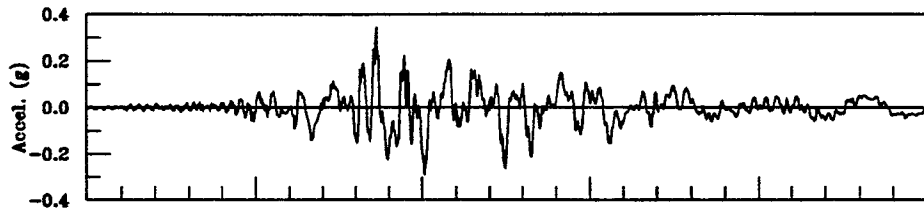
a) Recorded accelerogram at the north wall at the roof level (sensor 4)
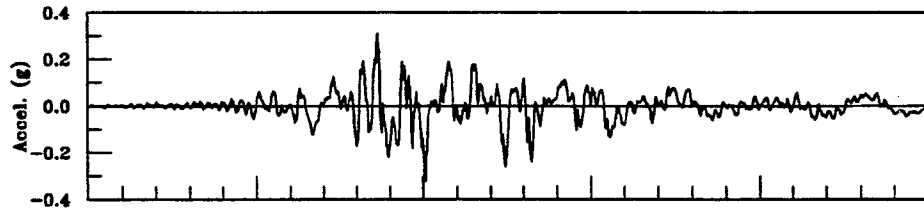
b) Recorded accelerogram at the south wall at the roof level (sensor 6)
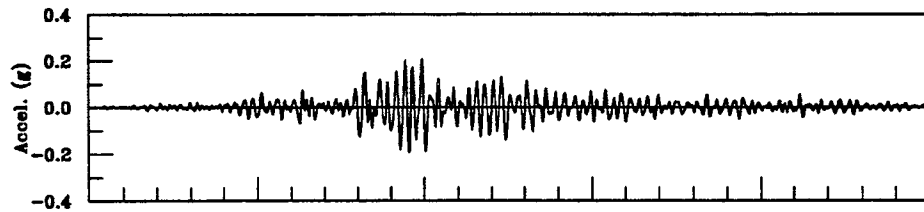
c) Predicted accelerogram at the south and north walls at the roof level (discrete model)
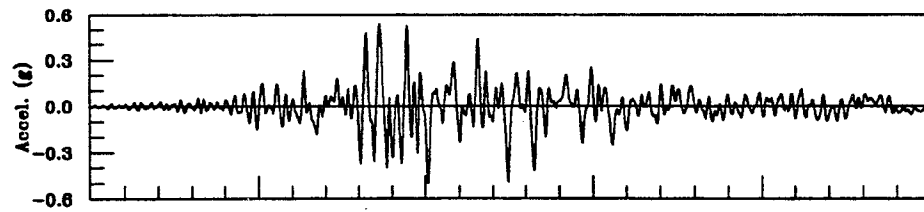
d) Recorded accelerogram at the diaphragm at the roof level (sensor 5)
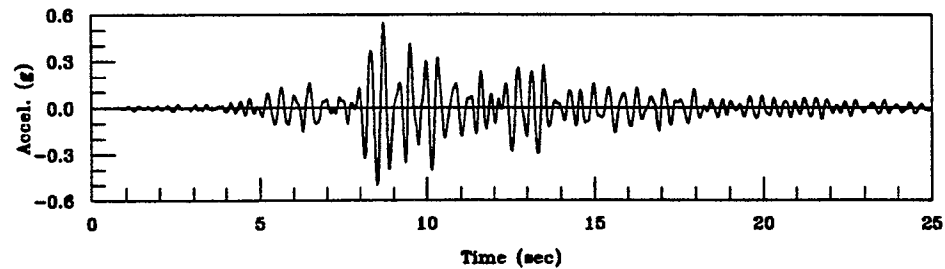
e) Predicted accelerogram at the diaphragm at the roof level (discrete model)

Figure 5.13 Recorded vs predicted accelerations in the E–W direction

81
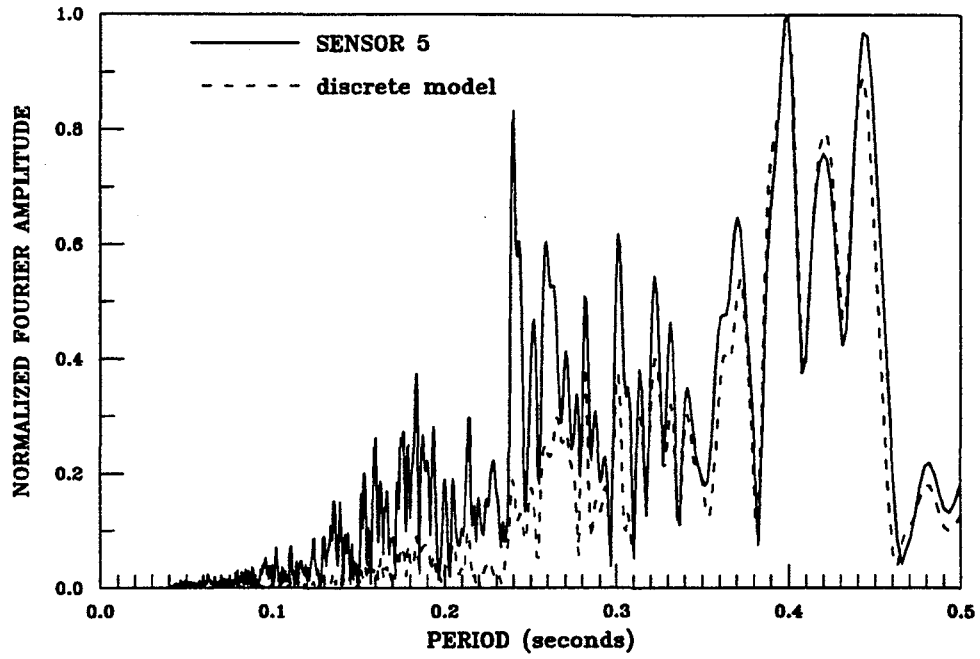
Figure 5.14 Normalized Fourier amplitude spectra for the diaphragm (E–W)

Figure 5.15 Normalized Fourier amplitude spectra for the walls (E–W)

1st and 2nd Mode   Third Mode   Fourth Mode

Fifth Mode   Sixth Mode   Equivalent system
(DOF = in-plane action)
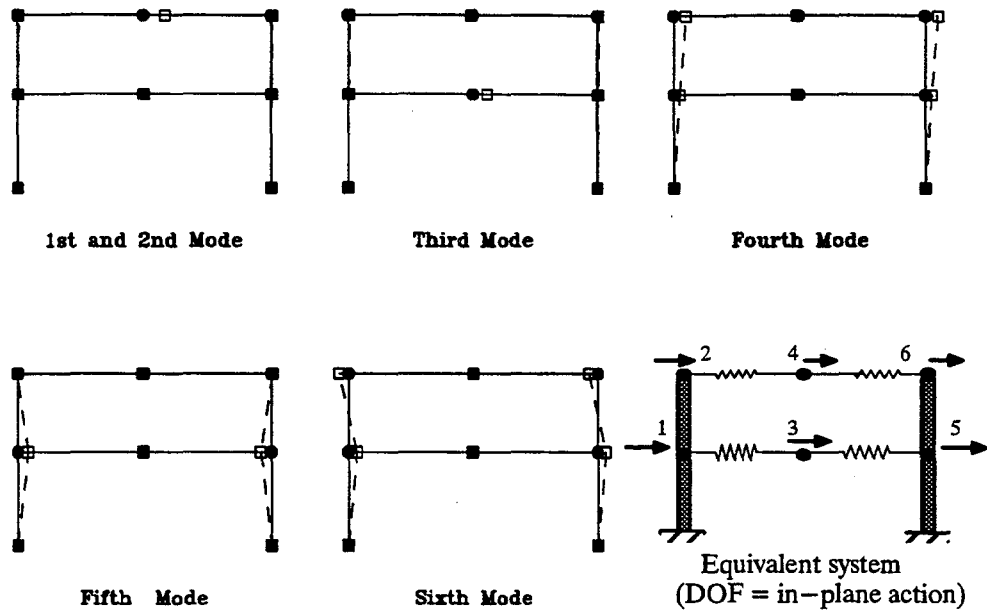
Figure 5.18 Schematic representation of the mode shapes for the fixed–base discrete model
of the building in the N–S direction

1st and 2nd Mode   Third Mode   Fourth Mode

Fifth Mode   Sixth Mode   Equivalent system
(DOF = in-plane action)
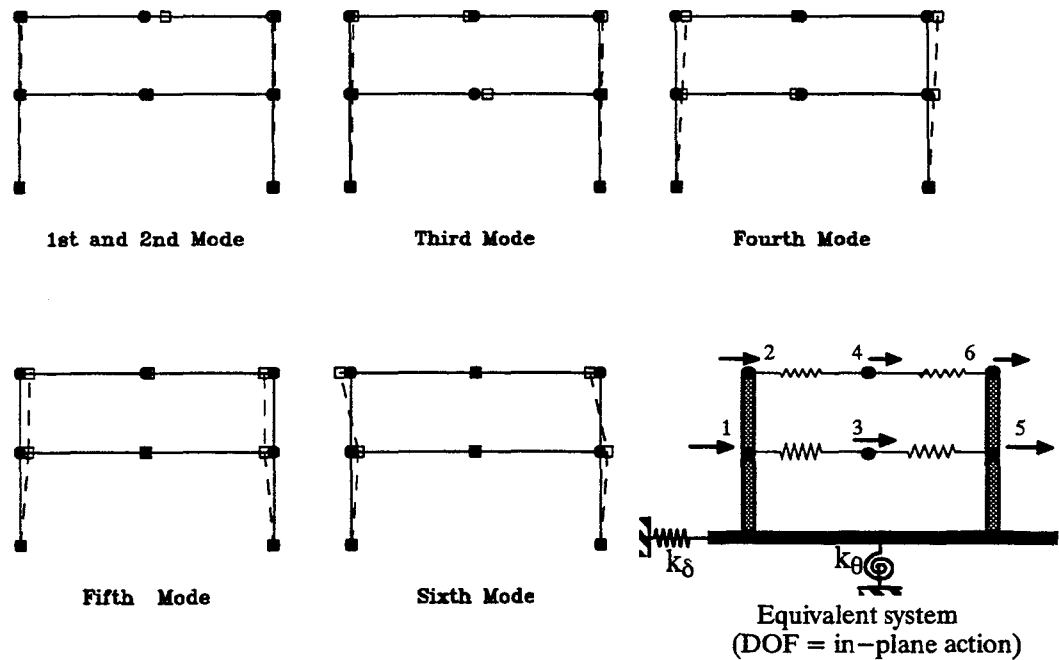
Figure 5.19 Schematic representation of the mode shapes for the flexible–base discrete model
of the building in the N–S direction
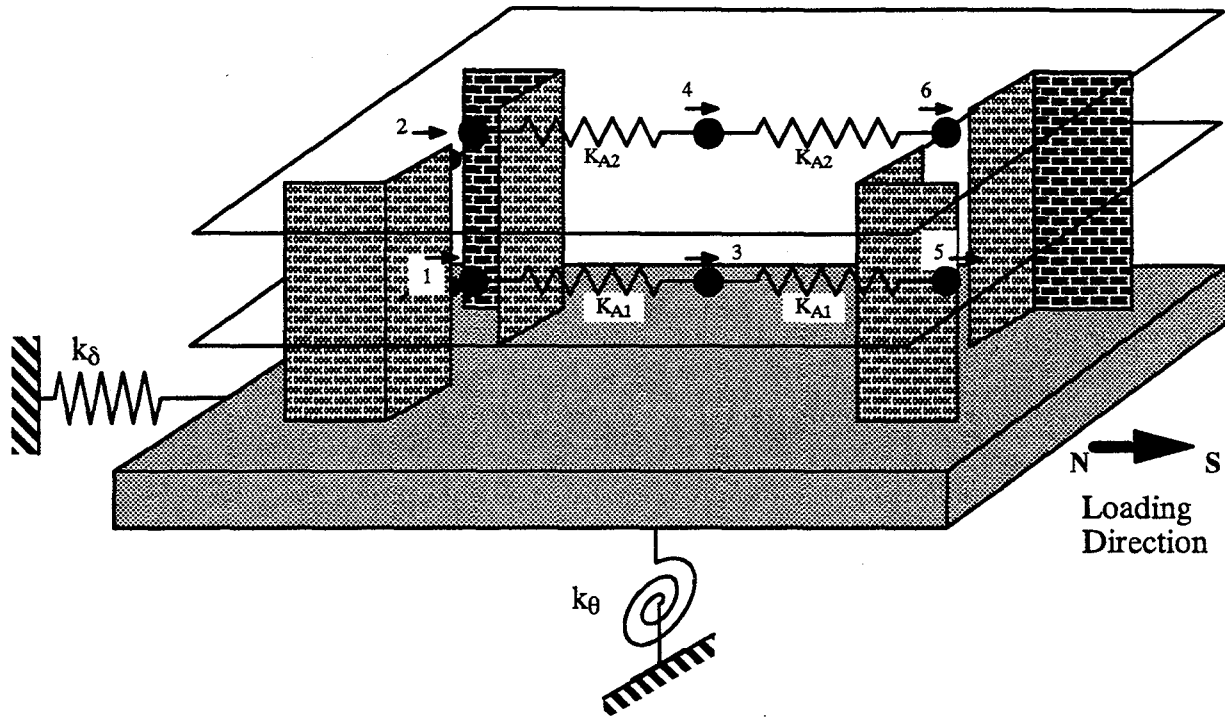
Figure 5.16 Discrete MDOF dynamic model considering soil−structure interaction
for the N−S direction
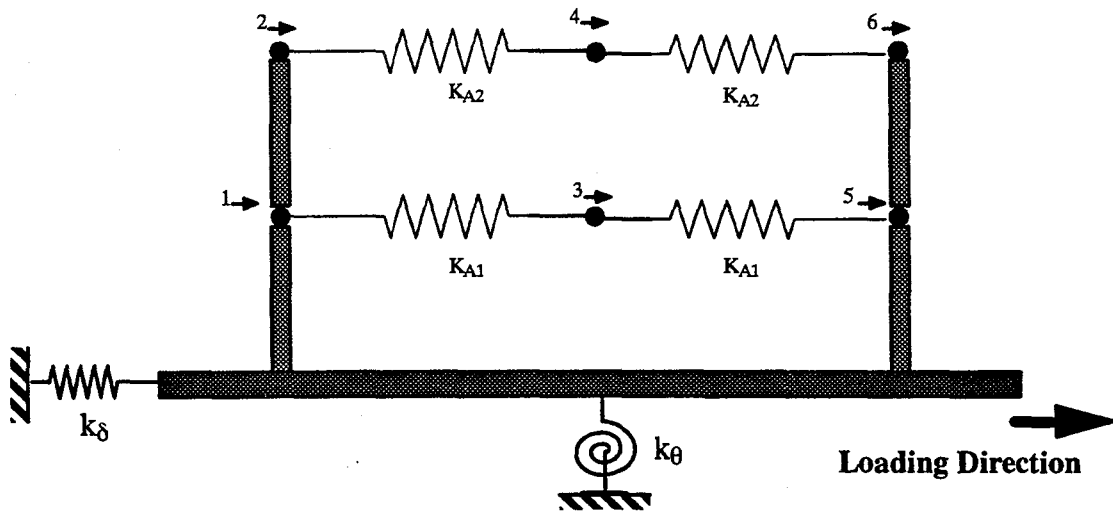
Figure 5.17 Schematic representation of the discrete MDOF dynamic model of Fig. 5.16
as an equivalent system of condensed beam elements and elastic springs
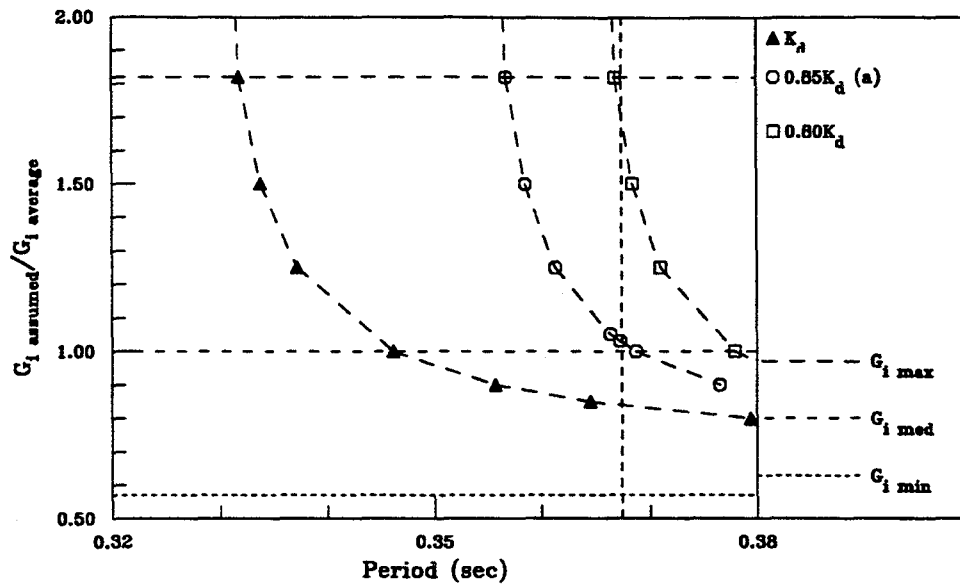
Figure 5.20 Sensitivity of the natural period of the discrete model with respect to the variability of the stiffnesses of the soil and the diaphragms (N–S direction)
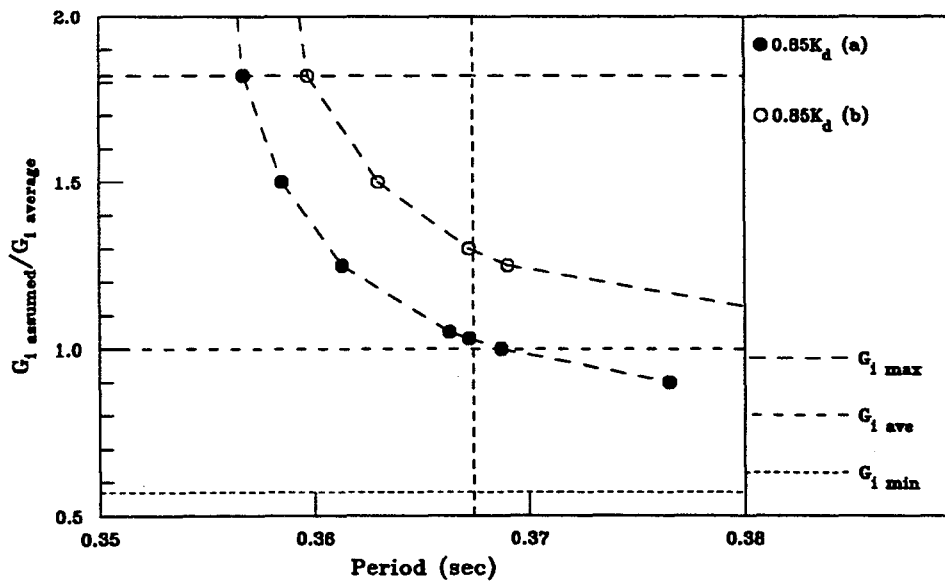
Figure 5.21 Sensitivity of the natural period of the discrete model with respect to the variability of the stiffness of the soil and the walls (N–S direction)
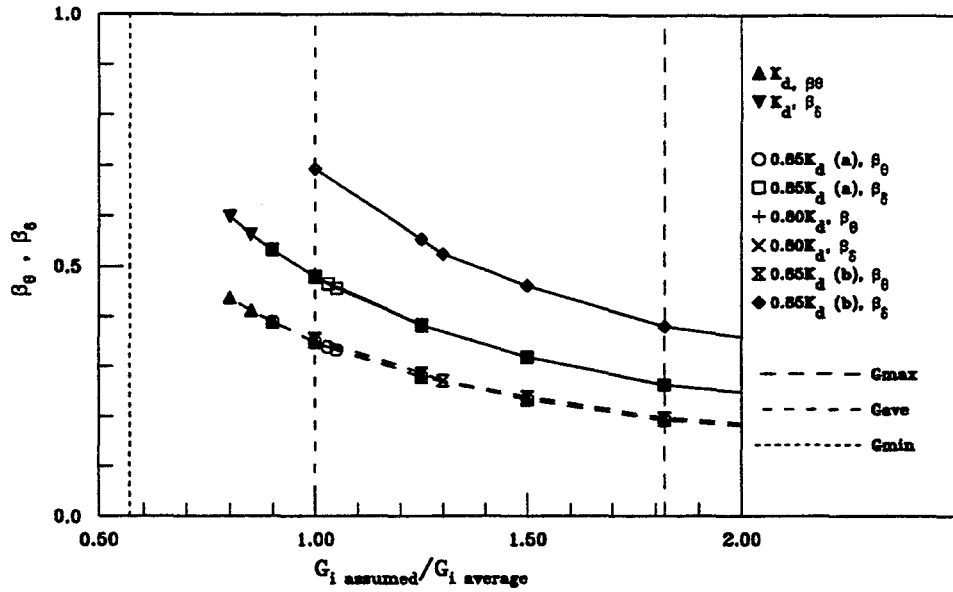
Figure 5.22 Sensitivity of the soil–structure interaction parameters β_θ and β_δ to the variability of the stiffnesses of the soil, walls and diaphragms (N–S)
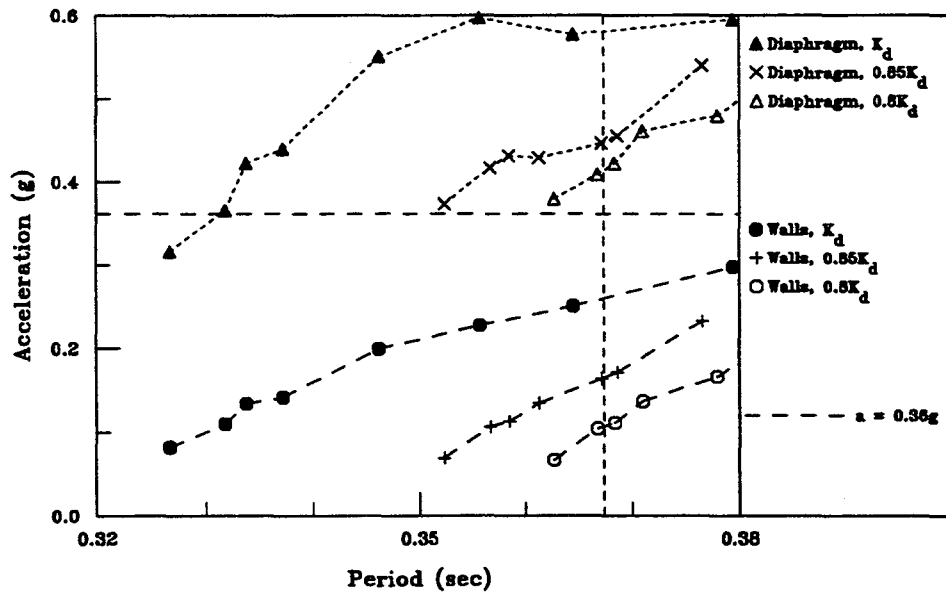
Figure 5.23 Sensitivity of peak accelerations at the roof level predicted with the discrete model to the variability of the stiffness of the diaphragms (N–S direction)
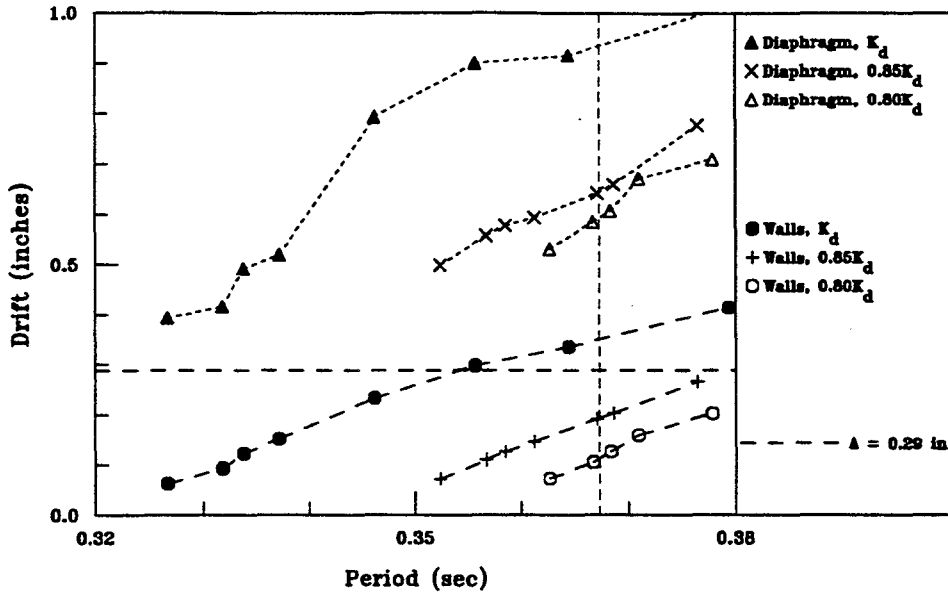
Figure 5.24 Sensitivity of maximum dynamic drifts at the roof level predicted with the discrete model to the variability of the stiffnesses of the diaphragms (N–S)
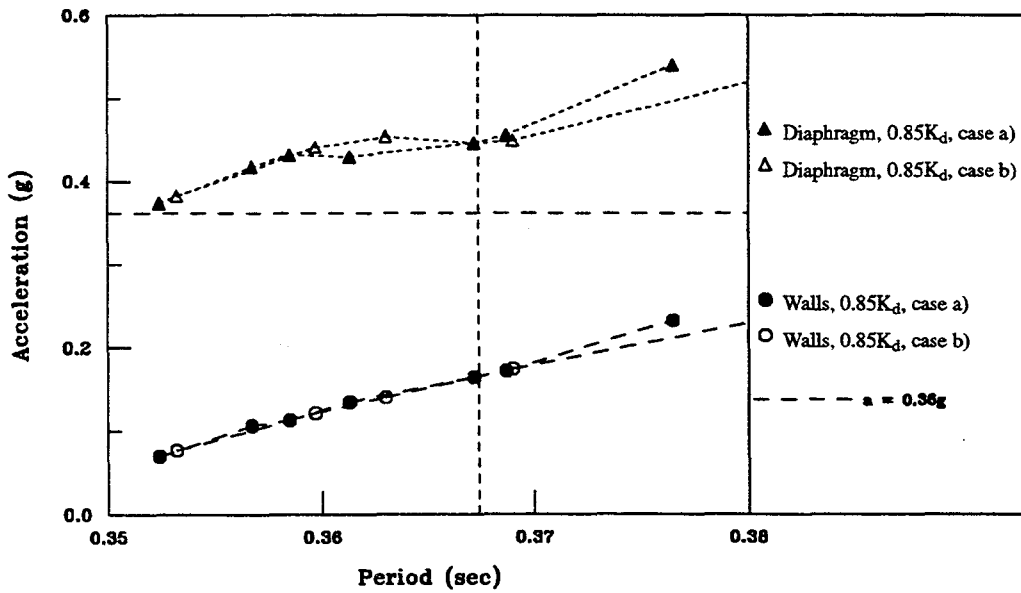
Figure 5.25 Sensitivity of peak accelerations at the roof level predicted with the discrete model to the variability of the stiffnesses of the walls (N–S)

87
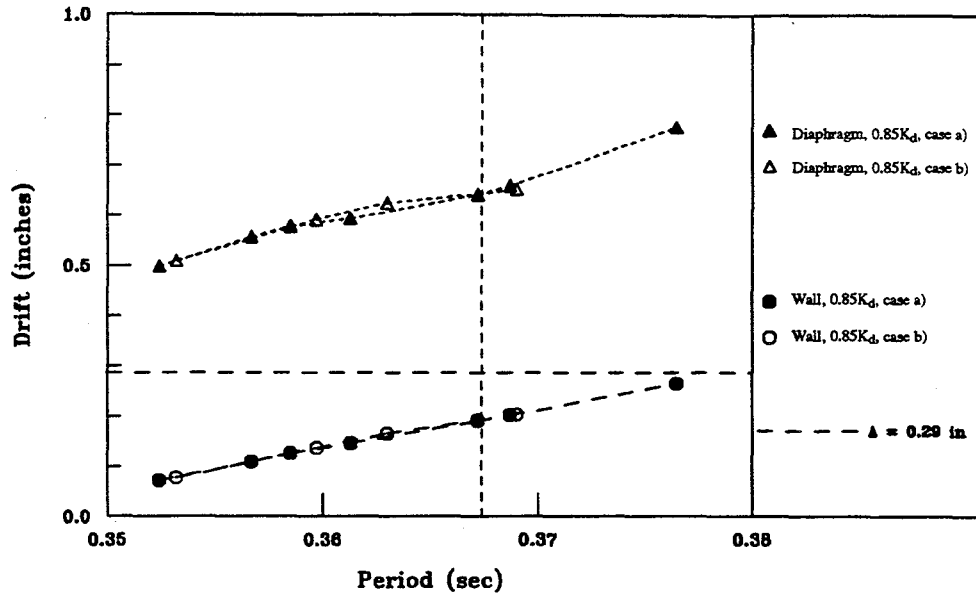
Figure 5.26 Sensitivity of maximum dynamic drifts at the roof level predicted with the discrete model to the variability of the stiffnesses of the walls (N–S)
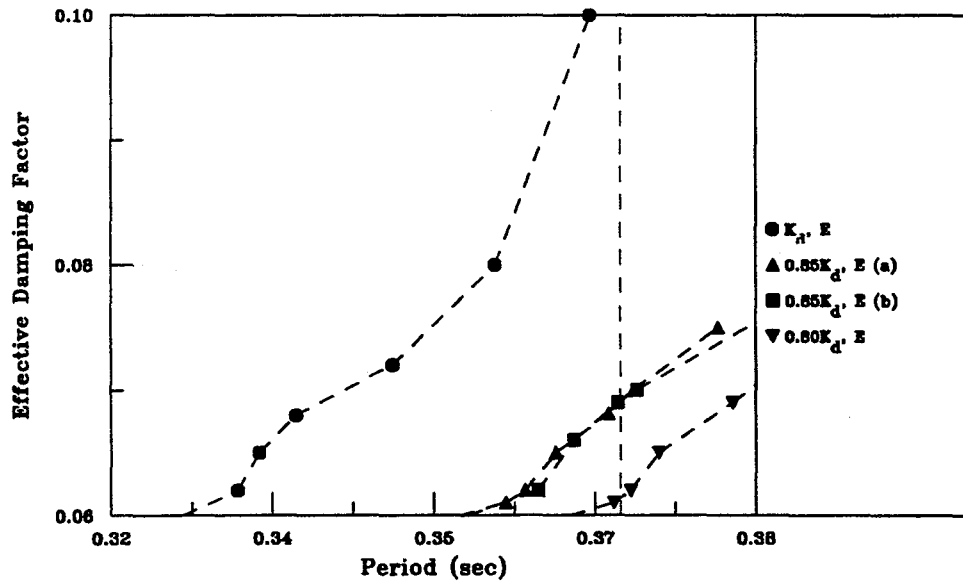
Figure 5.27 Effective damping factors used for the sensitivity studies in the N–S direction expressed as function of the natural period of the discrete models
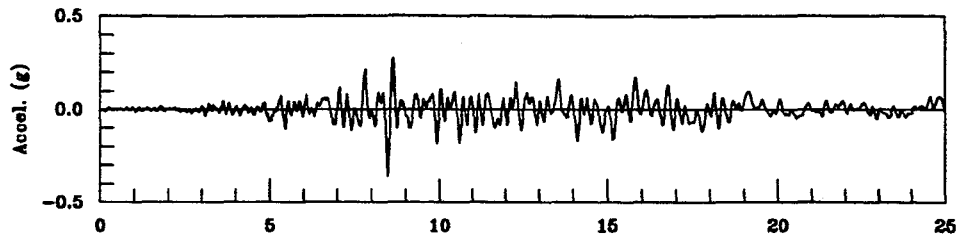
a) Recorded accelerogram at the diaphragm at the roof level (sensor 7)
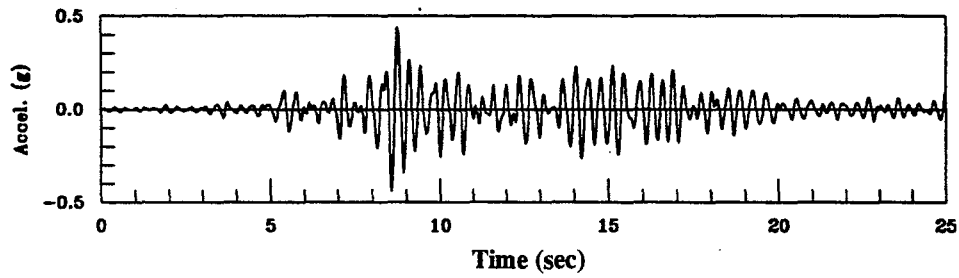
b) Predicted accelerogram at the diaphragm at the roof level (discrete model)

Figure 5.28 Recorded vs predicted accelerations in the N–S direction

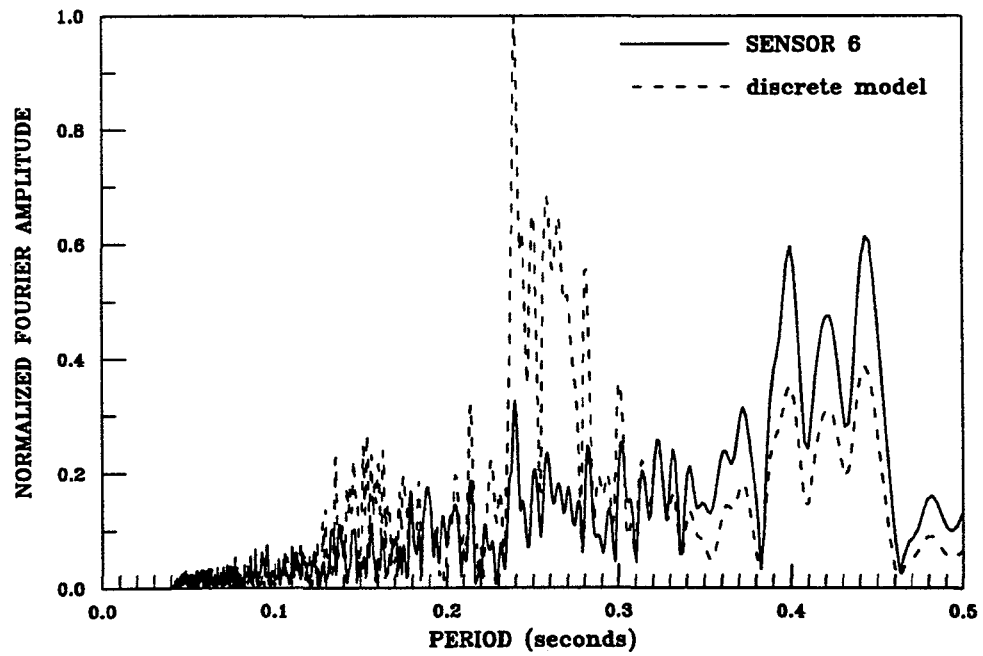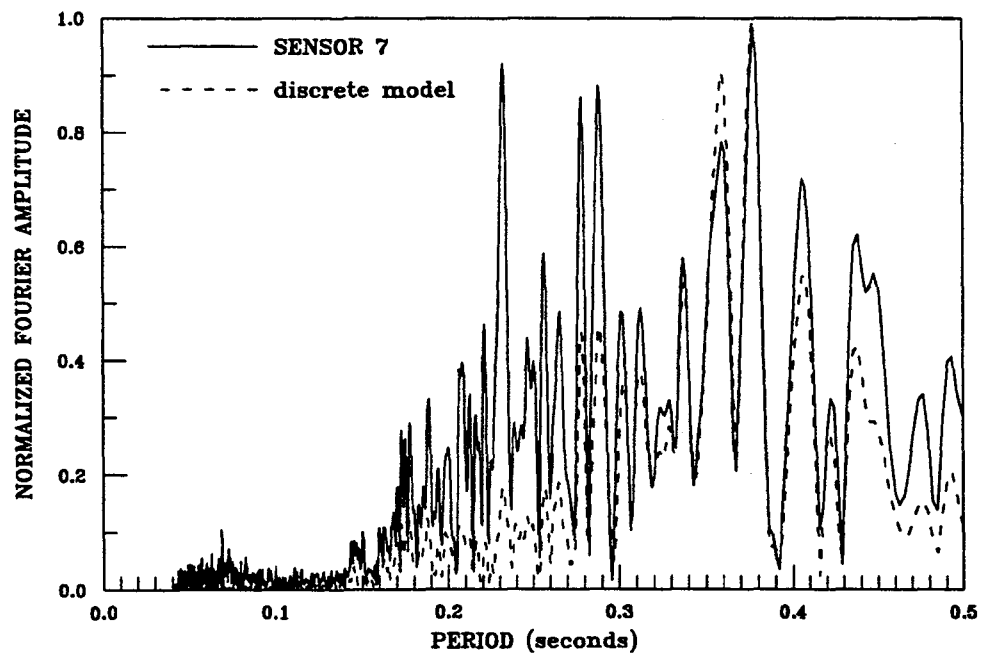Figure 5.29 Normalized Fourier amplitude spectra for the diaphragm (N–S)

89

CHAPTER 6
CORRELATION OF MEASURED RESPONSE
WITH CODE ESTIMATES

Estimates of dynamic responses offered by state−of−the−art seismic codes such as the 1988 UBC code (Ref. 16) and the NEHRP provisions (Refs. 21, 22) and the dynamic response measured at the instrumented two−story office building at Palo Alto are compared to assess the effectiveness of those provisions in the evaluation of the response of this particular case of study. It is beyond the scope of this work to evaluate the validity of those code provisions for masonry structures with flexible diaphragms. However, some valuable insight can be obtained from this comparison. The measured dynamic responses of interest are : 1) natural period; 2) maximum lateral drift; and, 3) base shear. The correlation between the measured response with this code estimates are presented in the following sections.

6.1 Natural Period

The measured natural periods of the building determined from the Fourier amplitude spectra of the recorded roof motions (Chapter 3) were 0.40 seconds in the E−W direction and 0.367 seconds in the N−S direction. These periods are relatively long for a two−story building, and they are a direct consequence of the flexibility of the diaphragms, especially the roof diaphragm. Most seismic codes do not differentiate structural systems with flexible diaphragms from those with rigid diaphragms to estimate the natural period of the structure. This can be misleading and dangerous for current engineering practice. Therefore, it might be interesting to establish a comparison between these periods and the estimates obtained from recommendations of current seismic codes.

6.1.1 1988 UBC Code

The provisions to estimate the structure period of the 1988 UBC code are contained in Section 2312(e)2B (Ref. 16). Two different methods are presented. Method A is an approximate

method intended for all buildings, and the period estimation is given by Equation 12–3 of the UBC code, which is :

$$T = C_t \, (h_n)^{\frac{3}{4}} \qquad \qquad \text{... 6.1)}$$

where :

T = fundamental period of vibration, in seconds, of the structure in the direction under consideration.

h_n = height of the building.

C_t = numerical coefficient which depends on the type of structural system.

The value of C_t for structures with masonry shear walls may be computed as :

$$C_t = \frac{0.1}{\sqrt{A_c}} \qquad \qquad \text{... 6.2)}$$

where A_c is the combined effective area, in square feet, of the shear walls in the first story of the structure. The value of A_c shall be determined from Equation 12–4 of the UBC code, which is :

$$A_c = \Sigma A_e \left[0.2 + \left(\frac{D_e}{h_n} \right)^2 \right] \qquad \qquad \text{... 6.3)}$$

where :

A_e = the minimum cross–sectional shear area in any horizontal plane in the first story, in square feet, of a shear wall.

D_e = the length, in feet, of a shear wall in the first story in the direction parallel to the applied forces.

The value of (D_e/h_n) used in Equation 6.3 shall not exceed 0.9. Method A of the UBC code makes no distinction between rigid diaphragms building systems and flexible diaphragms building systems. Therefore, the procedure could be indistinctly used to estimate the natural

period of two structural systems which behave completely different. The UBC formulation was based upon experimental data from structural systems with rigid diaphragms. Thus, good correlations with the identified natural periods of the building cannot be expected.

Estimates of the fundamental periods of the building in both the E−W and the N−S direction were obtained according to Method A of the UBC code and the geometry of the structure presented in Figs. 2.1 to 2.3. The estimated fundamental periods according to the 1988 UBC Method A were 0.30 seconds for the E−W direction and 0.21 seconds for the N−S direction. These estimates correlated poorly with the identified natural period of the structure in both directions, but they were closer than what it was found in a recent study (Ref. 33). The estimates correlated very poorly for an hypothetical case where the diaphragms of the building were rigid and a fixed based condition existed. This was not expected, and is in complete disagreement to what was observed in a recent study (Ref. 33). The fundamental periods of vibration for such a hypothetical structure would be 0.13 seconds for the E−W direction and 0.15 seconds for the N−S direction (Tables 5.4 and 5.8). Method A seems unreliable to estimate the natural period of shear wall structures with flexible or rigid diaphragms.

Method B of the UBC code to estimate the natural period of a building structure is based on Rayleigh quotient. In Method B, the fundamental period is calculated using the structural properties and deformational characteristics of the resisting elements in a properly substantiated analysis, according to Equation 12−5 of the code :

$$T = 2\pi \sqrt{\frac{\sum_{i=1}^{n} w_i \delta_i^2}{g \sum_{i=1}^{n} f_i \delta_i}} \qquad \qquad ... 6.4)$$

where :

w_i = that portion of the total seismic load which is located at or assigned to level i respectively.

δ_i = horizontal displacement at level i relative to the base due to applied lateral forces, f_i.

f_i = lateral force at level i.

g = acceleration due to gravity.

Method B can be applied to any structural system and it shall render reasonable estimates of the natural period if an appropriate model of the structure under study is carried out. In order to evaluate this method, the estimates for the natural periods of the firehouse in both directions were obtained from Equation 6.4 and the results given by the discrete models presented in Chapter 5. These values are presented in Tables 6.1 and 6.2.

Table 6.1 Data obtained from the discrete model of Fig. 5.1 to estimate the natural period of the building in the E−W direction using Equation 6.4				
DOF	Mass ($lb-sec^2/in$)	acceleration (g)	Static lateral force (kips)	Static lateral displacement (in)
1	1014.50	0.16	63.6	0.17
2	457.33	0.18	33.2	0.20
3	1017.52	0.40	197.1	0.38
4	468.90	0.50	99.8	1.04
5	1014.50	0.16	63.6	0.17
6	457.33	0.18	33.2	0.20

For the discrete model in the E−W direction (Fig. 5.1), the accelerations predicted at the time of peak response were used to compute the lateral forces and the horizontal displacements, δ_i. These data are presented in Table 6.1. The estimated natural period in the E−W direction based upon the data of Table 6.1 and Equation 6.4 was 0.37 seconds. This period corresponds is 7.5% shorter than the identified natural period obtained from the Fourier amplitude spectra of the roof records in the E−W direction.

For the discrete model in the N−S direction (Fig. 5.16), the accelerations predicted at the time of peak response were used to compute the lateral forces and the horizontal displacements, δ_i. These values are presented in Table 6.2. The estimated natural period in the N−S direction computed from the data of Table 6.2 and Equation 6.4 was 0.35 seconds, which is very close to the natural period of 0.367 seconds identified for the N−S direction (4.6% shorter).

Table 6.2 Data obtained from the discrete model of Fig. 5.16 to estimate the natural period of the building in the N−S direction using Equation 6.4				
DOF	Mass $(\text{lb}-\text{sec}^2/\text{in})$	acceleration (g)	Static lateral force (kips)	Static lateral displacement (in)
1	1014.50	0.11	41.8	0.13
2	457.33	0.16	29.0	0.20
3	1017.52	0.40	158.4	0.37
4	468.90	0.45	80.8	0.64
5	1014.50	0.11	41.8	0.13
6	457.33	0.16	29.0	0.20

According to these results, Method B of the 1988 UBC code to estimate the natural period of a building structure renders a good correlation for this case of study. This might be an indication of the utility of Method B for any building structure provided that appropriate hypothesis are made during the analysis of the structure. A good correlation was possible because the proposed discrete model represented reasonably well the overall behavior of the building at Palo Alto. If a model that cannot consider the flexibility of the diaphragms and/or soil−structure interaction would have been used, then, a poorer correlation would have been obtained. The accuracy of Method B depends on the applicability of the selected model to the structure under study.

6.1.2 NEHRP Provisions

The National Earthquake Hazards Reduction Program (NEHRP) recommend provisions for the development of seismic regulations for new buildings (Refs. 21, 22). The provisions to determine the fundamental period of a structure are contained in Section 4.2.2 of this provisions. The NEHRP provisions establish that the estimate of the natural period of the building shall be based upon established methods of mechanics and the properties of the structural system in the direction of analysis, and it makes the assumption that the base of the building is fixed. The natural period computed with this method shall not exceed:

$$T \leq C_a T_a \qquad \qquad ... 6.5)$$

where :

T = the fundamental period of the building.

T_a = the approximate fundamental period of the building.

C_a = coefficient for upper limit on calculated period (Table 4−A, Ref. 21).

Alternatively, the fundamental period may be taken equal to the approximate fundamental period of the building, T_a. For moment−resisting structures, the approximate fundamental period, T_a, is determined according to Equation 6.1, which is the same criterion issued by the 1988 UBC code. For all other buildings, T_a is computed as :

$$T_a = 0.05 \frac{h_n}{\sqrt{L}} \qquad \qquad ... 6.6)$$

where :

h_n = the height in feet above the base to the highest level of the building.

L = the overall length of the building, in feet, at the base in the direction being analyzed.

Equations 6.5 and 6.6 were used to estimate the fundamental period of the firehouse in both directions. The coefficient for upper limit on the calculated period, C_a, was equal to 1.2,

according to Table 4−A of Ref. 21. The computed natural periods for the building were 0.16 seconds for the E−W direction and 0.12 seconds for the N−S direction. The estimated fundamental periods correlated poorly with the identified natural periods of 0.40 and 0.367 seconds for the E−W and N−S direction respectively. A good correlation could not be expected because Equation 6.6 is in essence a simplistic procedure expressed in function of general geometric measurements, based upon a reduced set of experimental data for reinforced concrete shear wall buildings (Ref. 22). Equation 6.6 can be expected to provide underestimated values of periods of vibration for other building types (Ref. 22). However, considering it for a first, quick, and crude approximation to estimate the natural period of a shear (bearing) wall building structure, Equation 6.6 is somewhat useful.

Soil−structure interaction effects are also taken into account by the NEHRP provisions. In fact, the recommendations are entirely based on the ATC 3−06 provisions (Ref. 3). The effective fundamental period of the building can be determined with Equation 6−3 of both provisions (Refs. 3, 21) as follows :

$$\tilde{T} = T \sqrt{1 + \frac{\bar{k}}{k_y}\left(1 + \frac{k_y \bar{h}^2}{K_\theta}\right)} \qquad \text{... 6.7)}$$

where :

$\tilde{T}$ = the effective fundamental period of the building.

T = the fundamental period of the fixed−base building.

$\bar{k}$ = the stiffness of the building when fixed at the base.

$\bar{h}$ = the effective height of the building which shall be taken as 0.7 times the total height, h_n, except that for buildings where the gravity load is effectively concentrated at a single level, it shall be taken as the height to that level.

k_y = the lateral stiffness of the foundation, defined as the static horizontal force at the level of the foundation necessary to produce a unit deflection at that level, the force and the deflection being measured in the direction in which the

structure is analyzed.

k_θ = the rocking stiffness of the foundation, defined as the static moment necessary to produce a unit average rotation of the foundation, the moment and rotation being measured in the direction in which the structure is analyzed.

The foundation stiffnesses k_y and k_θ shall be computed by established principles of foundation mechanics. The stiffness of the building when fixed at the base is defined by Equation 6−4 of both provisions (Refs. 3, 21) as follows :

$$\overline{k} = 4\pi^2\left(\frac{\overline{W}}{gT^2}\right) \qquad \ldots 6.8)$$

where :

$\overline{W}$ = the effective gravity load of the building.

g = the acceleration due to gravity.

Estimates of the effective natural period in both directions were obtained using Equation 6.7 and the data provided by the discrete models that showed the best correlation with the identified structure (Chapter 5). The effective gravity load of the building was considered as the estimated total weight of the building (1,830. kips). The effective height of the building was defined as 16.8'. Using the discrete model of Fig. 5.1, the estimated natural period for the fixed−base building for the E−W direction was 0.39 seconds. The associated lateral and rocking stiffnesses of the foundation, k_y and k_θ, were estimated as 8,524 k/in and 5.462×10^9 k−in/rad respectively. These values were obtained for the discrete model with the best correlation. Then, the effective fundamental period of the firehouse in the E−W direction computed according to Equation 6.7 was 0.42 seconds. This estimated period is 4.5% higher than the identified natural period the building in the E−W direction (0.40 seconds).

For the N−S direction, the estimated natural period for the fixed−base building was 0.35 seconds. This estimation was obtained from the discrete model presented in Fig. 5.16. The associated lateral and rocking stiffnesses of the foundation, k_y and k_θ, were estimated as

30,427 k/in and 9.500×10^8 k−in/rad respectively. These values were obtained for the discrete model with the best correlation. The effective fundamental period of the firehouse in the N−S direction computed according to Equation 6.7 was 0.37 seconds, that is, equal to the identified natural period of the building in the N−S direction of 0.37 seconds.

The computed effective natural periods with Equation 6.7 correlated well with the identified natural periods of the building. Equation 6.7 constitutes a more sophisticated procedure to estimate the natural period of a building structure, and it requires more detailed information. Equation 6.7 was developed from analyses in which the structure is assumed to respond in its fixed−base fundamental mode, and it considers the foundation weight to be negligible in comparison to the weight of the structure (Refs. 3 and 22).

6.2 Drift Limits

The maximum dynamic in−plane drift of the building between the walls at the roof level and the base obtained from the recorded motions was 0.41 inches (E−W direction, Chapter 3). This drift is compared to the established limits given by the recommendations of current seismic codes.

6.2.1 1988 UBC Code

The story drift limitations of the 1988 UBC code are contained in Section 2312(e)8 of the code (Ref. 16). Calculated drifts shall include translational and torsional deflections. The code establishes that for buildings less than 65 feet in height, such as the instrumented building at Palo Alto, the calculated story drift δ shall not exceed :

$$\delta \leq \frac{0.04h}{R_w} \qquad \qquad ... 6.9)$$

nor :

$$\delta \leq 0.005h \qquad \qquad ... 6.10)$$

where :

R_W = numerical coefficient (response reduction modification factor).

h = story height.

These drifts limits may be exceeded when it is demonstrated that greater drifts can be tolerated by both the structural elements and non structural elements that could affect life safety. For a masonry shear wall structural system, the 1988 UBC code allows a response reduction factor R_w equal to 6 (Table No 23−O, Ref. 16). Therefore, Equation 6.10 is in this case the limiting criterion.

Considering "h" as the height of the building at the roof level, with value of 24', the maximum dynamic drift experienced at the central wall at the roof level as $0.0014h$ (E−W direction). Therefore, the maximum dynamic drift at the walls was within the allowable limits of the 1988 UBC code despite of the significant amount of diaphragm action observed at the building. The dynamic story drifts at the first and the second stories should have been under these limits for all walls as a consequence.

6.2.2 NEHRP Provisions

The deflections and drift limits of the NEHRP provisions are addressed in their Section 3.8 (Ref. 21). It is stated that the story drift, Δ, shall not exceed the allowable limit Δ_a as obtained from Table 3−C of the provisions for any story. For seismic hazard exposure group III of the provisions (buildings having essential facilities that are necessary for post earthquake recovery, category that applies for the instrumented building at Palo Alto), the allowable story drift limit Δ_a is :

$$\Delta_a = 0.010 h_{sx} \qquad \text{... 6.11)}$$

and for hazard exposures groups I and II the allowable story drift limit is increased by 50% :

$$\Delta_a = 0.015 h_{sx} \qquad \text{... 6.12)}$$

where :

99

h_{sx} = story height below level x.

If we take the height of the building at the roof level as h_{sx} with a value of 24', the maximum dynamic drift experienced at the central wall at the roof level of $0.0014h_{sx}$ (E−W direction) will fall well below the allowable limits of the NEHRP provisions (Equations 6.11 and 6.12). Dynamic story drifts for all walls at the first and the second stories should have been below these limits as well. It can be concluded that the maximum dynamic drift at the building is consistent with the extent of damage observed and with the prescribed code limits.

6.3 Design Base Shear

Computed base shears obtained based upon the recorded peak accelerations and statics are compared to those which would be estimated by the recommendations of current seismic codes.

6.3.1 1988 UBC Code

The total design base shear in a given direction shall be determined according to Section 2312(e)2A and from Equation 12−1 of the code (Ref. 16) :

$$V = \frac{ZIC}{R_w} W \qquad \qquad ...6.13)$$

where :

V = total base shear.

W = total seismic dead load.

Z = seismic zone factor.

I = importance factor.

R_w = numerical coefficient (response reduction factor).

C = numerical coefficient.

The numerical coefficient C defines the design spectra shape based upon the period range and the soil type under consideration, and is defined in Equation 12−2 of the code written below:

100

$$C = \frac{1.25S}{T^{2/3}} \qquad \qquad \text{... 6.14)}$$

where :

> S = site coefficient for soil characteristics.
>
> T = fundamental period of vibration, in seconds, of the structure in the direction under consideration.

The value of the numerical coefficient C need not to exceed 2.75 and may be used for any structure regardless of the soil type or structure period, and the minimum value of the ratio C/R_w shall be 0.075 (Ref. 16).

Design base shears for the building in both the E−W and N−S directions were estimated from Equations 6.13 and 6.14. The fundamental periods of vibration used in Equation 6.14 were those computed from Method A and Method B of the code as presented in Section 6.1.1. Site coefficient for soil characteristics, S, was identified as type S_2 (Table No 23−J, Ref. 16) and taken as 1.2. Palo Alto, California, is located in zone 4 of the seismic zone map. Then, the seismic zone factor Z was taken as 0.4 (Table No 23−I, Ref. 16). The response reduction factor R_w for a masonry shear wall structural system is equal to 6 according to the 1988 UBC code (Table No 23−O, Ref. 16). The importance factor I for special occupancy facilities is 1.00 (Table No 23−L, Ref. 16). The total weight of the structure was 1,830 kips.

Computed design base shears under these assumptions are presented in Table 6.3, where they are compared to those maximum base shears based upon the peak accelerations recorded at the structure. In this particular case, the underestimation of the structural period from Method A does not have an impact in the determination of the design base shear as compared to the more accurate Method B. The reason of this it that both computed structural periods fall within the flat area of the design response spectra of the UBC code (short period range).

Table 6.3 Estimated 1988 UBC design base shears vs computed maximum base shears from recorded motions					
Loading Direction	Structure Period		C	UBC Code Design Base Shear	Computed Base Shear
	Method	T (sec)			
E−W	A	0.30	2.75	0.18W	0.32W
E−W	B	0.37	2.75	0.18W	0.32W
N−S	A	0.21	2.75	0.18W	0.28W
N−S	B	0.35	2.75	0.18W	0.28W

In the E−W direction, the design base shears computed according to the UBC code were 1.78 times smaller than those computed base shears from the recorded motions. In the same fashion, the design base shears computed in the N−S direction according to the UBC code were smaller than to those computed base shears from the recorded motions (about 1.56 times smaller). This is a direct consequence of using a response modification factor of 6 for this type of structures, that could be high and no conservative. It is beyond the scope of this work to assess suitable response modification factors for reinforced grouted brick shear wall systems with flexible diaphragms.

6.3.2 NEHRP Provisions

For the NEHRP provisions, the design seismic base shear in the direction of analysis of a building considered to be fixed at the base, shall be determined according to Section 4.2 and from Equation 4−1 of the provisions (Ref. 21) :

$$V = C_s W \qquad\qquad ... 6.15)$$

where :

V = design seismic base shear in the direction being analyzed.

C_s = seismic design coefficient.

W = total gravity load of the building.

W shall be taken equal to the total weight of the structure and applicable portions of other components (Ref. 22). The value of the seismic design coefficient C_s may be determined in accordance with Equations 4−2, 4−3 or 4−3a of the provisions, as appropriate. Equation 4−2 written below requires calculation of the fundamental period of the building :

$$C_s = \frac{1.2A_vS}{RT^{2/3}} \qquad \text{... 6.16)}$$

where :

A_v = coefficient representing effective peak velocity−related acceleration.

S = coefficient for the soil profile characteristics of the site.

R = response modification factor.

T = fundamental period of the building in the direction being analyzed.

To account for the effects of soil−structure interaction, the base shear determined from Equation 6.15 may be reduced according to Equations 6−1 and C6−7 of the NEHRP provisions to :

$$\tilde{V} = V - \Delta V \qquad \text{... 6.17)}$$

$$\Delta V = \left[C_s - \bar{C}_s \left(\frac{\beta}{\tilde{\beta}} \right)^{0.4} \right] \overline{W} \qquad \text{... 6.18)}$$

where :

$\tilde{V}$ = reduced seismic base shear, which shall in no case be taken less than $0.7V$.

ΔV = reduction on the seismic base shear to account for soil−structure interaction effects.

C_s = seismic design coefficient computed from Equation 6.16 using the fundamental period of the fixed−base structure.

$\tilde{C}_s$ = seismic design coefficient computed from Equation 6.16 using the fundamental period of the flexibly supported structure.

β = fraction of critical damping for the structure alone.

$\tilde{\beta}$ = fraction of critical damping for the structure−foundation system.

$\overline{W}$ = effective gravity load of the building, which shall be taken as $0.7W$, except that for buildings where the gravity load is concentrated at a single level, it shall be taken equal to W.

Design base shears for the building for the E−W and N−S directions were estimated from Equations 6.15 to 6.18. The fundamental periods of vibration used were those computed from Equations 6.5 and 6.7 for the fixed−base and flexibly supported cases (Section 6.1.2). The coefficient for the soil profile characteristics of the site, S, was identified as type S_2 (Table 3−A, Ref. 21) and taken as 1.2. The coefficient representing effective peak velocity−related acceleration, A_v, was defined as 0.4 for Palo Alto, California, from the seismic zone map presented in Figure 1−4 of the NEHRP provisions (Ref. 21). This coefficient also identifies a seismicity index for this zone of 4. The response reduction factor R for reinforced masonry shear wall system is equal to 3.5 according to the NEHRP provisions (Table 3−B, Ref. 21). The total weight of the structure at the base was 1,830 kips.

Computed design base shears under these assumptions are presented in Table 6.4 for the fixed−base case and in Table 6.5 for the case when soil−structure interaction is considered. A quick review of the values for the fixed−based assumption (Table 6.4), makes evident that the design base shears computed from the NEHRP provisions are overestimated in both directions with respect to the computed base shears from the recorded motions. The computed elastic design base shears from the NEHRP provisions are 1.75 times higher in the E−W direction and 2.43 times higher in the N−S direction. The NEHRP provisions are conservative for this case study. The correlation could have been better if the identified natural periods of the structure should have been used in the estimate of the design base

shears. If this is done, the design base shears according to Equation 6.15 would be 0.30W in the E−W direction (T_{EW} = 0.40 seconds) and 0.32W in the N−S direction (T_{NS} = 0.37 seconds). The response modification factor specified by the NEHRP provisions seems to be adequate for reinforced masonry shear walls according to this particular case study.

Table 6.4 Estimated NEHRP design base shears (fixed−base) vs computed base shears from the recorded motions				
Loading	Estimated Period (sec)	C_s	NEHRP Design Base Shear	Computed Base Shear
E−W	0.16	0.56	0.56W	0.32W
N−S	0.12	0.68	0.68W	0.28W

The computed reduced design base shears including soil−structure interaction are summarized in Table 6.5 . Here, the fixed−base periods considered are the ones obtained from the discrete models (Chapter 5). The design base shears for the fixed−base system under this consideration were 0.31W for the E−W direction and 0.33W for the N−S direction. The fraction of critical damping for the structure alone, β, was taken as 0.06, and the fraction of critical damping for the structure−foundation system, $\tilde{\beta}$, was taken as 0.065 for the E−W direction and 0.069 for the N−S direction. This is in agreement with the assumptions made for the best−correlation discrete models of Chapter 5. The effective gravity load of the building, $\overline{W}$, was taken as 1281 kips (0.7W).

Table 6.5 Estimated NEHRP design base shears (soil−structure interaction) vs computed base shears from the recorded motions					
Loading Direction	Estimated Period		ΔV	NEHRP Design Base Shear	Computed Base Shear
	Fixed (sec)	Flexible (sec)			
E−W	0.39	0.42	0.02W	0.29W	0.32W
N−S	0.35	0.37	0.02W	0.31W	0.28W

If soil−structure interaction was considered, the reduced computed design base shears were very much improved. The Design base shear have a very good correlation with the computed base shears from the recorded motions. The computed reduced design base shears considering soil−structure interaction effects according to the NEHRP provisions were only 1.10 times smaller in the E−W direction and 1.11 times higher in the N−S direction with respect to the computed maximum base shears from the recorded motions. Therefore the NEHRP provisions has a good correlation with what was measured. This suggest that the response modification factor R=3.5 proposed for reinforced masonry shear wall structures may be adequate for such structures.

6.4 Summary

Some observations can be highlighted from the previous comparisons made between the measured or computed dynamic response of the building in relation to estimates computed by state−of−the−art seismic codes : the UBC 1988 code (Ref. 16) and the NEHRP provisions (Refs. 21, 22).

Regarding the estimates of the fundamental structural periods, it can be concluded that the approximate formulas proposed by the 1988 UBC code and the NEHRP provisions, which are based upon experimental data and that are expressed in function of geometrical properties (Equations 6.1 and 6.5 respectively), are not necessarily suitable for masonry shear wall structures with flexible diaphragms. On the other hand, the proposed formulas to estimate the fundamental period using the structural properties and deformational characteristics of the resisting elements in a properly substantiated analysis (Equations 6.4 and 6.7) are adequate if suitable models are selected for the analysis. Similar conclusions were arrived at a recent study (Ref. 33).

The maximum dynamic drift at the walls computed from the recorded motions was under the allowable limits of both the 1988 UBC code and the NEHRP provisions. This drift is consistent with the extent of damage observed at the building.

The estimates of the design base shear by the 1988 UBC code correlated poorly with respect to those determined from the recorded motions. The response modification factor $R_W = 6$ adopted by the UBC code for masonry shear wall structures could lead to unconservative determination of the forces to be considered in such structures. On the other hand, the NEHRP provisions for initial design are conservative for this particular case study. In addition, the NEHRP provisions when soil–structure interaction was considered had a good correlation with the computed base shear from the recorded motions. This suggest that the response modification factor $R = 3.5$ proposed by the NEHRP provision for reinforced masonry shear walls might be suitable for this type of structures.

The 1988 UBC code and the NEHRP provisions do not distinguish between the seismic design of structures with flexible diaphragms from the design of structures with rigid diaphragms. Given the radical difference between the dynamic behavior of structures with flexible and rigid diaphragms, this code practice does not seem to be appropriate for structural systems with flexible diaphragms despite the inherit factors of safety contained in both codes.

CHAPTER 7
SUMMARY AND CONCLUSIONS

A case study has been presented describing seismic response of an instrumented grouted brick wall structure subjected to the Loma Prieta Earthquake. The subject structure is a two-story office building located at Palo Alto, California. Recorded peak ground accelerations were as high as 0.21g and peak roof accelerations as high as 0.53g. Considerable amplifications of the peak accelerations between the ground and the roof were observed. The building withstood the Loma Prieta Earthquake with little damage.

The objectives of this study were to :

1) assess the applicability of the simplified discrete MDOF dynamic model for the seismic evaluation of the two-story office building at Palo Alto and similar masonry shear wall buildings with flexible diaphragms.

2) correlate the recorded, observed and computed response at the two-story office building at Palo Alto with estimates of dynamic response and prescribed allowable stress limits by state-of-the-art masonry and seismic codes.

7.1 Survival of the Structure

The building had enough nominal capacity to resist the seismic shear forces to which it was subjected. However, the nominal moment capacity of the structure was tight to resist the expected maximum overturning moments at the time of peak recorded responses. The walls should have yielded at the time of severe ground shaking. Additional sources of strength and energy dissipation should have played a key role in the ability of the structure to survive the Loma Prieta Earthquake. The building was designed and according to code provisions.

7.2 Appropriateness of Code Provisions

Current seismic codes do not consider the design or evaluation of structures with flexible diaphragms explicitly (i.e., response modification factors and simplified formulas to estimate

the natural period of a building). Given the radical difference between the dynamic behavior of structures with flexible and rigid diaphragms, code practice is not appropriate for structural systems with flexible diaphragms despite the inherit factors of safety contained in the codes.

7.2.1 Design Base Shear

Base shears were underestimated by the 1988 UBC code as a direct consequence of allowing a high response modification factor for grouted–brick shear wall buildings ($R_W = 6$). On the other hand, base shears were within bounds with the NEHRP procedure when the natural period of the structure was closely estimated. The response modification factor adopted by the NEHRP provisions ($R=3.5$) seems to be more proper for this type of structural systems.

7.2.2 Fundamental Period

The approximate period formulas given by the 1988 UBC code and the NEHRP provisions are not necessarily suitable for masonry structures with flexible diaphragms. Estimated natural periods using the 1988 UBC Method A (Equation 6.1, $T_{E-W}=0.30$ sec. and $T_{N-S}=0.21$ sec.) and NEHRP provisions (Equation 6.5, $T_{E-W}=0.16$ sec. and $T_{N-S}=0.12$ sec.) clearly did not represent the diaphragm flexibility which extended the natural period of vibration ($T_{E-W}=0.40$ sec. and $T_{N-S}=0.37$ sec.).

7.3 Suitability of the Discrete MDOF Dynamic Model

The discrete MDOF dynamic model can be understood as an equivalent system of condensed beams (representing the cantilever walls) linked by elastic springs (representing the flexible diaphragms). Response is calculated at the translational degrees of freedom of these elements. The elastic discrete modeling has the capability to include the flexibility of the diaphragms, rotations of the walls, and soil–structure interaction effects through generalized translational and rotational springs at the base. However, the modeling does not consider the dynamic constraints imposed by the walls running in the perpendicular direction of analysis. Computation up to 25,000 time steps of dynamic response of a discrete model with as many

as 6 degrees of freedom can be done in less than one minute on a workstation or an advanced personal computer (386 or 486).

Recorded dynamic response of the subject building were represented reasonably well with the discrete model (waveforms, natural period estimates, frequency contents and peak responses). Variations between measured and computed response were obtained within ranges of variation of material properties and the soil.

The current study reinforces the perception that the discrete model constitutes a promising analytical tool for the seismic evaluation of low−rise masonry structures with flexible diaphragms, as it was found out in a recent study (Ref. 33). Although the discrete model has been developed for the study of masonry shear wall structures with flexible diaphragms, the concept could be easily extended to other structural systems with flexible diaphragms.

7.4 Suggested Research

Further research is needed on evaluation methods for masonry structures. In−situ dynamic tests (ambient vibrations, forced vibration) can provide relevant information about the dynamic characteristics of these structures, and they are helpful to corroborate the applicability of numerical models. Case studies of more masonry structures are desired, especially those of instrumented buildings. More buildings need to be instrumented as well as free−field ground motions adjacent to them so that results of this study can be extrapolated.

This research work has prompted out the necessity to improve the understanding of the behavior of structural systems with flexible diaphragms. Further research is needed on behavior of different types of diaphragms (plywood, flexible reinforced concrete, etc) to define : 1) damping characteristics; 2) the contribution of joists and sheathing to the lateral stiffness; and, 3) their nonlinear behavior. This information can be used to : 1) develop simplified nonlinear dynamic models; 2) obtain suitable response modification factors; and, 3) obtain empirical formulas to estimate the fundamental period.

110

7.5 Concluding Remarks

The seismic evaluation of masonry buildings can be enhanced. The knowledge gained through this research has been possible thanks to the availability of instrumented data from a grouted brick wall building during the Loma Prieta Earthquake. The discrete model used in this study proved again to be a helpful analytical tool for the evaluation of low−rise masonry structures with flexible diaphragms. However, further case studies of instrumented low−rise masonry buildings with flexible diaphragms are required to corroborate the effectiveness of the discrete model. In addition, case studies of instrumented high−rise masonry structures are needed to develop suitable simple models to compute their dynamic response, since inelastic behavior has been observed in these structures. Further research on the dynamic response of different types of masonry construction is therefore needed to develop an improved methodology for seismic evaluation of masonry structures with flexible diaphragms.

LIST OF REFERENCES

[1] ASCE, "Seismic Analysis of Safety Related Nuclear Structures and Commentary on Standard for Seismic Analysis of Safety Related Nuclear Structures," *ASCE Standard*, September 1986.

[2] ASCE, "Building Code Requirements for Masonry Structures (ACI 530−88/ASCE 5−88)," *ASCE*,18 pages.

[3] ATC (Applied Technology Council), "Tentative Provisions for the Development of Seismic Regulations for Buildings," *ATC Publication ATC 3−06, NBS Special Publication 510*, Washington, D. C., June 1978.

[4] Bathe, K. J. and E. L. Wilson, "Numerical Methods in Finite Element Analysis," Prentice Hall, 1976.

[5] Breyer, D. E, "Design of Wood Structures," Second Edition, Mc Graw Hill, 1988.

[6] Clough, R. W. and J. Penzien, "Dynamics of Structures," International Edition, Mc Graw Hill, 1982.

[7] CSMIP, "Plots of Processed Data for Palo Alto − 2−Story Office Building from the Santa Cruz Mountains (Loma Prieta) Earthquake of October 17, 1989," Confidential Report.

[8] EERC, "Preliminary Report of the Seismological and Engineering Aspects of October 17, 1989 Santa Cruz (Loma Prieta) Earthquake," Report No. UCB/EERC−89/14, October 1989.

[9] EERI, "Loma Prieta Earthquake October 17, 1989 Preliminary Reconnaissance Report," November 1989.

[10] EERI, "Loma Prieta Earthquake Reconnaissance Report," *Earthquake Spectra*, Supplement to Volume 6, May 1990.

[11] Elnashai, A., J. Bommer and A. El−Ghazoulli, "The Loma Prieta (Santa Cruz, California) Earthquake of 17 October 1989 : Seismological, Geotechnical and Structural Field Observations," ESEE Report 89/11, December 1989.

[12] Ghaboussi, J.,"Generalized Differences in Direct Integration Methods for Transient Analysis, "*Proceedings, NUMETA 87 International Conference of Numerical Methods in Engineering : Theory and Applications*, Swansea, U.K., July 1987, Vol II, T3.

[13] Ghaboussi, J.,"CE 498–CM Class Notes (Numerical Methods in Computational Mechanics), "University of Illinois at Urbana Champaign, Spring Semester, 1989.

[14] Gurfinkel, G., "Wood Engineering," Kendall/Hunt Publishing Company, Second Edition, June 1981.

[15] Hjelmstad, K. D. and D. A. Foutch, "Response Spectrum Analysis of Buildings with Flexible Bases," Unpublished Paper, University of Illinois at Urbana–Champaign, 1988.

[16] International Conference of Building Officials, "Uniform Building Code, 1988 Edition," International Conference of Building Officials, Whittier, California, 1988.

[17] International Masonry Institute, "The Loma Prieta, California, Earthquake of October 17, 1989; Observations Regarding the Performance of Masonry Buildings," February 1990.

[18] Kariotis, J. C., "Seismic Behavior of Unreinforced Masonry Buildings Shaken by the Loma Prieta Earthquake," *Structures Congress '91 Compact Papers, Ninth ASCE Structures Congress*, Indianapolis, Indiana, May 1991, pp. 30–33.

[19] Lew, M., R. Chieruzzi and K. W. Campbell, "Correlations of Seismic Velocity with Depth," *Proceedings, International Conference on Recent Advances in Geotechnical Earthquake Engineering and Soil Dynamics*, University of Missouri–Rolla, Rolla, Missouri, May 1981, p.p. 13–22.

[20] Masonry Promotion Groups of Southern California, "1988 Masonry Codes and Specifications," 1988.

[21] National Earthquake Hazards Reduction Program (NEHRP), "Recommended Provisions for the Development of Seismic Regulations for New Buildings," Part 1, Provisions, Federal Emergency Management Agency, 1988 Edition.

[22] National Earthquake Hazards Reduction Program (NEHRP), "Recommended Provisions for the Development of Seismic Regulations for New Buildings," Part 2, Commentary, Federal Emergency Management Agency, 1988 Edition.

[23] Newmark, N. M. and E. Rosenblueth, "Fundamentals of Earthquake Engineering," Prentice Hall, 1971.

[24] Newmark, N. M. and W. J. Hall, "Earthquake Spectra and Design," Monograph Series, EERI, 1987.

[25] NIST, "Performance of Structures During the Loma Prieta Earthquake of October 17, 1989," NIST Special Publication 778, January 1990.

[26] Parlett, B. N., "The Symmetric Eigenvalue Problem," Prentice Hall, 1980.

[27] Paulson, T. A. and D. P. Abrams, "Measured Inelastic Response of Reinforced Masonry Building Structures to Earthquake Motions," Civil Engineering Studies, Structural Research Series No. 555, University of Illinois at Urbana—Champaign, October 1990.

[28] Rubin, S., "Concepts in Shock Data Analysis," Shock and Vibration Handbook, Vol. 2, Mc Graw—Hill, 1961, pp. 23—1 to 23—37.

[29] Schneider, R. and W. L. Dickey, "Reinforced Masonry Design," Prentice Hall, Second Edition, 1987, pp. 400—417

[30] SEAOC, "Reflections on the October 17, 1989 Loma Prieta Earthquake," Structural Engineers Association of California (SEAOC), April 1991.

[31] Seed, H. B., C. Ugas and J. Lysmer, "Site Dependent Spectra for Earthquake—Resistant Design," *Bulletin of the Seismological Society of America,* Vol. 66, No. 1, February 1976, pp. 221—243.

[32] Shakal et al, "CSMIP Strong—Motion Records from the Santa Cruz Mountains (Loma Prieta), California Earthquake of 17 October 1989," Report OSMS 89—06, 1989.

[33] Tena—Colunga, A., "Response of an Unreinforced Masonry Building During the Loma Prieta Earthquake," Ph. D. Thesis, University of Illinois at Urbana—Champaign, May 1992.

[34] Tena—Colunga, A., "Seismic Evaluation of Unreinforced Masonry Structures with Flexible Diaphragms," Earthquake Spectra, Vol. 8, No. 2, May 1992, p.p. 305—318.

[35] Tissell, J. R. and J. R. Elliot, "Plywood Diaphragms," *Research Report 138,* American Plywood Association, April 1983.

[36] TMS Codes and Standard Committee, "Commentary to Chapter 24, Masonry, of the Uniform Building Code 1988 Edition," The Masonry Society (TMS), 1990.

[37] United States Department of Agriculture, "Wood Handbook : Wood as an Engineering Material," *Agriculture Handbook 72,* 1988.

[38] Wiegel, R. L. (Editor), "Earthquake Engineering," Prentice Hall, 1970.